Investigation of the *Folliculin (Flcn)* tumor suppressor gene in energy metabolism

Ming Yan

Department of Biochemistry
McGill University
Montréal, Canada

Dec., 2015

A thesis submitted to McGill University in partial fulfillment of the requirements for the degree of Doctor of Philosophy.

ABSTRACT

Birt–Hogg–Dubé (BHD) syndrome is an autosomal dominant hereditary disorder characterized by skin fibrofolliculomas, lung cyst, spontaneous pneumothorax and renal cell carcinoma (RCC). This condition is caused by germline mutations of *folliculin (Flcn)* gene, which encodes a 64-kDa protein named folliculin (FLCN). The AMP-actived protein kinase (AMPK) is a master regulator of cellular energy homeostasis. FLCN interacts with AMPK through FLCN-interacting proteins (FNIP1/2). Molecular function of FLCN and how FLCN interacts with AMPK in energy metabolism are largely unknown. We used mouse embryonic fibroblasts (MEFs) and adipose specific *Flcn* knockout mouse model to investigate the role of *Flcn* and its function associated with AMPK in energy metabolism.

We found that loss of FLCN constitutively activates AMPK, which in turn leads to elevation in peroxisome proliferator-activated receptor gama coactivator 1 α (PGC-1α), which mediates mitochondrial biogenesis and increase reactive oxygen species (ROS) production. Elevated ROS induces hypoxia-inducible factor (HIF) transcriptional activity and drives Warburg metabolic reprogramming. These findings indicate that *Flcn* exert tumor suppressor activity by acting as a negative regulator of AMPK-dependent HIF activation and Warburg effect.

To investigate the potential role of FLCN/AMPK/ PGC-1α in fat metabolism, we generated an adipose-specific *Flcn* knockout mouse model. *Flcn* KO mice exhibit elevated energy expenditure associated with increased O2 consumption, and are protected from diet-induced obesity. Importantly, loss of FLCN leads to increase in AMPK-dependent PGC-1 α and ERR α signaling, which are recognized as thermogenic and/or key regulators of mitochondrial biogenesis. Accordingly, several mitochondrial genes including uncoupling protein 1 (UCP1) are upregulated in *Flcn* KO white adipose tissue (WAT). As a consequence, the *Flcn* KO mice are more resistant to cold exposure associated with a higher UCP1 expression, which promotes fat burning by heat.

Taken together, FLCN is a negative regulator of AMPK. Loss of *Flcn* results in AMPK dependent PGC-1 α activation, which 1) drives tumorigenic metabolic adaptation

by ROS induced HIF activity, 2) inhibits fat accumulation by increased FAO and UCP1 expression.

Résumé

Le syndrôme Birt-Hogg-Dubé (BHD) est une maladie autosomale dominante héréditaire charactérisée par des troubles de la peau, des kystes pulmonaires, des pneumothorax spontanés et l'apparition de tumeurs rénales. Cette condition est causée par des mutations germinales dans le gène codant pour la protéine de 64 kDa nommée folliculine (FLCN). La protéine AMPK (*AMP-activated protein kinase*) est une clé de voute de l'homéostasie énergétique de la cellule. FLCN interagit avec AMPK par le biais de l'interaction avec les FNIP, les *FLCN-interacting proteins*. On ignore toujours le détail des fonctions moléculaires de FLCN, ainsi que de son impact sur le métabolisme cellulaire à travers son interaction avec AMPK. Dans le cadre des travaux présentés dans cette thèse, nous avons utilisé des fibroblastes embryonniques de souris (MEFs) et des souris avec une délétion ciblé du gène *Flcn* dans le tissus adipeux de façon à étudier le rôle de FLCN dans l'homéostasie du métabolisme énergétique.

Nous avons découvert que la répression ou la délétion de FLCN entraine une activation constitutive d'AMPK qui promeut l'activité de PGC-1α (*peroxisome proliferator-activated receptor gama coactivator 1α*), menant à une biogénèse accrue des mitochondries et de la production d'espèce réactive d'oxygène (ROS). Cette augmentation de ROS active le facteur de transcription HIF afin de favoriser une reprogrammation du métabolisme vers la glycolyse aérobie (effet Warburg). Ces résultats démontrent que FLCN jouent le rôle de suppresseur de tumeur en réprimant l'activation d'HIF dépendante d'AMPK, bloquant ainsi les changements du métabolisme pro-tumoraux.

De façon à étudier le rôle potentiel de la voie FLCN/AMPK/PGC-1α dans le métabolisme des adipocytes, nous avons généré un modèle de souris aillant une inactivation ciblée du gène *Flcn* au niveau des tissus adipeux. Dans ces expériences, les souris portant la délétion génétique démontraient une augmentation de leur métabolisme avec une plus grande consommation d'O2, leur conférant ainsi une protection contre l'obésité. Nous expliquons cette observation par le fait que la perte de FLCN entraîne une activation de la voie AMPK et de ces effecteurs PGC-1α et ERRα, qui sont reconnus comme des facteurs clés favorisant la biogénèse et l'activité des mitochondries. Ainsi, dans

les tissus adipeux des souris porteuses de la délétion, plusieurs gènes associés au métabolisme énergétique sont augmentés, notamment UCP1 (*uncoupling protein 1*). Par conséquent, les souris porteuses de la délétion Flcn démontrent une thermogène accrue lors de l'exposition au froid, puisque le tissu adipeux de ces souris est énergétiquement plus actif.

En conclusion, FLCN est un régulateur négatif de la voie d'AMPK. Ainsi, la répression de FLCN hyperactive la voie d'AMPK et son effecteur PGC-1 α, ce qui entraîne: 1) une adaptation métabolique oncogénique dépendante de l'activité de HIF et 2) une inhibition de l'accumulation des lipides via une activation de leur oxydation.

TABLE OF CONTENTS

ACKNOWLEDGEMENTS

First, I would like to thanks my supervisor, Dr. Arnim Pause, who gave me an opportunity for my Ph.D. study in his laboratory, He offered me an excellent and exciting project with unlimited support, advice and patience until achievement.

Second, I would also like to thank my RAC committee, Dr. Julie St-Pierre, Dr. Russell Jones and Dr. Nahum Sonenberg for their kind and best guidance.

A special thank to Dr. Vincent Giguère for his invaluable advice and shared treasured reagents and his Postdoc Étienne Audet-Walsh for kind collaboration and fantastic discussion on the chapter 3 project.

A great thanks to all colleagues, past and present members of the Dr. Pause laboratory, for their friendship and great fun over more than five years. A special thank you to our laboratory manager Dr. Marie-Claude Gingras for her valuable work on chapter 2 and for keeping the lab running smoothly.

I thank all of my family and my wife Yiyao for love, support and encouragement to follow my dreams. Finally, to my son Alex, you are the greatest gift from God. I am so proud of you.

Lastly, I would like to thank CIHR's doctoral research award funding me over 3 years as well as FRSQ, Canderel, and MICRTP for my research and travel finance awards.

LIST OF FIGURES

CHAPTER 1

CHAPTER 2

CHAPTER 3

CHAPTER 4

LIST OF TABLES

LIST OF ABBREVIATIONS

A	Alanine
ACC	Acetyl-CoA carboxylases
ADP	Adenosine diphosphate
AGE-1	Ageing alteration-1
AICAR	5-aminoimidazole-4-carboxamide-1-β-D-ribonucleoside
AMP	Adenosine monophosphate
AMPK	5'AMP-activated protein kinase
ATP	Adenosine triphosphate
ATP	Adenosine 5'-triphosphate
BHD	Birt-Hogg-Dube
C-	Carboxy
C	Cysteine
CAMKK	Ca2+/calmodulin-activated protein kinase kinases
cDNA	Complementary DNA
DMEM	Dulbecco's Modified Eagle's Medium
DMSO	Dimethyl sulphoxide
DNA	Deoxyribonucleic acid
ds	Double-stranded
DTT	Dithiothreitol
EDTA	Ethylenediaminetetraacetic acid
EGTA	Ethylene glycol tetraacetic acid
ERR	Estrogen-related receptor
ER	Endoplasmic reticulum
FAS	Fatty acid synthesis
FAO	Fatty acid oxidation
FLCN	Folliculin
FNIP1	Folliculin-interacting protein 1
FNIP2	Folliculin-interacting protein 2
FTC133	Follicular thyroid carcinoma cells 133

GABARAP	GABA receptor-associated protein
GEFs	Guanine nucleotide exchange factors
Glu	Glutamic acid
GLUT1	Glucose transporter 1
GLUT4	Glucose transporter 4
GPDH	Glycerol-3-phosphate dehydrogenase
GTP	Guanosine-5'-triphosphate
H2O2	Hydrogen peroxide
HIF1	Hypoxia inducible factor 1
HIF2	Hypoxia inducible factor 2
HRP	Horseradish peroxidase
IP	Immunoprecipitation
K	lysine
kb	Kilobase pairs
kDa	Kilodaltons
KO	Knock out
Leu	Leucine
MEFs	Mouse embryonic fibroblasts
MiT	microphthalmia transcription
mTOR	Mammalian target of Rapamycin
N-	Amino
OXPHOS	Oxidative phosphorylation
PAS	Periodic acid schiff
PAGE	polyacrylamide gel electrophoresis
PBS	Phosphate buffered saline
PCR	polymerase chain reaction
PGC1	Proliferator-activated receptor gamma 1 co-activator
PPARs	Peroxisome proliferator-activated receptors
R	Arginine
Rag	Recombination activating gene
RCC	Renal cell carcinoma

RNA	Ribonucleic acid
RNAi	RNA interference
ROS	Reactive oxygen species
S	Serine
shRNA	Small hairpin RNA
TCA	Tricarboxylic acid
TFE3	Transcription factor E3
TFEB	Transcription factor EB
TGF-β	Transforming growth factor beta
Thr172	Threonine 172
TNF-α	Tumor necrosis factor alpha
TSC2	Tuberous sclerosis complex 2
UCP	Uncoupling protein
UTR	Untranslated region
VEGF	Vascular endothelial growth factor
VHL	Von Hippel-Lindau
WAT	White adipose tissue
WT	Wild-type

CONTRIBUTION OF AUTHORS

Chapter 2

In chapter 2, I performed the following experiments:

2.1: A, C, D, E, F, G, and H

2.2: C, F, and G

2.3: A, B, C, D, E, and F

2.4: A, B, C, D, E, F, and G

2.6: A, D, E, F, and G

Marie-Claude Gingras performed the following experiments:

2.1: G, H

2.2: A, B, E

2.4: D, F, and H

2.5: A, B, C

2.6: B, C

Elaine A. Dunlop performed experiment 2.1: B

Yan Nouet performed experiments: 2.5: D, E

Fanny Dupuy performed experiments: 2.5: A, B, C

Mitian Kamps & Maurice A.M. Van Steensel performed experiment 2.7: A, B

Chapter 3

In chapter 3, I performed all experiments except those for figure 3.2 D, E (Haematoxylin and eosin stain) and 3.6 D (UCP1 antibody immunohistochemistry) on mouse adipose tissue. They were accomplished at the McGill histology facility and Étienne Audet-Walsh and I performed the imaging. Étienne Audet-Walsh also performed figure 3.5 C, D and G for ChiP-qPCR analysis. Sanaz Manteghi and I perform figure 3.4 C for ERRE luciferase report assay. Benjamin Walker helped with the metabolic cage data analysis for figure1, Chatherine Rosa Dufour helped with mouse cold exposure experiment.

CHAPTER 1:

INTRODUCTION

1.1 Birt-Hogg-Dubé syndrome

1.1.1 Epidemiology

Birt–Hogg–Dubé (BHD) syndrome is an autosomal, dominantly inherited, genetic disorder, characterized by the development of fibrofolliculomas (benign skin tumors), pulmonary cysts and pneumothorax (collapsed lung), and predisposition to kidney cancers with clear cell, chromophobe, papillary or oncocytic features.

BHD disease was originally described in 1977 by three Canadian doctors; Birt, Hogg and Dubé. They identified a numbers of patients presenting small dome-shaped papular lesions from the hair follicle on forehead, face, neck and upper trunk that were inherited in an autosomal dominant manner [1]. Histological analysis of these cutaneous lesions revealed the characteristic dermatologic triad of fibrofoliculomas, trichodiscomas and acrochordons, which became known as the Birt-Hogg-Dubé (BHD) syndrome [1] [2] [3] [4]. Updated for 2015, approximately 432 families in the world have been diagnosed with BHD according to a conservative estimate (See table 1.1).

BHD syndrome is manifested in a manner similar to other hamartoma syndromes. These include tuberous sclerosis, which causes skin lesions similar to fibrofolliculomas, and von Hippel-Lindau disease, which causes hereditary kidney cancers. Hamartoma syndromes are caused by mutations of key tumor suppressor genes leading to malignant and benign tumors in multiple organs such as Cowden Syndrome caused by the loss of function of PTEN, Peutz-Jeghers syndrome by LKB1 and Tuberous Sclerosis complex by TSC1 or TSC2 tumor suppressors, respectively. Importantly, BHD syndrome is known to be associated with *Flcn* tumor suppressor gene only [5] [6] [7].

Table 1.1 BHD Families until 2015

Country	Number of families	References
USA	171	Toro *et al*. 2007, Unpublished
The Netherlands	56	Menko *et al*., 2012; Houweling *et al*., 2011; Unpublished
Japan	56	Nakamura *et al*., 2013; Tobino and Seyama, 2012; Furuya *et al*., 2012; Kashiwada *et al*. 2012; Tobino *et al*. 2011; Hayashi *et al*. 2010; Kunogi *et al*. 2010; Koga *et al*. 2009; Ishii *et al*. 2009; Imada *et al*. 2009; Misago *et al*., 2008; Gunji *et al*. 2007; Kawasaki *et al*. 2005; Takahashi *et al*. 2001
France	40	Zenone, 2013; Spring *et al*., 2013; van Denhove *et al*., 2011; Vinit *et al*. 2010; Steff *et al*., 2010; Kluger *et al*. 2010; Le Guyadec *et al*. 1998; Unpublished
UK	38	Felton and Madan, 2012; Byrne *et al*., 2012; Hopkins *et al*. 2011; Warwick *et al*. 2010; Stavrakoglou *et al*. 2010; Jarrett *et al*. 2009; Sundaram *et al*. 2009; Woodward *et al*. 2008; Unpublished
Italy	14	Attinà *et al*., 2013; Maffé *et al*. 2011; Palmirotta *et al*. 2008; Scalvenzi *et al*. 1998
Germany	12	Sander *et al*., 2013; Brehmer *et al*., 2013; Lichte *et al*., 2012; Michels *et al*. 2012; Sattler *et al*., 2012; Westermann *et al*. 2010; Janitzky *et al*. 2008; Lamberti *et al*. 2005; Gambichler *et al*. 2000; Walter *et al*. 1997
China	14	So *et al*. 2009; Ren *et al*. 2008,
Korea	6	Kim *et al*., 2012; Shin *et al*., 2011; Park *et al*., 2011; Bae *et al*., 2011; Kim *et al*. 2008
Spain	6	Mota-Burgos *et al*., 2013; Alonso-Gonzalez *et al*., 2011; Sempau *et al*., 2010; Truchuelo *et al*. 2011; Fuertes *et al*. 2009; De La Torre *et al*. 1999
Canada	3	Pierce *et al*., 2011; Souza *et al*. 2005; Birt *et al*. 1977
Switzerland	3	Fröhlich *et al*. 2008; Pittet *et al*. 2006
Australia	2	Cocciolone *et al*., 2010; Godbolt *et al*. 2003
Taiwan	2	Yang and Chiang, 2013; Furuya *et al*., 2012
Belgium	1	Schreuer *et al*., 2011
Brazil	1	Pimenta *et al*., 2012
Egypt	1	Fahmy *et al*. 2007
Finland	1	Painter *et al*. 2005
Iran	1	Jandaghi *et al*., 2013
Ireland	1	Lynch *et al*., 2011
Russia	1	Unpublished
Sweden	1	Khoo *et al*. 2001
Turkey	1	Tefekli *et al*., 2012
Total	**432**	

This is a conservative estimate of the number of BHD families. References were only included where it could be determined that the patients in the cohort were unique and not reported elsewhere in the literature. Thus, the actual number of BHD families is likely to be higher.

(Adapted from BHD literature database in BHD Foundation and [8, 9] [10])

1.1.2 Birt-Hogg-Dubé disease clinical manifestations

1.1.2.1 Fibrofolliculomas

Clinically, fibrofolliculomas are hallmark for BHD syndrome. Fibrofolliculomas are defined as multiple anastomosing nests and strands of two to four epithelial cells arose from a central follicle. The dermatologic diagnosis of BHD disease is recognized in individuals who have five or more facial or truncal papules with at least one histologically confirmed fibrofolliculoma [11]

1.1.2.2 Pulmonary cysts and pneumothorax

Pulmonary cysts are air filled structure within the lung parenchyma that has a thin-walled, well-defined lesion between 1 and 4 mm. Most patients (89%) with BHD syndrome have multiple bilateral and multifocal lung cysts on chest CT [12]. Individuals with BHD syndrome and a family history of pneumothorax have a statistically significant increased risk of pneumothorax compared to individuals with BHD syndrome without a family history of spontaneous pneumothorax. BHD patients have a 50-fold increased risk for spontaneous pneumothorax compared to family members who do not have BHD syndrome [13]. The pulmonary cysts and repeated episodes of pneumothorax are the clinical hallmarks for diagnosis of families affected by the syndrome [14]

1.1.2.3 Renal cell carcinoma

Renal cell carcinoma (RCC) is common type of cancerous kidney diseases. Yearly, more than 6000 Canadian individuals are diagnosed with RCC and almost 30% are estimated to die because often detected at the late stages [15]. Human RCC is believed to arise from a variety of specialized nephron cells and is comprised of several histological cell types including chromophobe and collecting duct RCC, clear cell and papillary RCC. Each type has differences in genetics [16]. For example, von Hippel-Lindau syndrome (VHL syndrome) typically develop clear cell RCC only, hereditary papillary renal cancer (HPRC) develop bilateral and multifocal type 1 papillary RCC, and hereditary leiomyomatosis and renal cell cancer (HLRCC) usually develop solitary renal tumors from tubo-papillary to type 2 papillary renal cancer to collecting duct renal cell cancer [17].

Unlike other causative RCC genes disorder, BHD-associated renal tumors are

heterogeneous and increase the risk of developing all renal tumor subtypes including chromophobe RCC (chRCC), benign renal oncocytoma, mixed oncocytic hybrid RCC, clear-cell RCC (ccRCC), and papillary type I RCC with a variety of histology. The risk of developing renal tumors is seven fold greater in BHD affected individuals when compared with their unaffected siblings [18]. The most frequent histologic tumour type in BHD-affected individuals is the hybrid oncocytic tumour (50%) with features of chRCC and renal oncocytoma. Additionally, patients with BHD are at risk of developing chRCC (35%), ccRCC (9%) and, less frequently, renal oncocytoma (5%) [19] [20].

1.1.2.3 Other phenotypic manifestations

A large number of other clinical features have been reported in BHD patients with lipomas, parathyroid adenomas, thyroid nodules, thyroid cancer, and parotid oncocytomas [11, 21-23]. However, whether these incidental phenotypes are truly correlative with BHD syndrome is under investigation.

1.1.2.4 Colorectal polyps and colorectal cancer

Multiple cases of colon cancer have been described in affected individuals [22], but the evidence associating colonic neoplasm and BHD syndrome is conflicting. Indeed, BHD was reported to be associated with colonic polyposis and colorectal cancer in some families [24-26]. Khoo et al. found a high incidence of colorectal polyps and CRC in BHD patients with confirmed *Flcn* germline mutations, suggesting that some BHD families are at increased risk of colorectal neoplasia, and indicating that FLCN may be involved in colorectal tumourigenesis. However, others failed to observe any significant risk for colon polyps and cancer [11, 13]. Zbar et al. (2002) found no association between BHD and colonic polyps or colorectal cancer (CRC) in a study involving a large cohort of 111 BHD syndrome patients [13, 27].

Consequently, other clinical manifestations have been possibly linked to the BHD syndrome including endometrial cancer [28, 29]. Similarly, an increase risk for colorectal, endometrial as well as gastric cancers can also be observed in patients with hereditary non-polyposis colorectal cancer (HNPCC) or Lynch syndrome due to inherited mutation that impair DNA mismatch repair [29]. Further studies are required to confirm the association

of BHD with these cancers.

1.1.2.5. Thyroid nodules

Three cases of thyroid cancer in affected individuals have been reported [22, 23]. In a French case series, thyroid nodules and/or cysts were detected by ultrasonography in 13 (65%) of 20 individuals with BHD; no medullary carcinoma or other thyroid carcinomas were detected. None of the affected individuals with thyroid nodules and/or cysts had a familial history of thyroid cancer. Overall, nine (90%) of ten families affected by BHD with germline pathogenic variants in FLCN had individuals with thyroid nodules [30].

1.1.2.6 BHD therapy

Currently, surgical intervention is the only therapy available for BHD-associated renal tumors. Erbium-YAG or fractional CO_2 laser ablation of folliculoma/trichodiscoma resulted in substantial improvement for a period of time, but relapse usually occurs [31, 32]. Nephron-sparing surgery is the treatment of choice for renal tumors whenever possible, depending on the size and location of the tumors [19].

Notably, there is currently no pharmacological treatment available to cure for any of the symptoms for BHD syndrome, but improved understanding of FLCN molecular function will hopefully lead to the development of effective strategy of therapy for this disease.

1.2 Folliculin (*Flcn*) gene

1.2.1 Identification of the *Flcn* gene

In 2001, the first BHD-associated gene locus was mapped to chromosome 17p11.2, named Folliculin (*Flcn*), and subsequently identified as being inactivated in individuals with BHD syndrome [33, 34]. In 2002, *Flcn*, the only gene known to cause BHD syndrome, was identified in spanning approximately 20 kb of genomic DNA and comprising 14 exons, encodes a 579 amino acid with a predicted size of 64 kDa protein, folliculin (FLCN), which is expressed in most tissues including the skin and its appendages, the lungs (type 1 pneumocytes) and the kidney (distal nephron). The sequence

has no significant homology to any known protein, but it is highly conserved across species including Canis lupus familiaris, Bos Taurus, Mus musculus, Rattus norvegicus, Gallus gallus, Xenopus tropicalis, and Drosophila melanogaster, suggesting an important biological role [35].

1.2.2 *Flcn* mutations

Although mutations can occur anywhere including exons and introns, 50% of the mutations reported are caused by insertions or deletions in the 8 cytosine nucleotides of exon 11. Screening of nine BHD families found that eight had truncating mutations (seven frameshift, one nonsense) in *Flcn*, five of which were in exon 11. And an additional 53 BHD families screen found that 22 had mutations in exon 11, suggesting it is a mutation 'hot spot' [12, 36-39].

The loss of FLCN expression observed in almost all histologic subtypes of renal carcinoma and a second somatic mutation necessary for renal cancer provide further support for its function as a tumor suppressor gene that fits the classic two-hit model [4]. To date, 149 unique *Flcn* germline mutations spanning all 14 exons have been identified in BHD syndrome are predominantly mutations (insertion/deletion, nonsense, splice site) [40] that result in premature protein truncation and presumed loss of FLCN function. In addition, nine large intragenic deletions or duplications were expected to severely disrupt protein structure or, at a minimum, to delete the last exon [20].

1.3 Folliculin and its interacting proteins

1.3.1 FLCN protein

FLCN encodes for a 579 amino acid protein (64kDa), consisting of a short hydrophobic N-terminal sequence, one N-glycosylation site, three myristoylation sites and a glutamic acid-rich coiled coil domain centrally located in the protein [35]. The N- and C-terminal domains of FLCN are connected through a 40 amino acid disordered linker region. This region contains a bipartite tryptophan (WD-WQ) motif, which has been shown to be a binding motif for kinesin light chain 1, which is an intracellular trafficking protein [41]. C-terminal domain (residues 341-579) of FLCN, determined by X-ray crystallography were found to form alpha-sheet with helices packed on one side, followed by an all helical region. This fold is remarkably similar to that of DENN-domain proteins, which function as Rab guanine nucleotide exchange factors (GEFs) [35]. No transmembrane domains or organelle localization signals have been determined within the FLCN sequence [42].

1.3.2 Folliculin-interacting proteins: FNIP1/FNIP2/AMPK complex

FLCN as an AMPK-binding partner has been first reported to be involved in the AMPK signaling pathway [43]. FLCN interacts with AMPK via a 130-kDa protein binding to FLCN, named folliculin-interacting protein 1 (FNIP1). FNIP1 interacts with the C-terminus of FLCN and with 5'-AMP-activated protein kinase (AMPK). A second FLCN interacting protein, folliculin-interacting protein 2 (FNIP2) was identified by bioinformatics searches for homologous FNIP1. FNIP2 has 49% homology with FNIP1 and, like FNIP1, binds to the carboxyl terminus of FLCN and interacts with AMPK [44]. FNIP1 and FNIP2 are both required for localization of FLCN to lysosomes during amino acid starvation, [45] where FLCN interacts with the RAG proteins in order to activate mTORC1 signaling [46, 47].

AMP-activated protein kinase (AMPK) is an evolutionarily conserved serine/threonine protein kinase playing a key role in cellular and whole-body energy homeostasis. AMPK is a heterotrimeric complex composed of a catalytic α subunit and

two regulatory subunits (β and γ). When cellular energy levels drop, AMP or ADP bind to the γ regulatory subunit of AMPK and induce an allosteric conformational change. This change leads to the activation of AMPK by phosphorylation of a threonine residue (Thr-172) within the activation loop of the kinase domain. Once activated, AMPK maintains energy balance by switching cells from an anabolic (ATP consumption) to catabolic (ATP production) state. Two upstream kinases, liver kinase B1 (LKB1) and calcium/calmodulin-dependent protein kinase kinase (CaMKKβ) are reported to be responsible for phosphorylation of AMPK [48]. Activation of AMPK leads to a concomitant increase in the phosphorylation of acetyl-CoA carboxylase (ACC), a downstream targets gene of AMPK [49]. ACC is an important enzyme for synthesis of malonyl-CoA, a precursor for both of fatty acid synthesis (FAS) and fatty acid oxidation (FAO). Phosphorylation of ACC by activated AMPK leads to inhibition of ACC and subsequent suppression of FAS while promoting mitochondrial β-oxidation in liver [50]. It has been reported that constitutively active AMPK-α1, an isoform of AMPKα, in liver generated by transgenic mice exhibits resistance to high fat diet-induced obesity [51]. Activation of AMPK in mouse adipose tissue leads to increase in fatty acid oxidation [52].

Correspondingly, AMPK has been shown to downregulate the expression of cyclooxygenase (COX)-2 [53], which contributes to progression of certain human cancers and inflammatory disorders (Figure1.2). However, several controversial reports revealed that AMPK acts as a driver of tumorigenesis in cancer development. Its physiological role on AMPK-dependent functions is still poorly characterized (Figure 1.1).

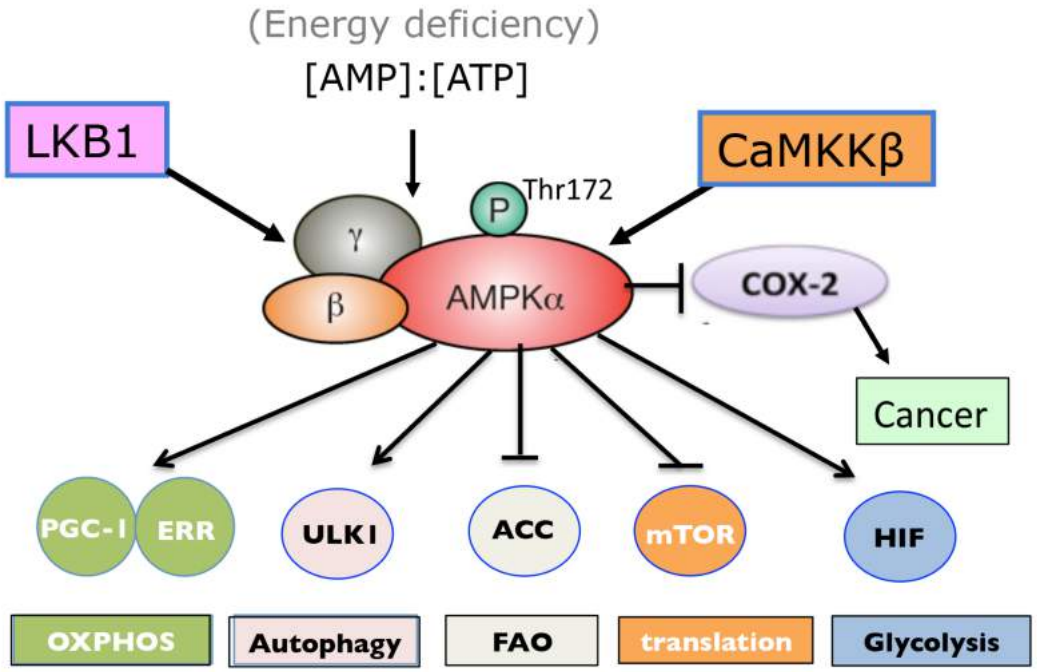

Fig 1.1 Functional deregulation of AMPK leading to tumor suppression

AMPK is activated when AMP/ATP or ADP/ATP ratios in the cells rise due to various physiological stresses, such as hypoglycemia and hypoxemia, leading to the activation of LKB1. Metformin and phenformin can also mimic these stressors and lead to AMPK activation in an LKB1-dependent manner. CaMKKb activates AMPK in response to calciumincrease. Catabolic pathways, such as fatty acid oxidation, are activated by AMPK. For example, AMPK phosphorylation leads to the inactivation of acetyl CoA carboxylase (ACC2). On the other hand, AMPK inhibits anabolic pathways, such as fatty acid synthesis, mediated by ACC1. One of the most well-known pathway of AMPK is through the TSC1/TSC2 complex, leading to the downregulation of mTOR, which can also be activated downstream of the PI3K-AKT and Ras-Raf-MEK-ERK signaling pathways. The mTOR pathway suppresses apoptosis via its effect on the tumor suppressors p53 and p27 and inhibits autophagy by suppressing UNC-51-likekinase1 (ULK1) and ULK2. AMPK downregulates these effects of mTOR, thus leading to increased apoptosis and autophagy-mediated cell death. In dependent of mTOR, AMPK phosphorylates and activates ULK1 and ULK2, thus triggering autophagy. Furthermore,

AMPK has been shown to downregulate the expression of cyclooxygenase (COX)-2, which contributes to the pathophysiological progression of certain human cancers and inflammatory disorders. AMPK is necessary for the expression of xeroderma pigmentosum C (XPC) to promote DNA repair follow in UV damage.
(Adapted from [54])

1.3.3 Other FLCN-interacting proteins

ULK1 and GABARAP are other FLCN-interacting proteins known for their involvement in the autophagy process [55]. Moreover, the regulatory particle triple-A ATPase 4 (Rpt4) and Plakophilin-4 (PKP4), which are involved in ribosomal RNA synthesis and cytokinesis and Rho signaling respectively, have been also shown to interact with FLCN [56-58]. However, how these interactions are linked to the cellular mechanism of FLCN is not fully elucidated.

1.4 Folliculin-associated signaling pathways

FLCN has been implicated in numerous signaling pathways and cellular processes including mTOR signaling, HIF signaling, mitochondrial biogenesis, stress resistance, autophagy, PGC-1 α signaling, and TGF-β signaling.

1.4.1 mTOR signaling

FLCN and AMPK interaction, mediated by FNIP1 and FNIP2, has been shown to regulate mTOR signaling [43, 44]). AMPK, an important energy-sensing enzyme that monitors cellular energy status, is a negative regulator of mechanistic target of rapamycin mTOR [59]. mTOR is the master controller of protein synthesis and cell growth. [60]; [61]. Wee et. al reported that an 8-week course of topical rapamycin reduced the size and redness of skin lesions in two siblings with Familial Multiple Discoid Fibromas (FMDF), characterized by the presence of fibrofolliculomas, suggesting that dysregulated mTOR signaling may contribute to the development of skin lesions in BHD syndrome [62].

Recent studies showed that FLCN-FNIP1/2 complex interacts with RAG proteins on the surface of lysosomes to modulate mTORC1 activity upon amino acid stimulation [47, 63]. mTORC1 is activated through a multimeric protein complex, which contains the

Ras-related GTP binding (Rag) family of GTPases (RagA/B and RagC/D), whose bound nucleotide state (GDP/GTP) determines the recruitment of mTORC1 to the lysosome (Tsun, et al. 2013). Evidence by Petit et al. provides a somewhat different mechanism. Their findings support a role of FLCN and FNIP1, acting as a guanine exchange factor (GEF) for RagA, which results in GTP loading of RagA/B and recruitment and activation of mTOR (Petit, et al. 2013).

In both studies, the interaction between FLCN and the Rag proteins was found to activate mTORC1 signaling in response to amino acid stimulation. These studies provide strong support of a role for FLCN in facilitating mTORC1 activation at the lysosome surface in an amino-acid-sensitive manner via the Ras-related GTPases.

1.4.2 HIF signaling

Hypoxia-inducible factor-1 (HIF-1) is a dimeric transcriptional complex that has been recognized primarily for its role in the maintenance of oxygen and energy homoeostasis [64]. The HIF-1α subunit is O2 labile and is degraded by the proteasome following prolyl-hydroxylation and ubiquitination in normoxic cells [65]. HIF-1 is one of the principal mediators of homeostasis in human tissues exposed to hypoxia, which presents in many solid tumors. The most common causes of tissue hypoxia are inflammation and/or insufficient circulation [66]. HIF-1 plays a key role in the development and regulation of certain cancers, such as kidney, lung and cardiovascular tumors [67]. HIF-1 blockade may be beneficial to prevent tumor angiogenesis and tumor growth [68].

Preston et al. [69] observed that increased hypoxia-inducible factor (HIF) signaling in FLCN-null cells lead to the increased activity of glycolytic enzymes, thus causing these cells to favor glycolytic rather than lipid metabolism, as seen in the Warburg effect [70]. The Warburg effect states that cancerous cells produce energy by glycolysis and lactic production in the cytosol rather than by pyruvate oxidation in the mitochondria [70]. Additionally, HIF-1 α expression is increased in cystic lung tissue segmental resection from a BHD patient, suggesting that under normal conditions, FLCN inhibits HIF

signaling [71]. HIF signaling pathway regulates a number of different genes involved in angiogenesis, erythropoiesis, cell survival and metastasis, and is an oncogene in several cancer types [72].

Interestingly, it has been reported that AMPK increased the transcriptional activity of HIF in hypoxia without affecting its stability via an unknown mechanism [73]. However, how AMPK is activated upon loss of FLCN is still not clear. Consequently, how FLCN and AMPK/FNIPs interact mechanistically, and how they regulate HIF transcriptional activity and metabolic adaptation in normoxia, and whether this effect linking to tumor suppression maintain largely unknown.

1.4.3 Autophagy signaling

Autophagy is a process of self-degradation of cellular components in which double-membrane autophagosomes sequester organelles or portions of cytosol and fuse with lysosomes or vacuoles for breakdown by resident hydrolases [74]. Several reports have identified a role for FLCN in autophagy. Possik et al. observed that loss of *Flcn* in a *Caenorhabditis elegans* model led to constitutive AMPK activation and induction of autophagy [75]. In contrast, Dunlop et al. showed that autophagy was impaired in FLCN-deficient kidney cell lines and BHD renal tumors. This report supports a mechanism by which FLCN, modulated by ULK1-like autophagy activating kinase and in complex with FNIP1/2, positively regulates autophagy through interaction with GABARAP (GABA receptor--associated protein), a component of the autophagosome machinery [55].

1.4.4 TGF-β signaling

The transforming growth factor beta (TGF-β) signaling is involved in many cellular processes in the developing embryo including cell growth, cell differentiation, apoptosis, cellular homeostasis and other cellular functions. Two independent studies have shown that FLCN regulates TGF-β signaling: Hong et al. used microarray analysis to show [76] that FLCN regulates several components of the TGF-β pathway in UOK-257 cells. They reported that FLCN controlled the transcriptional activity of basic-helix-loop-

helix transcription factor E3 (TFE3), a member of the microphthalmia transcription (MiT) family involved in TGF-β-induced activation of the PAI-1 promoter [77]. They observed that TFE3 was normally maintained in the cytoplasm without stimulus. FLCN deficiency leads to TFE3 relocalization to the nucleus where it can perform its transcriptional regulation. They further demonstrated that TFE3 nuclear localization was correlated with decreased TFE3 phosphorylation and increased activity in a number of FLCN-deficient human and mouse renal tumors and in UOK-257 kidney cancer cell line. Others observed a general loss of TGF-β mediated transcription and chromatin modifications in FLCN-null murine ES cells. They found that loss of the *Flcn* tumor suppressor gene results in apoptotic resistance due to aberrant TGFβ-mediated transcription [78].

1.4.5 PGC-1α signaling

The peroxisome proliferator-activated receptor γ, co-activator 1α (PGC-1α) was initially identified through its functional interaction with the nuclear receptor, peroxisome proliferator-activated receptor γ (PPARγ) in brown adipose tissue (BAT), a mitochondria-rich tissue involved in regulating the process of adaptive thermogenesis in response to cold [79]. Subsequent study determined that PGC-1α serves as an inducible transcriptional coactivator playing a critical role in the regulation of mitochondrial biogenesis and cellular energy metabolism [80, 81].

Klomp et al. [82] found that the loss of FLCN in BHD-associated renal tumors resulted in mitochondrial dysfunction, as indicated by upregulation of two transcription factor genes, PGC-1α and TFAM (transcription factor A, mitochondrial), involved in mitochondrial biogenesis. They proposed that loss of FLCN leads to dysfunction of PGC-1α-OXPHOS-TFAM signaling axis. Additionally, Hasumi et al. added that deletion of FLCN in mouse muscle lead to an increase in both PGC-1α expression and mitochondrial oxidative phosphorylation. [83].

Boström and colleagues reveal that overexpression of PGC-1α in mouse muscle induced a brown-like adipose tissue gene program, and overexpressing PGC-1α showed markedly increased in brown adipose tissue (BAT)-associated uncoupling protein 1

(Ucp1) in the subcutaneous inguinal fat [84]. Normally, UCP1 in BAT plays a nonshivering thermogenesis function through an increase in energy expenditure by heat loss in mitochondria [80]. Other study demonstrated that expression of UCP1 in white adipose tissue (WAT) is largely induced through a β3-adrenergic receptor agonist [85] and cold exposure [86]. Importantly, PGC-1α dependent upregulation of UCP1 leads concomitant browning of the WAT in which alter fat metabolism and improve obesity and type 2 diabetes [87]. Interestingly, it is still largely unknown how a single transcriptional coactivator can mediate such broad systemic effects and, particularly, how muscle-specific expression can influence whole-body metabolism.

Recently, Ohno et al. showed that PPAR-γ ligands, coupled with PRDM16 (a determinant for the development of BAT), could switch subcutaneous white adipose cells to a BAT program [88]). Moreover, other molecules such as AMPK and PPAR-δ have been put forward as exercise mimetic for browning [89]. An important investigation should be to identify the specific molecular pathways that underlie browning. Taken together, it will be interesting to explore fat metabolism upon FLCN deletion, which might lead to elevation in PGC-1α and browning of the WAT in the AMPK dependent manner (Figure 1.2).

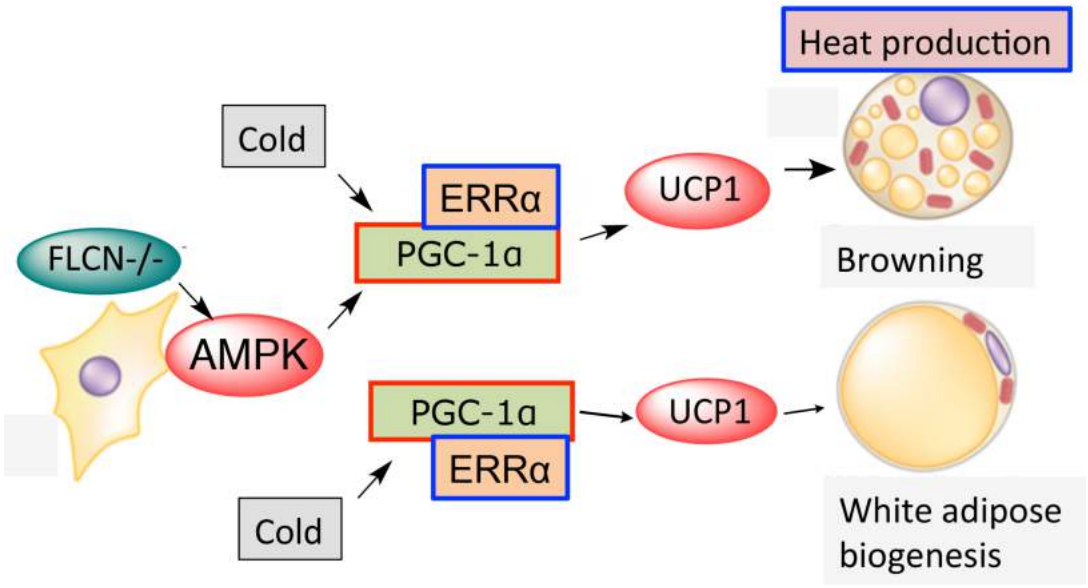

Fig 1.2 PGC-1α is an adaptive thermogene, inducible by cold exposure in WAT and BAT

Cold exposure results in a marked induction of PGC-1α expression in BAT and browning of white adipose tissue (WAT). PGC-1α is a powerful transcriptional co-activator of nuclear hormone receptors, including PPARα and PPARY, RARα and ERRα. PGC-1α is able to coordinate the transcription of genes that are involved in thermogenesis with the induction of UCPs, genes of the mitochondrial respiratory chain such as ATP synthase and the cytochrome c oxidase subunits (COX) II and IV, and mitochondrial biogenesis. FLCN might play a major role in this process through recruiting the PGC-1a coactivator in AMPK dependent manner. Upon cold exposure, FLCN deletion might lead to elevation in PGC-1α and increase higher expression of thermogenic genes including upregulation of UCP1, which leads concomitant browning of the WAT, alters fat metabolism and promotes more heat.

Adapted from [79, 90, 91]

1.4.6 FLCN loss drives AMPK-dependent cellular metabolism

Basically, all kind of cells needs to generate energy to build all the components necessary to grow and survive, a process known as “cellular metabolism”. Cancer cells often generate energy through altered metabolic reprogramming to fuel their high metabolic rate and rapid proliferation. One of the primary metabolic adaptations associated with cellular transformation is an increase in glycolytic activity. Glucose is normally catabolized in cells via two independent biochemical pathways: glycolysis, the non-oxidative glucose catabolism to generate 2 molecules of ATP and pyruvate per glucose molecule, and the tricarboxylic acid (TCA) cycle/oxidative phosphorylation (OXPHOS) system in mitochondria, which oxidizes glycolysis-derived pyruvate to generate 36 molecules of ATP per glucose molecule. In contrast to non-transformed cells, cancer cells convert the majority of glucose-derived pyruvate to lactate, a phenomenon now known as the “Warburg Effect”, which is commonly used to describe a metabolic phenotype in which tumor cells engage in high rates of glucose uptake and lactate production regardless of oxygen concentration [70].

AMPK is a central sensor of cellular energy status. The kinase is activated by increases in cellular AMP by three mechanisms: 1) allosteric activation; 2) promotion of Thr172 phosphorylation by kinase, for instance, LKB1; (iii) inhibition of Thr172 dephosphorylation. Of these thus allowing the system to act as a sensor of cellular energy [92].

FLCN phosphorylation was first identified by Baba [43]. Further research has shown that FLCN interaction with AMPK is modulated by the phosphorylation of FLCN on critical site of serine 62. Importantly, FLCN-S62A mutant resulted in reduced binding to AMPK and enhanced activation of AMPK through Thr172 phosphorylation [93]. FLCN also appears to be phosphorylated at Ser302 by unknown kinases downstream of mTORC1 [94]. Interestingly, it has been reported that AMPK increased the transcriptional activity of HIF in FLCN-null cells in hypoxia without affecting its stability via an unknown mechanism [69]. However, how AMPK is activated upon loss of FLCN, and how FLCN and AMPK/FNIPs interact mechanistically are not clear. Understanding how cancer cells generate energy to deal with stressful situations in FLCN and AMPK molecular signaling

may provide new metabolic strategy of therapy for BHD and/or other cancers.

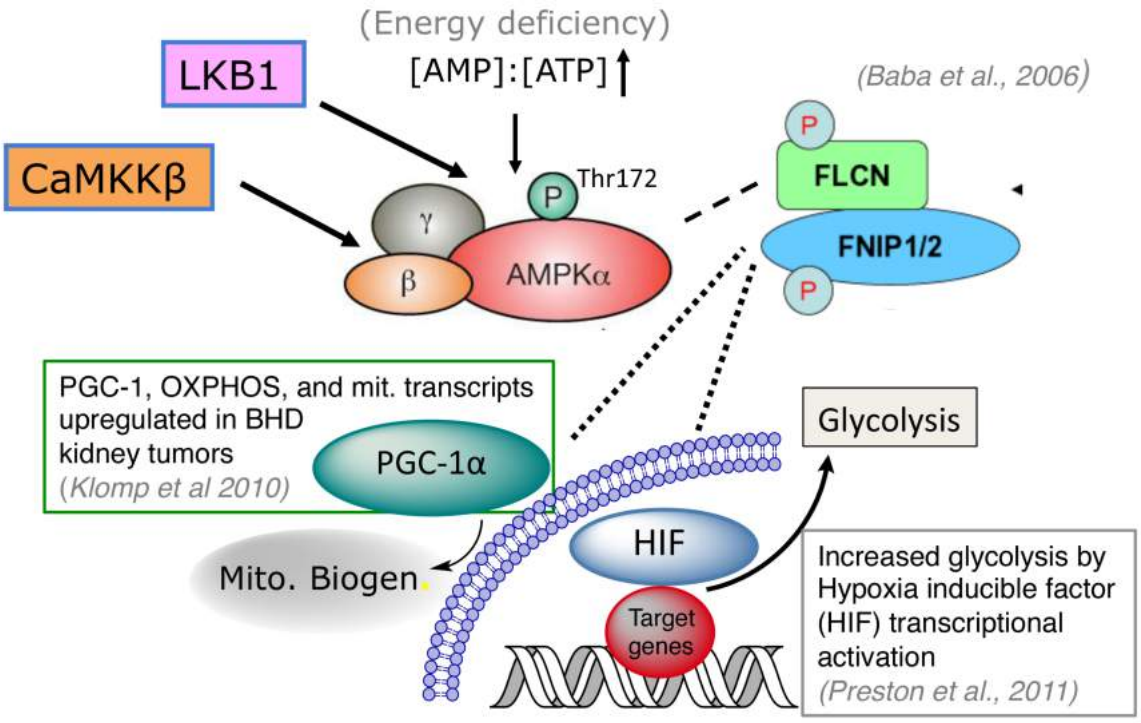

Figure 1.3 FLCN-interacting proteins and associated pathways that might contribute to renal tumorigenesis under FLCN deficiency

FLCN interacts with AMPK through interacting proteins FNIP1 and FNIP2. AMPK phosphorylates FNIP1, FNIP2 and FLCN. FLCN also has a rapamycin-sensitive phosphorylation site. FLCN has potential roles in regulation of HIF1α expression, TFE3/TFEB transcriptional activity, and PGC1α expression that drives mitochondrial biogenesis.

Abbreviations: AMPK, 5'-AMP-activated protein kinase; FLCN, folliculin; FNIP1, folliculin interacting protein 1; FNIP2, folliculin interacting protein 2; HIF1α, hypoxia inducible factor 1 alpha; PGC1α, (also known as PPARGC1A) peroxisome proliferator-activated receptor gamma coactivator 1alpha;

Adapted from [20, 95]

1.5 OVERVIEW OF THE THESIS

Birt-Hogg-Dubé (BHD) syndrome is a rare autosomal dominant hereditary disorder characterized by predisposition to develop hair follicle tumors, lung and kidney cysts, and renal cell carcinoma. This syndrome is caused by germline mutations of *Folliculin* (*Flcn*) tumor suppressor gene that encodes a 64-kDa protein named folliculin (FLCN). The clinical phenotype in BHD syndrome is likely well established recently. However, the function of tumor suppressor *Flcn* in molecular mechanism remains elusive.

AMP-activated protein kinase (AMPK) is a highly conserved serine/threonine protein kinase playing a key role in cellular and whole-body energy homeostasis. FLCN has been shown to be phosphorylated by AMPK and to interact with AMPK through FLCN-interacting proteins (FNIP1/2), suggesting an involvement of FLCN in cellular energy metabolism through the AMPK signaling pathways.

It is largely unknown how FLCN regulates AMPK and what downstream cascades of AMPK are modulated by FLCN. Thus, understanding the role of FLCN in the modulation of AMPK activity will provide insight into how *Flcn* mutation causes BHD syndrome. The study presented in this thesis therefore focuses on characterization of the FLCN-AMPK pathways in cellular energy metabolism.

Chapter 1 presents a literature review to introduce the BHD syndrome and its important clinical aspects. It discusses about FLCN and its interaction/binding proteins, especially AMPK as key gatekeeper of energy homeostasis. Also a brief overview of what is currently known about how FLCN acts as a tumor suppressor and on the molecular signaling pathways in which FLCN deficiency could drive tumorigenesis.

In Chapter 2 consists of our work highlighting that FLCN exerts tumor suppressor function by regulating metabolic reprogramming via AMPK-dependent HIF-1α signaling.

We show that loss of FLCN constitutively activates AMPK, which in turn leads to elevation of PGC-1α to mediate. Consequently, that leads to increased ROS levels that induces hypoxia-inducible factor (HIF) transcriptional activity and drives Warburg metabolic reprogramming. Therefore, we characterized a novel tumor suppressor mechanism of FLCN through uncovered a novel HIF activation mechanism through the AMPK/PGC-1α /HIF signaling pathway: Loss of FLCN favors metabolic transformation that confers a tumorigenic advantage through activation of AMPK.

In Chapter 3, we demonstrate that deletion of FLCN in mouse adipose tissues leads to a complete metabolic reprogramming of white adipocytes toward a brown-like phenotype. This metabolic switch allows these mice to exhibit a strong browning phenotype associated with increase energy expenditure and mitochondrial activity to prevent high fat diet-induced obesity by burning more lipids. Additionally, these mice have increased resistance to cold exposure associated with browning of white adipose tissue (WAT), a phenomenon known usually as adaptive thermogenesis that relies on heat production in brown adipocytes mitochondria through uncoupled respiration. We revealed that FLCN ablation leads to chronic hyperactivation of AMPK, which in turns induces and activates two key transcriptional regulators of cell metabolism, PGC-1α and ERRα. Together, the AMPK/PGC-1α/ERRα axis positively modulates the expression of nuclear-encoded mitochondrial genes to promote mitochondrial activity and lipid metabolism.

Finally, in Chapter 4, we summarize the major findings presented in Chapters 2 and 3 and discussions about significance of the research described in this thesis, and other projects we are currently working on, and then future perspectives of FLCN study will complete this chapter.

Chapter 2:

The tumor suppressor *folliculin* regulates AMPK-dependent metabolic transformation

Authors/Affiliation

Ming Yan,[1,2,6] Marie-Claude Gingras,[1,2,6] Elaine A. Dunlop,[3] Yann Nouët,[1,2] Fanny Dupuy,[1,4] Zahra Jalali,[1,2] Elite Possik,[1,2] Barry J. Coull,[5] Dmitri Kharitidi,[1,2] Anders Bondo Dydensborg,[1,2] Brandon Faubert,[1,4] Miriam Kamps,[5] Sylvie Sabourin,[1,2] Rachael S. Preston,[3] David Mark Davies,[3] Taren Roughead,[1,2] Laëtitia Chotard,[1,2] Maurice A.M. van Steensel, [5] Russell Jones,[1,4] Andrew R. Tee,[3] and Arnim Pause, [1,2]

[1]Goodman Cancer Research Center, McGill University, Montréal, Québec, Canada

[2]Department of Biochemistry, McGill University, Montréal, Québec, Canada

[3]Institute of Cancer and Genetics, Cardiff University, Cardiff, Wales, United Kingdom

[4]Department of Physiology, McGill University, Montréal, Québec, Canada

[5]Department of Dermatology, Maastricht University, Maastricht, The Netherlands

[6] These authors contributed equally to this work.

Published for this article: *J Clin Invest.* 2014 Jun:124(6):2640-2650.

2.1 Abstract

The Warburg effect is a tumorigenic metabolic adaptation process characterized by augmented aerobic glycolysis, which enhances cellular bioenergetics. In normal cells, energy homeostasis is controlled by AMPK; however, its role in cancer is not understood, as both AMPK-dependent tumor -promoting and -inhibiting functions were reported. Upon stress, energy levels are maintained by increased mitochondrial biogenesis and glycolysis, controlled by transcriptional coactivator PGC-1α and HIF, respectively. In normoxia, AMPK induces PGC-1α, but how HIF is activated is unclear. Germline mutations in the gene encoding the tumor suppressor folliculin (*Flcn*) lead to Birt-Hogg-Dubé (BHD) syndrome, which is associated with an increased cancer risk. FLCN was identified as an AMPK binding partner, and we evaluated its role with respect to AMPK-dependent energy functions. We revealed that loss of FLCN constitutively activates AMPK, resulting in PGC-1α–mediated mitochondrial biogenesis and increased ROS production. ROS induced HIF transcriptional activity and drove Warburg metabolic reprogramming, coupling AMPK-dependent mitochondrial biogenesis to HIF-dependent metabolic changes. This reprogramming stimulated cellular bioenergetics and conferred a HIF-dependent tumorigenic advantage in FLCN-negative cancer cells. Moreover, this pathway is conserved in a BHD-derived tumor. These results indicate that FLCN inhibits tumorigenesis by preventing AMPK-dependent HIF activation and the subsequent Warburg metabolic transformation.

2.2 Introduction

Kidney cancer is a metabolic disease since renal cancer genes including *VHL*, *MET*, *TSC1*, *TSC2*, *FH* and *SDH*, are involved in metabolic sensing and adaptation to fluctuations in oxygen, energy and nutrient status [96]. Intriguingly, aberrant Hypoxia Inducible Factor (HIF) driven gene-expression is a shared feature observed upon deregulation of these pathways. To maintain cellular homeostasis under energy stress, HIF mediates transcription of genes that favour glycolysis (*HK2* and *LDHA*) and energy supply (*GLUT1* and *VEGF*). HIF induction occurs via protein stabilisation of its regulatory alpha subunit and/or an increase in transcriptional activity of the HIF complex (encompassing α and β subunits). While HIF activation in response to hypoxia has been extensively described, its role in normoxia and tumorigenic metabolic adaptation are poorly defined [97, 98].

Germline mutations in the Folliculin (*Flcn*) gene lead to Birt-Hogg-Dubé (BHD) syndrome characterized by lung cysts, pneumothorax susceptibility, renal cell carcinoma (RCC), and skin tumors [99]. We recently reported that loss of the tumor suppressor FLCN leads to increased HIF transcriptional activity and a higher glycolytic rate in human kidney cancer cells, which is a recurrent characteristic of cancer metabolic adaptation referred to as the Warburg effect [69, 100]. HIF-α protein levels are regulated by oxygen-dependent prolyl-hydroxylation, sequential VHL binding and degradation of HIF-α via the proteasome [101]. Interestingly, it has been demonstrated that AMP-activated protein kinase (AMPK) increased the transcriptional activity of HIF without affecting its stability via an unknown mechanism [102]. AMPK is a heterotrimeric enzyme that monitors the energy status and maintains energy homeostasis under metabolic stress by activating catabolic processes and inhibiting anabolic processes [103]. However, the role of AMPK in metabolic transformation is still unclear as both oncogenic and tumor suppressor functions have been reported [104]. Interestingly, FLCN and its binding partner folliculin-interacting-protein (FNIP) are known interactors of AMPK [43, 105]. However, it is unknown how FLCN and AMPK interact mechanistically, how they regulate HIF transcriptional activity and metabolic adaptation in normoxia, and whether this effect is linked to tumor suppression.

Here we used untransformed cells to investigate the effect of FLCN on cellular metabolism and signalling pathways linked to AMPK. We show that loss of FLCN binding to AMPK results in AMPK activation and uncover a novel-signalling pathway that directly couples AMPK-dependent mitochondrial biogenesis to HIF-driven aerobic glycolysis through mitochondrial ROS production in physiological conditions. The concomitant induction of mitochondrial oxidative phosphorylation with aerobic glycolysis results in excess production of ATP and metabolic intermediates, a cancer adaptation mechanism also known as the Warburg effect. We reveal that this metabolic transformation is conserved in human cancer cells, renal tumors from BHD patients, and that this mechanism confers a tumorigenic advantage upon loss of FLCN.

2.3 Results

2.3.1 Loss of FLCN increases ATP levels through enhanced HIF-dependent aerobic glycolysis.

To study the cellular role of FLCN, we generated syngenic paired *Flcn*$^{+/+}$ (wild-type: WT) and *Flcn*$^{-/-}$ (knockout: KO) mouse embryonic fibroblast (MEF) lines and employed a stably rescued FLCN cell line derived from the KO MEF (Resc) (Figure 2.1A). Consistent with our earlier work, we observed that *Flcn* KO cells display a 2-fold increase in HIF activity when compared to *Flcn* WT or Resc MEFs in hypoxia using a HIF reporter assay (Figure 2.1B) [69]. Under normoxic conditions, HIF-induced target genes (*HK2*, *LDHA*, *GLUT1* and *VEGF*) expression was increased by 2-fold upon loss of FLCN (Figure 2.1C). Loss of FLCN in MEFs did not affect the levels of HIF-1α or HIF-2α protein, which we reported previously in human renal cancer cells (Figure 2.1D). Moreover, we tested whether the HIF-1α subunit drives the increased HIF target gene expression in *Flcn* KO MEFs under normoxia by using two independent shRNAs for HIF-1α, (Figure 2. 1E & F). Together with our previous results, we concluded that under both hypoxic and normoxic conditions, FLCN controls HIF transcriptional activity. However, we observed that in hypoxia, the augmented HIF-α protein levels potentiate the HIF transcriptional activity and thus intensify the difference observed between FLCN-positive and FLCN-negative cells [69].

Interestingly, *Flcn* KO MEFs exhibited an increased rate of aerobic glycolysis characterized by an augmentation of glucose uptake and lactate production, leading to an increased extracellular acidification rate (ECAR) (Figure 2.1G). Consistently, the ATP levels were increased in *Flcn* KO MEFs, compared to WT (Figure 2.1H). Stable downregulation of HIF-1α confirmed that the increased aerobic glycolysis and ATP levels observed in *Flcn* KO cells depends on HIF-1α activation (Figure 2.1F & H). Altogether, our data strongly suggest that *Flcn* deficiency enhances HIF-transcriptional activity, which drives aerobic glycolysis, increasing cellular ATP levels in normoxic conditions.

2.3.2 Increased mitochondrial biogenesis enhances ROS production and activates HIF.

In aerobic conditions, cells preferentially use oxygen to efficiently produce ATP through mitochondrial oxidative phosphorylation (OXPHOS). It was initially thought that aerobic glycolysis associated with the Warburg effect was accompanied by impaired mitochondrial activity [106]. However, recent reports have shown that most cancer cells have normal mitochondrial function and that OXPHOS is not dispensable and actively contributes to energy and biosynthetic precursor production, which constitute a tumorigenic advantage [107-109]. It has been recently reported that conditional loss of FLCN in mouse kidney and muscle resulted in increased mitochondrial function [110]. To confirm this finding in our cellular model, we acutely measured the rate of mitochondrial respiration in *Flcn* KO MEFs compared to WT and Resc cells and show that loss of FLCN significantly increases total mitochondrial respiration (Figure 2.2A). Using oligomycin, an ATP synthase inhibitor that suppresses mitochondrial ATP turnover, we determined the amount of proton leak over total mitochondrial respiration. Interestingly, we did not observe a significant difference in the percentage of proton leak to total ATP turnover (Figure 2.2A). Next, we examined the mitochondrial abundance and efficiency and observed that loss of FLCN resulted in 1.2-fold increase in mitochondrial abundance and potential using mitochondrial dyes (Figure 2.2B). These effects were reversed by FLCN re-expression in KO cells. Strikingly, the mitochondrial membrane potential per mitochondrial mass (Pot/Load) was unchanged in cells devoid of FLCN (Figure 2.2B), suggesting that the increase in mitochondrial respiration observed in *Flcn* KO MEFs is

caused by an increase in mitochondrial mass. To determine whether FLCN functions similarly in other cell lines, we measured the relative mitochondrial levels in the UOK257 kidney cancer devoid of FLCN. We confirmed the increased mitochondrial abundance upon loss of FLCN by quantitative PCR to determine the ratio of mtDNA/nDNA in UOK257 and MEF lines (Supplemental Figure 2.S1A). In agreement with these results, patients with BHD syndrome are predisposed to develop renal oncocytomas, which are tumors characterized by abundant mitochondria, suggesting extensive mitochondrial accumulation due to years of FLCN deficiency in BHD-derived tumors [111].

Since enhanced mitochondrial load is likely to increase the production of ROS, a side product of mitochondrial respiration, we quantified the relative levels of cellular ROS using the CM-H2DCFDA general oxidative stress indicator. We observed that loss of FLCN is associated with a significant 1.7-fold increase of intracellular ROS levels, which was rescued by FLCN re-expression (Figure 2.2C). Consistently, we observed a 3-fold increase of ROS levels in UOK257 cells devoid of FLCN (EV) when compared with UOK257 rescued for FLCN expression (Figure 2.S1B). ROS accumulation causes DNA and protein damage, which affects cellular functions. Therefore, we hypothesized that the increased ROS levels conferred by loss of FLCN could lead to cellular damage. We measured protein carbonylation and 8-hydroxydeoxyguanosine (8-OHdG) levels, two major oxidized forms of ROS-dependent protein and DNA damage, respectively. We did not observe a difference in the levels of protein carbonylation (Figure 2.2D) or 8-OHdG (Figure 2.2E) between WT and *Flcn* KO cells, suggesting that the increased ROS levels are not causing long-term damage in *Flcn* KO cells. Since the ROS assay was performed on live cells using a probe irreversibly oxidized upon contact with ROS, one attractive explanation would be that a higher rate of mitochondrial ROS production is measured rather than ROS steady state levels. To test this hypothesis, we incubated the cells with the CM-H2DCFDA dye in a time course experiment and measured ROS levels (Figure 2.2F). Interestingly, while we observed an increase in ROS signal over time in both *Flcn* WT and KO conditions, the fold difference between WT and KO conditions increased over time, confirming an enhanced ROS production in KO cells.

Whereas ROS were initially described as harmful to the cell, beneficial and physiological roles of ROS as signalling molecules are now widely acknowledged [112]. Interestingly, increased ROS production upon mitochondrial dysfunction is well known to

activate HIF under hypoxic conditions [113, 114]. Moreover, heightened mitochondrial ROS levels are also known to drive HIF activation in normoxia. Indeed, a recent study in *C. elegans* showed an upregulation of HIF activity in response to mitochondrial ROS production promoting longevity [115]. In addition, mitochondrial ROS-dependent HIF activation has been shown to modulate the immune response in long-lived *Mclk1*$^{+/-}$ mouse mutants [116] and HIF activation was reported to be both AMPK- and ROS-dependent in prostate cancer cells [102]. Finally, HIF activation by mitochondrial ROS caused invasive growth and angiogenesis in melanoma cells [117]. Therefore, we hypothesized that the increased production of mitochondrial ROS observed in *Flcn* deficient cells might be responsible for the HIF transcriptional activation. To test this possibility, we treated WT and *Flcn* KO MEFs with the anti-oxidant N-acetyl cysteine (NAC) and determined the effect on the transcriptional activation of HIF target genes (Figure 2.2G). In *Flcn* KO MEFs, NAC reduced mRNA expression of HIF target genes to an equivalent level to the WT MEFs treated with NAC. We also confirmed a similar effect using the HIF-reporter assay in hypoxic conditions (Supplemental Figure 2.S1C). Collectively, these data reveal that ROS enhances HIF transcriptional activation in *Flcn* KO MEFs.

2.3.3 Increased PGC-1α expression in FLCN-null cells enhances ROS production.

Mitochondrial biogenesis is largely controlled by a transcriptional network dependent on the peroxisome proliferator-activated receptor gamma coactivator 1 α (PGC-1α) [118]. It has been suggested that through mitochondrial biogenesis, PGC-1α indirectly stimulates HIF target gene expression [119]. Therefore, we quantified PGC-1 expression and observed a 3-fold increase in both the PGC-1α and PGC-1β transcripts upon loss of FLCN, which was restored by FLCN re-expression (Resc), suggesting that the increased mitochondrial biogenesis is driven by PGC-1 in FLCN null cells (Figure 2.3A). Consistently, we observed a 2-fold increase in PGC-1α protein levels by western blot (Figure 2.3B), and a corresponding increase in PGC-1α target genes (*COX7a, ATP5j, NDUFB5*) and co-activators (*TFAM, NRF1, NRF2*) (Figure 2.3C). We also observed a reduction of PGC-1α expression after FLCN reintroduction in the FLCN-deficient (EV) UOK257 kidney cell line (Supplemental Figure 2.S2). However, we could not confirm PGC-1β protein expression with commercially available antibodies. In line with this work,

it was previously reported that tumours from BHD patients harbour an induced PGC-1α transcription profile associated with a high expression of mitochondria and OXPHOS-associated genes [82]. Furthermore, PGC-1α and its target genes are consistently upregulated in 30 thyroid oncocytomas when compared to normal tissue [120]. Mitochondria-rich oncocytoma tumors, which are observed in kidneys of patients with BHD disease, might severely affect organ functionality and are also observed in other organs such as the thyroid gland, suggesting that the PGC-1α dependent mitochondrial biogenesis observed upon loss of FLCN is not restricted to BHD syndrome.

It is accepted that PGC-1α increases ROS production through its effect on mitochondrial biogenesis. However, PGC-1α simultaneously enhances cellular antioxidant defense mechanisms to neutralize the damaging effect caused by ROS, and generally PGC-1α upregulation is not associated with elevated intracellular ROS levels [121, 122]. To determine if PGC-1α upregulation was responsible for the increased production of ROS in our cell lines, we downregulated PGC-1α in *Flcn* KO MEFs (Figure 2.3D) and quantified ROS level (Figure 2.3E). In contrast with control (siNT), the knockdown of PGC-1α isoform in *Flcn* KO MEFs significantly reduced ROS levels, suggesting PGC-1α dependent ROS production (Figure 2.3E). To confirm that PGC-1α-dependent ROS production mediates HIF activation in *Flcn* KO MEF cells, we determined the levels of expression of HIF-target genes upon PGC-1α knockdown and observed a significant decrease (Figure 2.3F). Together, these data suggest that PGC-1α is upregulated upon loss of FLCN and stimulates mitochondrial biogenesis and ROS production, which drive HIF transcriptional activation.

2.3.4 AMPK activation in FLCN-deficient cells promotes PGC-1α upregulation.

FLCN has been linked to the AMP-dependent protein kinase (AMPK) signalling pathway as FLCN binds to AMPK through FNIPs [43, 69, 105]. The FLCN-AMPK interaction is controlled by the phosphorylation of FLCN on two sites (serine 62 and 302), suggesting possible regulatory roles in AMPK-dependent energy sensing and maintenance of energy homeostasis [93, 94]. Through allosteric interactions with AMP and ADP, AMPK acutely monitors adenylate charge fluctuations. Under energetic or cellular stress conditions, AMPK enzymatic function is activated by phosphorylation of its threonine 172

(Thr172) catalytic site by the upstream kinase, LKB1 [103]. Active AMPK is known to upregulate PGC-1α gene-expression and to directly phosphorylate PGC-1α [123]. The impact of FLCN loss on mitochondrial biogenesis, accompanied with high PGC-1α expression levels made us speculate that AMPK is involved in the PGC-1-ROS dependent activation of HIF. By western blot, we confirmed that loss of FLCN activates AMPK (pAMPKα) and increases AMPK target gene phosphorylation (pACC) in normoxia and in the absence of energetic stress (Figure 2.4A). To test whether AMPK activation upon *Flcn* loss is responsible for increased PGC-1α expression and activity, we downregulated FLCN in AMPKα null cells (*Ampk*$^{-/-}$) using shRNA (sh*Flcn*) or empty vector control (shEV) (Figure 2.4B). While *Flcn* knockdown resulted in the robust increase in pAMPKα and accumulation of PGC-1α protein (Figure 2.4B) and transcript (Figure 2.4C) in control cells (*Ampk*$^{+/+}$), the expression levels of PGC-1α remained unchanged in the *Ampk*$^{-/-}$ cells. Similarly, ROS production was increased in the *Ampk*$^{+/+}$ cells upon *Flcn* downregulation while ROS levels remain unchanged in the *Ampk*$^{-/-}$ cells (Figure 2.4D). Our data reveal that in the absence of FLCN, AMPK drives a sequential chain of events leading to upregulation of PGC-1α, increased mitochondrial biogenesis, ROS production and HIF activation, which stimulates aerobic glycolysis.

To further substantiate the notion that FLCN binding to AMPK prevents its activation, we rescued FLCN expression in KO MEFs with an empty vector (Flag-EV), Flag-FLCN-WT or the non-phosphorylatable Flag-FLCN-S62A mutant. This point mutation has been previously reported to reduce the affinity of FLCN to AMPK in a HEK293T over-expression system [93]. To validate this observation, we immunoprecipitated FLCN complexes containing AMPK in MEF lines described above. As expected, we observed reduced binding of the FLCN S62A mutant to AMPK and FNIP1 (Figure 2.4E). Strikingly, reduced interaction of FLCN-S62A mutant with AMPK enhanced the phosphorylation of AMPK (Figure 2.4F), suggesting that binding of FLCN to the AMPK-FNIP1 complex blocks AMPK activation. To test this notion further, we asked whether the FLCN-dependent regulation of PGC-1α expression was dependent on the association of FLCN to AMPK. Consequently, the FLCN-S62A mutant failed to restore the levels of PGC-1α protein expression (Figure 2.4F) and transcript levels (Figure 4G) to a level observed with Flag-FLCN WT. Similarly, the S62A mutant failed to repress HIF target gene activation (*HK2, GLUT1, VEGF*) (Figure 2.4G), revealing a loss of

function phenotype for the S62A mutant. Our data uncover a new FLCN function as a negative regulator of AMPK and show that loss of FLCN binding to AMPK is a critical signaling event that leads to AMPK/PGC-1α/HIF activation.

2.3.5 Loss of FLCN leads to metabolic transformation.

Our data reveal that loss of FLCN in untransformed MEFs induces metabolic reprogramming, characterized by PGC-1α-dependent mitochondrial biogenesis and HIF-driven aerobic glycolysis. However, while FLCN-deficient MEFs exhibit increased amounts of ATP, they do not acquire a proliferative advantage *in vitro* (Supplemental Figure S3) or spontaneous transformation features such as anchorage-independent growth or in vivo tumorigenic potential per se (Gingras, unpublished observations). To further characterize the metabolic profile associated with loss of FLCN, we used an approach combining GC/MS and LC/MS analyses to monitor the intracellular steady state levels of metabolites (Figure 2.5A, Supplemental Table S1). As expected, the glycolysis intermediates (Glucose, Fructose 6-phosphate/Glucose 6-Phosphate [F6P/G6P], Fructose 1, 6-bisphosphate [F1,6 bisP], Dihydroxyacetone phosphate/Glyceraldehyde 3-phosphate [DHAP/G3P], 3-Phosphoglyceric acid [3PGA]) were augmented in the *Flcn* KO MEFs. Consistently, the intermediates of the pentose phosphate pathway (Ribose 5-phosphate/Ribulose 5-phosphate [R5P/RL5P]) and the levels of serine (Ser, pSer), both known as critical intermediates for nucleotide biosynthesis, were also significantly increased in the *Flcn* KO MEFs. In agreement with the observed increase in mitochondrial number, respiration and OXPHOS, the TCA cycle metabolites were increased (citrate [Cit.], α-Ketoglutarate [α-KG], succinate [Succ.] and Fumarate [Fum.]) in *Flcn* KO MEFs. It has been reported that glycolytic cancer cells increase their consumption of glutamine and use it as a source of carbon to feed the TCA cycle and facilitate the production of biosynthetic precursors [124]. Consistently, we observed an increase in Glutamine (Gln) levels in *Flcn* KO MEFs. Surprisingly, the metabolic signature of the *Flcn* KO cells suggested a highly proliferative profile, while their proliferation rates were similar to WT MEF in cell culture (Supplemental Figure S3).

Next, we defined the profile of glucose and glutamine consumption by performing mass isotopomer labeling experiments in cells pulsed with [^{13}C]-labeled glucose (Figure

5B, Supplemental Table S2) or glutamine (Figure 2.5C, Supplemental Table S2) and examined the amount of ^{13}C contribution of these carbon fuels to metabolite pools. Consistent with the metabolic signature, we observed an increased accumulation of glycolytic intermediates derived from the labelled glucose, in the *Flcn* KO MEFs suggesting an increased glycolytic rate. Indeed, the total abundances of pyruvate, lactate and alanine derived from the labelled glucose were increased by 1.5 to 2 fold in *Flcn* null cells, as a characteristic feature of the Warburg effect. Our data further reveals a significant amount of [^{13}C]-Citrate derived from the labelled glucose, which was not increased in *Flcn* KO MEFs, while the other TCA intermediates are mainly unlabelled (Gingras, unpublished observations). These results might be explained by the utilization of citrate for the generation of lipid precursors and membrane synthesis, which would imply that a different source of carbon might fuel the TCA cycle. Consistent with this notion, we observed a significant level of [^{13}C]-glutamine uptake in MEFs, which was drastically increased in *Flcn* KO MEFs compared to wild-type (Figure 2.5C). However, this uptake was not associated with a higher TCA cycle utilization of glutamine, since labelled fumarate (Figure 2.5C), α-ketoglutarate and succinate (Gingras, unpublished observations) were similar in WT and *Flcn* KO MEFs (Figure 2.5C). Importantly, the level of m+5 citrate (five carbons labelled), which could only be derived from reductive carboxylation of the labelled glutamine, was significantly increased in *Flcn* KO MEFs compared to wild type. Conversely, the m+4 citrate derived from the classical TCA cycle reaction was decreased in *Flcn* KO MEFs (Figure 2.5C). This characteristic is frequent in glycolytic cancer cells, which sometime decrease their glucose-derived replenishment of the TCA cycle that must rely on alternative source of metabolites such as glutamine [125, 126]. Strikingly, it has been recently reported that HIF is necessary and sufficient to induce reductive carboxylation of glutamine in renal cell carcinoma to maintain lipogenesis and cell growth [127]. Our findings reveal that the increased uptake of glucose drives the glycolytic pathway to favour the generation of additional ATP, nucleotide precursors through the pentose phosphate and serine pathway and enhanced lactate and alanine production. While the glutamine uptake is significantly increased upon loss of FLCN, the glutamine flux into the TCA cycle is not enhanced. Rather, glutamine uptake might serve to produce citrate and lipids through glutamine reductive carboxylation.

Our data strongly suggest that glucose is the major source of energy in *Flcn* KO MEFs and that glutamine might be an alternative carbon source used for lipogenesis. Therefore, we investigated the dependency of *Flcn* KO MEFs to both sources of energy by evaluating their ability to survive under either glucose or glutamine deprivation. Under low glucose concentration (100 μM), *Flcn* KO MEFs exhibited a diminution of cell survival compared to wild-type MEFs (Figure 5D), while complete glutamine withdrawal lead to an increase in survival in *Flcn* KO MEFs compared to WT MEFs (Figure 2.5E). Collectively, our data reveal that FLCN deficient cells are "metabolically transformed" to favor aerobic glycolysis and depend on glucose to survive.

2.3.6 Loss of FLCN-mediated metabolic transformation confers tumorigenic advantage

AMPK has been proposed to be a contextual oncogene that may confer a survival advantage under selection pressure, suggesting an involvement in tumor progression rather than in tumor initiation [104]. To determine if the metabolic transformation induced upon loss of FLCN would promote a tumorigenic advantage in an established cancer cell line, we used the human follicular thyroid cancer cell line FTC-133 which are naturally deficient for FLCN expression that we stably rescued with an empty vector (EV) or FLCN expression vector (Resc) (Figure 2.6A) [128, 129]. In agreement with our previous results, FTC-133 control cells (EV) exhibited an increase in AMPK activation (Figure 2.6A); PGC-1 α levels (Figure 2.6A and 6E), mitochondrial biogenesis (Figure 2.6B and 6C) and ROS production (Figure 2.6D) compared to FLCN rescued FTC-133 cells. Moreover, the FTC-133 control cells displayed transcriptional upregulation of HIF target genes (Figure 2.6E) in absence of HIF-1α stabilization (Figure 2.6A). Consistently, we observed an increase in aerobic glycolysis (glucose uptake) and ATP levels in FTC-133 control cells (shScram), which was inhibited by FLCN re-expression (Resc) or HIF downregulation (shHIF-1α) (Figure 6F and Supplemental Figure 4A). Strikingly, these data suggest that the AMPK-PGC-1α-ROS-HIF identified in FLCN-null MEFs and UOK257 is conserved in the human FTC-133 cancer cell line. Similar to what we observed in *Flcn* KO MEFs, the metabolic advantage conferred by loss of FLCN did not lead to a proliferative advantage in FTC-133 cells, as the proliferation rate and cell size were comparable

between FTC-133 control and rescued cells (Gingras, unpublished observations). However, we observed a significant increase in the number of soft agar colonies in FTC-133 control cells (shScram) when compared to rescued cells (Figure 2.6G, Supplemental Figure S4B). Moreover, downregulation of HIF-1α completely abolished the increased colony numbers observed in control cells, which were reduced to a similar level observed in the rescued cells (Figure 2.6G, Supplemental Figure S4B). In agreement with these data, it has been reported that while FLCN reintroduction in FLCN-deficient UOK257 cells does not affect cell growth, it significantly decreased the anchorage independent and in vivo tumorigenic potential [130]. Using UOK257 cells, we confirmed a similar decrease in anchorage independent cell growth upon HIF-1α downregulation (Supplemental Figures 4C and 4D). Strikingly, FLCN deficiency in FTC-133 cells (shScram) was associated with an increased tumor volume and growth rate when compared to FLCN rescued cells or HIF-1α downregulated cell lines (shHIF-1α) (Figure 2.6H, Supplemental Figure S4E). To test the relevancy of our finding for human BHD disease, we performed immunohistochemistry staining on matching renal tumors and adjacent normal kidney tissues from a BHD patient. We observed increased HIF-1 nuclear translocation, associated with an increase in mitochondria number (MTC02), and HIF target gene expression (BNIP3, GLUT1, VEGF-A) (Figure 2.6I). Altogether, our data demonstrate that loss of FLCN induces an AMPK-HIF-dependent metabolic reprogramming resulting in an energetic advantage, which favors tumor progression in vivo.

2.4 Discussion

In accordance with our results, it was recently shown that upregulation of PGC-1α expression resulted in an increase of mitochondrial biogenesis and ATP production in a muscle-specific *Flcn* knockout mouse model [110]. Interestingly, all features observed in our FLCN-deficient cells have been independently linked with cancer promoting metabolic adaptations. Indeed, AMPK activation [104, 131-133], PGC-1 induction and mitochondrial biogenesis [134], increased ROS production [135] and HIF activation [136] have been described as steps leading to cellular metabolic reprogramming that favour tumor development in different cellular systems. Interestingly, while some AMPK-dependent signalling pathways inducing HIF have been reported, the exact mechanism

was still unclear [104]. Our work identifies an additional mechanism for AMPK to activate HIF and couples this activation to an AMPK downstream target: PGC-1α.

While HIF activation has been associated with tumor development in mammals, it leads to extension of lifespan in nematodes. Indeed, a loss of function mutation of the VHL tumor suppressor gene in *C. elegans* promotes HIF-α-dependent increase in life span [137]. Interestingly, promotion of *C. elegans* longevity upon transient AMPK-dependent increased ROS or upon ROS-mediated HIF-1 activation has been independently reported [115, 138, 139]. Together with these studies, our results suggest the existence of an AMPK driven pathway activating HIF-mediated metabolic adaptation through ROS, which appears conserved in lower organisms.

Classically, ROS is known to oxidize and inhibit the hydroxylases responsible for HIF degradation, leading to HIF stabilization and activation [136]. However, we reveal that ROS production can drive HIF transcriptional activation without affecting the protein levels of HIF-α. In accordance with our data, it has been shown in prostate cancer cells that H_2O_2 activates HIF, beyond what would be solely expected through increased HIF-1α stability (for example compared to MG132 treatment) [102]. Indeed, the use of a reporter system measuring *trans*-activation of HIF revealed that ROS but not MG132 stimulates HIF activity. Moreover, AMPK inhibition blocked this activation, suggesting that ROS could stimulate HIF-1 *trans*-activation via AMPK, which is in addition to any effect on HIF stabilization. In addition to the various transcriptional cofactors that might influence HIF activity, several HIF posttranslational modifications such as phosphorylation, S-nitrosylation and sumoylation, have been reported as potent modulators of HIF transcriptional activity [140]. Moreover, the MgcRacGAP cytoskeleton regulator has been recently identified as a novel inhibitor of HIF dimerization, affecting HIF transcriptional activity [141]. Further investigations will be required to decipher this mechanism, which is not within the scope of this study.

Since increased ROS and HIF activation have been independently shown to promote tumorigenesis, it would be worthwhile to further determine if this signalling connection from ROS to HIF is relevant to other types of cancers. Interestingly, it was recently shown that FLCN expression negatively correlates with PGC-1α activation in numerous tumors such as breast, cervix, colon, kidney, lung, lymph, ovary, pancreas, prostate, stomach,

thyroid, and vulva [82]. Specifically, the PGC-1α gene set and other OXPHOS gene sets correlated negatively with FLCN expression across all tumor types examined. Of interest, we also observed enhancement of PGC-1α expression, ROS production and HIF activation in a follicular thyroid carcinoma cell line that innately lacked FLCN and was not derived from a BHD patient. Our analogous observations in this cell line importantly confirm that our research findings presented in this manuscript have wider implications to other cancers, rather than being restricted to BHD patient tumors alone. Together, our study suggests that loss of FLCN expression leads to activation of the AMPK/PGC-1α/OXPHOS/HIF signaling axis, which is an important driver of sporadic tumors in multiple organs.

AMPK has been shown to drive anti-tumorigenic functions, revealing an AMPK metabolic tumor suppressor function [142, 143]. This notion is compatible with the fact that AMPK activates catabolic and inhibits anabolic processes, an unfavourable context for cell proliferation [104]. In contrast, several recent reports have also shown that gain of function of AMPK and PGC-1α are drivers of tumorigenesis via maintenance of metabolic homeostasis, promotion of metastasis and support of cancer cell survival [131-133, 144-148]. This concept is supported by the fact that loss of AMPK or its upstream activator LKB1 is associated with apoptosis under bioenergetically stressful conditions [144]. Based on these reports, it was proposed that AMPK tumor suppressor function might prevent tumor initiation through its ability to restrict cell proliferation, whereas AMPK activation permits metabolic adaptation and survival under energetic stress conditions and is beneficial for tumor progression and metastasis [104]. In agreement with this concept, the central regulatory role of LKB1 in pro-growth metabolism and tumor initiation has been recently reported [149]. Results presented here are consistent with an AMPK oncogenic function and uncover a signaling pathway that links AMPK activity to HIF via PGC-1α upregulation, mitochondrial biogenesis and ROS generation. Our study also reveals how loss of FLCN mediates aerobic glycolysis to drive a metabolic advantage in cancer cells when oxygen and nutrients are plentiful. Our findings have wider implications for cancers and human disease where HIF activity is known to be induced and shed further light on the tumor suppressor mechanism of FLCN.

2.5 Methods

See supplemental experimental procedures section for details regarding plasmids, primers, antibodies and reagents, for description of the cell lines and culture methods and for extended procedures used for RNA extraction, quantitative PCR (qPCR), real time PCR (qRT-PCR), protein extraction, immunoprecipitation, western blotting, immunohistochemistry, proliferation, soft agar and xenografts assays.

HIF Luciferase Reporter Assays

MEFs were transfected with the firefly luciferase HIF activity reporter pGL2-TK-HRE plasmid and the assays were carried out under hypoxia (1% oxygen) as described [150]. Briefly, 20 μl of cleared lysed cell supernatant was injected with 50 μl luciferase assay reagent II (Promega) into a luminometer. Luciferase levels were measured at 2 and 10 sec interval after initial injection. Results were normalized to TK-renilla reporter control. When indicated, the anti-oxidant, N-acetyl cysteine (NAC), was added to the cells for 16 h prior to transfection and maintained post-transfection.

Glucose uptake and lactate production assays

Glucose uptake were determined using the 2-(*N*-(7-Nitrobenz-2-oxa-1,3-diazol-4-yl) Amino)-2-Deoxyglucose (2-NBDG) fluorescent glucose analog (Invitrogen). Briefly, cells were incubated with 100 nM 2-NBDG for 1h and the mean fluorescent intensity was detected using FACSCalibur flow cytometer (BD Biosciences). Lactate production was determined in media collected from 48h seeded cells using the L-lactate assay kit (Eton Bioscience). Absorbance measurements were read at 490nm using a Spectramax spectrophotometer microplate reader (Molecular Devices) and data were normalized to the cell number.

Seahorse XF24 Extracellular Flux analysis

The extracellular acidification rate (ECAR) was determined using the XF24 Extracellular Flux Analyzer (Seahorse Bioscience). Briefly, 40,000 cells per well were seeded in 625 μl non-buffered DMEM containing 25mM glucose, 2mM glutamine and 10% FBS and were incubated in a CO_2-free incubator at 37°C for 1h. XF assays consisted

of sequential mix (3min), pause (3min) and measurement (5min) cycles and assays were performed three times in triplicates.

Protein and DNA damage assays

The extent of oxidative protein damage was measured using the OxyBlot Protein oxidation Detection Kit (Millipore) using 20 μg of total protein extract. Carbonylated proteins were detected by western blot and α-tubulin was used as loading control. The amount of DNA oxidative damage (8-OHdG) were quantified on 16 μg of purified genomic DNA using the OxiSelect™ Oxidative DNA Damage ELISA Kit (Cell Biolabs, Inc).

Respiration Assay

Respiration assays were performed as described [147, 151]. Briefly, $1x10^6$ cells were resuspended in PBS supplemented with 25 mM glucose, 1 mM pyruvate and 2% (w/v) BSA. Oxygen consumption was measured at 37°C using a Clark-type oxygen electrode. The ATP synthase inhibitor oligomycin (2.5 μg/10^6 cells) was used to determine the amount of proton leak over ATP turnover.

ROS, mitochondrial load and potential

Cellular ROS levels were determined using the general oxidative stress indicator CM-H2DCFDA (Invitrogen) and the mitochondrial mass and potential were determined using respectively the Mito-Tracker Green FM and Mito-Tracker Red CMXRos (Invitrogen). Briefly, subconfluent adherent cells were incubated for 30 min at 37°C or in time-course for 10, 30 or 60 minutes in serum-free media supplemented with the dyes. Then cells were incubated 10 min in complete DMEM, resuspended in 500 μL of PBS supplemented with 2% (v/v) FBS. Fluorescence intensity was detected using FACSCalibur flow cytometer (BD Biosciences). Cells not incubated with the dye or pretreated with 100 uM H_2O_2 were used as negative and ROS positive controls, respectively.

ATP quantification

ATP levels were determined by luminescence using CellTiter-Glo Luminescent Cell Viability Assay (Promega). Briefly, 5,000 subconfluent cells were loaded in 96-well

plate in triplicates. After addition of equal volume of CellTiter-Glo reagent, relative luminescence units (RLU) were measured using FLUOstar Omega microplate reader (BMG LabTech) and results were expressed as fold changes.

Metabolism

Metabolites from subconfluent cells cultured for 48h were extracted and quantified by GC/MS (TCA intermediates) or by LC/MS (glycolytic and pentose phosphate intermediates and amino acids) as described [131, 143]. Metabolites levels were normalized to the cell number and data are expressed as fold of the control wild-type cells. For the mass isotopomer experiment, 5 x 10^5 cells were cultured for 48h and pulsed using uniformly labelled ^{13}C-glucose (30 min) or ^{13}C-glutamine (1 h). Metabolites were extracted and GC/MS analyses were performed as described [131].

Statistics

Statistical analyses were performed using paired Student's *t* tests using Excel software (Microsoft). A *p* value less than 0,05 was considered significant. Results are expressed as fold difference relative to the controls conditions and are shown as mean ± SD or SEM of values obtained in at least three independent experiments.

Study approval

Maintenance and experimental manipulation of animals were performed according to the guidelines and regulations of the McGill University Research and Ethic Animal Committee and the Canadian Council on animal Care.

Acknowledgements:

We thank Dr. N. Sonenberg (McGill University, Montreal, Canada), Dr. M.C. Simon (University of Pennsylvania, Philadelphia, USA), Dr. G. Melillo (NCI, Frederick, MD, USA) and Dr. L. Schmidt (NCI, Bethesda, MD, USA) and Dr. E.R. Maher (University of Birmingham, Birmingham, UK) for materials. We are indebted to D. Avizonis, G. Bridon from the McGill University Goodman Cancer Research Center Metabolic Core Facility for their technical support and expertise. We thank Dr. J. St-Pierre and Dr. I. Topisirovic for critical reading of this manuscript and V. Chénard for technical

support. M.Y. and B.F. are supported by Canadian Institutes of Health Research (CIHR) Doctoral Research Award. This project is funded by the Association for International Cancer Research Career Development Fellowship (A.T.: 06-914/915), the Myrovlytis Trust (A.T., E.D., A.P.), the Terry Fox Foundation/CIHR team grant on Oncometabolism (A.P., R.J.: 116128, Metabolic Core Facility), the Dutch Cancer Society (M.V.S.: KWF U2009-4352), the Annadal Foundation and GROW (M.V.S, B.J.C). A.P. is a recipient of the Canada Research Chair in Molecular Oncology.

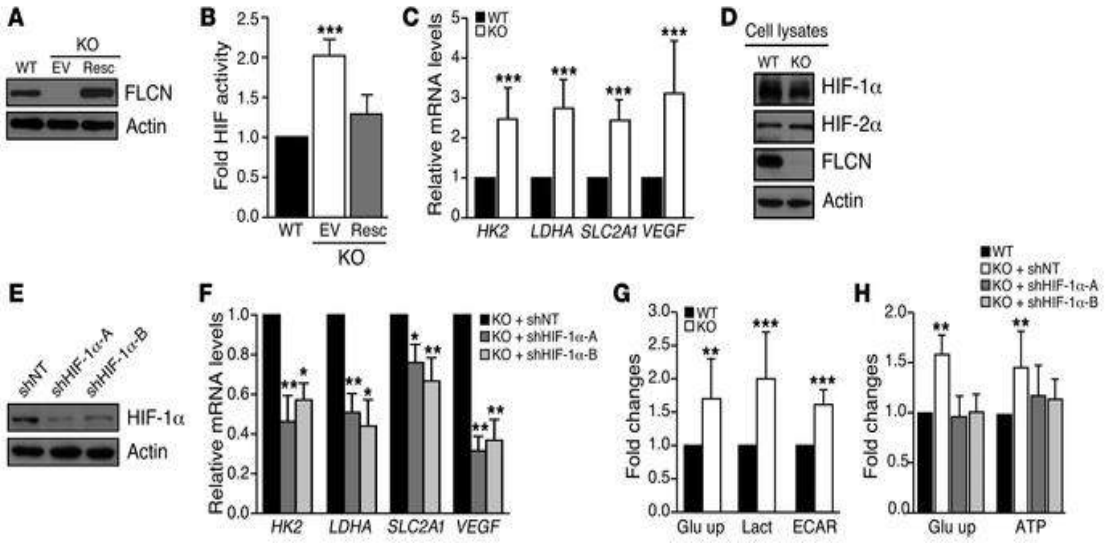

Figure 2.1

Loss of FLCN stimulates HIF-dependent glycolysis and ATP production.

(A, D, and E) Western blot analysis of FLCN, HIF-1α, and HIF-2α expression levels in the indicated MEF cell lines. Actin was used as loading control. Results are representative of 3 independent experiments. (B) Fold HIF activity assessed under hypoxic conditions using HIF reporter assay. (C and F) Relative mRNA expression of HIF target genes determined by qRT-PCR (C) in the indicated MEFs or (F) in KO MEFs downregulated (shHIF-1α cell lines) or not (shNT) for HIF-1α. (G) Fold change in glucose uptake (Glu up), lactate production (Lact), and extracellular acidification rate (ECAR) in the indicated MEFs. (H) Glucose uptake and ATP levels measured in the indicated MEF cell lines. Data in B, C, and F–H represent the mean ± SD of 4 independent experiments performed in triplicate. *P<0.05**P<0.01,***P<0.001.

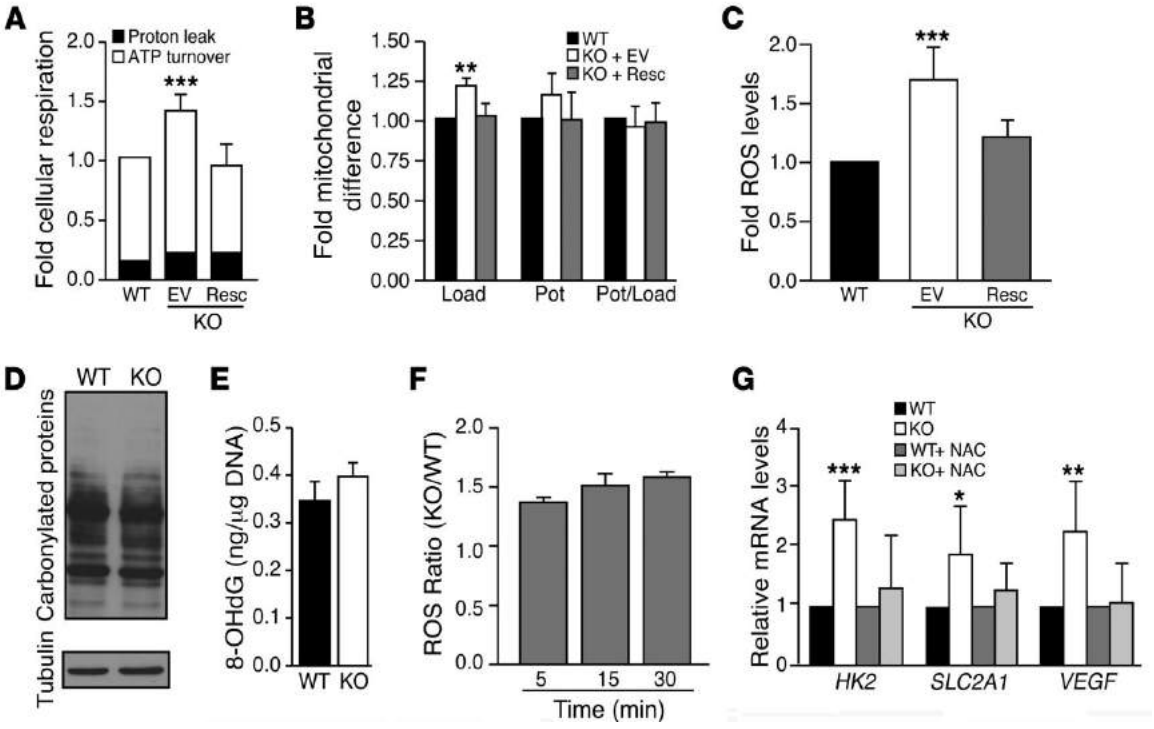

Figure 2.2 Enhancement of mitochondrial biogenesis upon loss of FLCN activates HIF in MEFs.

(A) Fold changes in total mitochondrial respiration, divided in ATP turnover and proton leak, determined following inhibition of ATP synthase by oligomycin treatment. (B) Fold changes in mitochondrial load and potential determined using MitoTracker Green FM and MitoTracker Red CMXROS, respectively. Pot, mitochondrial membrane potential; Load, mitochondrial mass. (C and F) Fold ROS levels assessed using the general oxidative stress indicator CM-H2DCFDA incubated with cells for (C) 30 minutes or (F) the indicated time points in a time course experiment. Data are expressed as fold ROS levels normalized to (C) WT or as (F) the KO/WT ROS ratio. (D) Extent of ROS-dependent protein and (E) DNA damage quantified using the OxyBlot Protein Oxidative Detection Kit and the OxiSelect Oxidative DNA Damage Kit, respectively. Data are representative of 3 independent experiments. (G) Relative mRNA expression of HIF target genes in MEFs treated with 10 mM of the antioxidant NAC for 24 hours. Data in A–C and E–G represent the mean ± SD of 4 independent experiments performed in triplicate. *$P < 0.05$, **$P < 0.01$, ***$P < 0.001$.

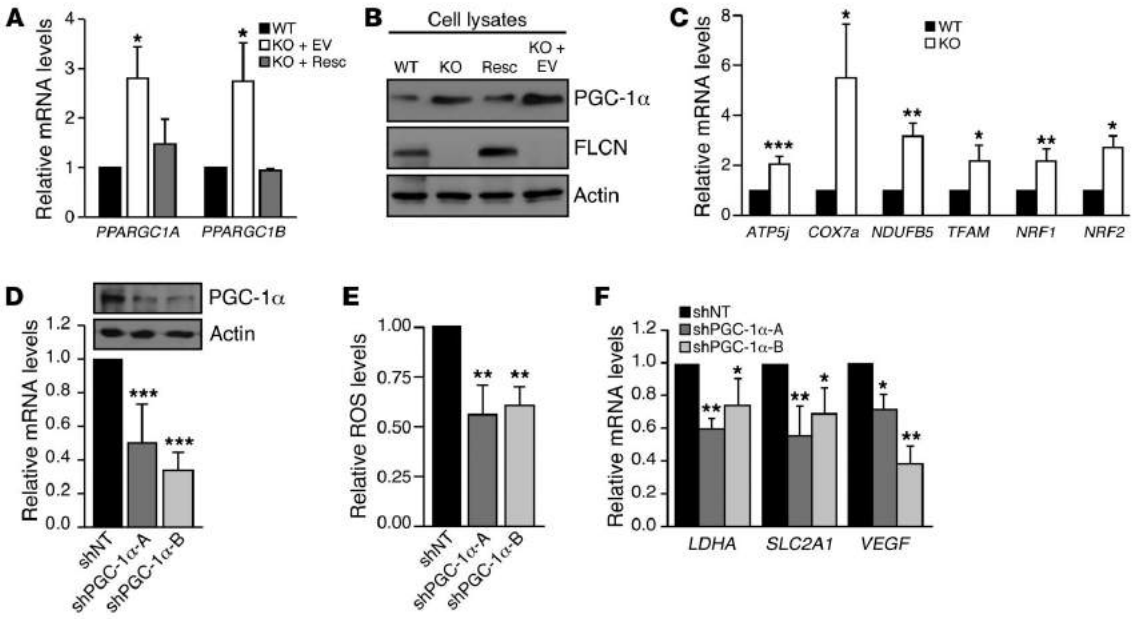

Figure 2.3 ROS-mediated HIF activation depends on PGC-1α upregulation in FLCN-null cells.

(A) PPARGC1A and PPARGC1B relative mRNA expression measured by qRT-PCR in the indicated MEFs. (B) Western blot analysis of the PGC-1α and FLCN expression levels. Actin was blotted as loading control. Results are representative of 3 independent experiments. (C) Relative mRNA expression of PGC-1α target genes and coactivators determined by qRT-PCR. (D) PGC-1α protein and relative mRNA expression levels in KO MEFs downregulated using shRNA for PGC-1α (shPGC-1α-A and -B) or control (shNT), as measured by Western blot and qRT-PCR. (E) Relative ROS levels and (F) HIF target gene expression determined in the indicated cell lines. Data represent the (A and D–F) mean ± SD or (C) mean ± SEM of 4 independent experiments performed in triplicate. *P < 0.05, **P < 0.01, ***P < 0.001.

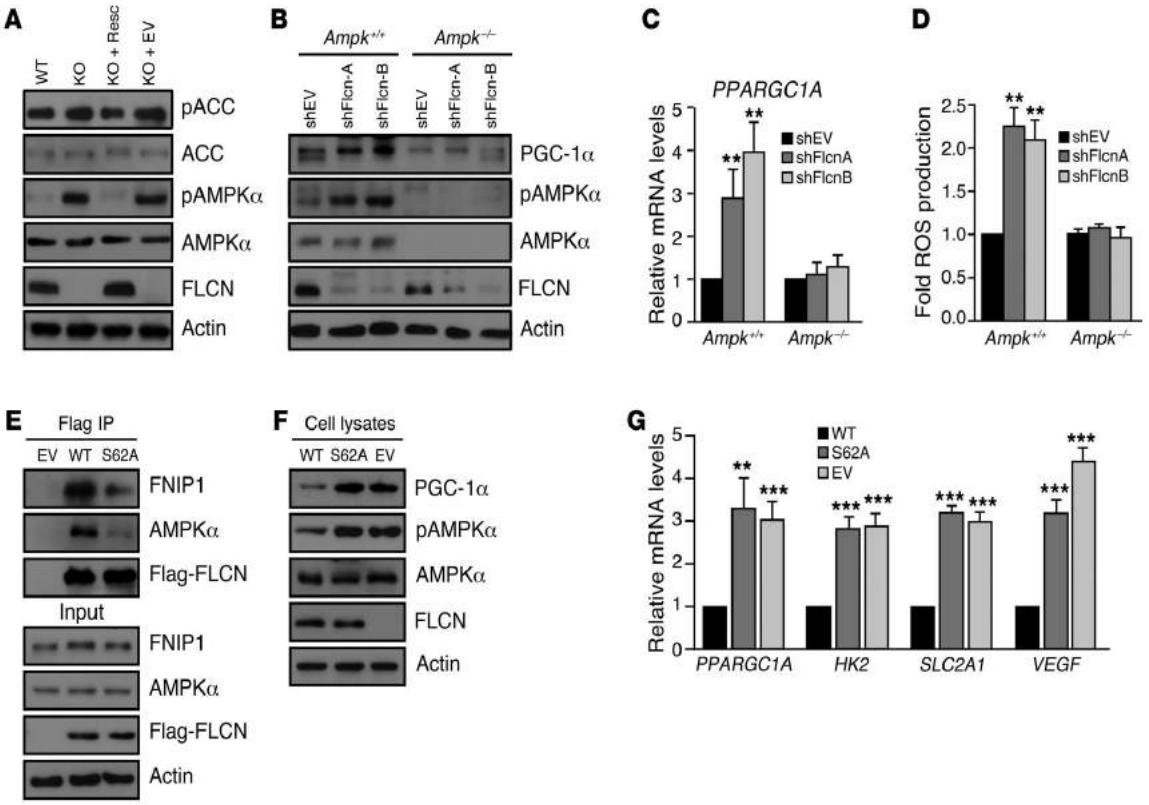

Figure 2.4 AMPK activation upon loss of FLCN binding drives the PGC-1α-ROS–mediated HIF induction.

(A) Western blot analysis of AMPK expression (AMPKα) and activation (pT172 AMPKα [pAMPKα]) levels and acetyl-CoA carboxylase (ACC) expression and activation (pS79 ACC [pACC]) levels in the indicated MEFs. Actin was used as loading control. (B) Western blot analysis of Ampk–/– or Ampk+/+ MEFs downregulated (shFlcn) for FLCN or not (shEV). Actin was used as loading control. (C) Relative PPARGC1A mRNA expression and (D) ROS production levels in the indicated MEFs. (E–G) Flcn KO MEFs were rescued with FLCN WT, FLCN S62A mutant (S62A), or EV constructs, and (E) the extent of FLCN binding to AMPKα and FNIP1 was determined by coimmunoprecipitation. The effect of the S62A mutation on (F and G) PGC-1α, (G) HIF target gene expression, and (F) AMPK activation (pT172 AMPKα) was assayed by (F) Western blot and (G) qRT-PCR. Results in A, B, E, and F are representative of 3 independent experiments and data in C, D, and G represent the mean ± SD of 4 independent experiments performed in triplicate. **P < 0.01, ***P < 0.001.

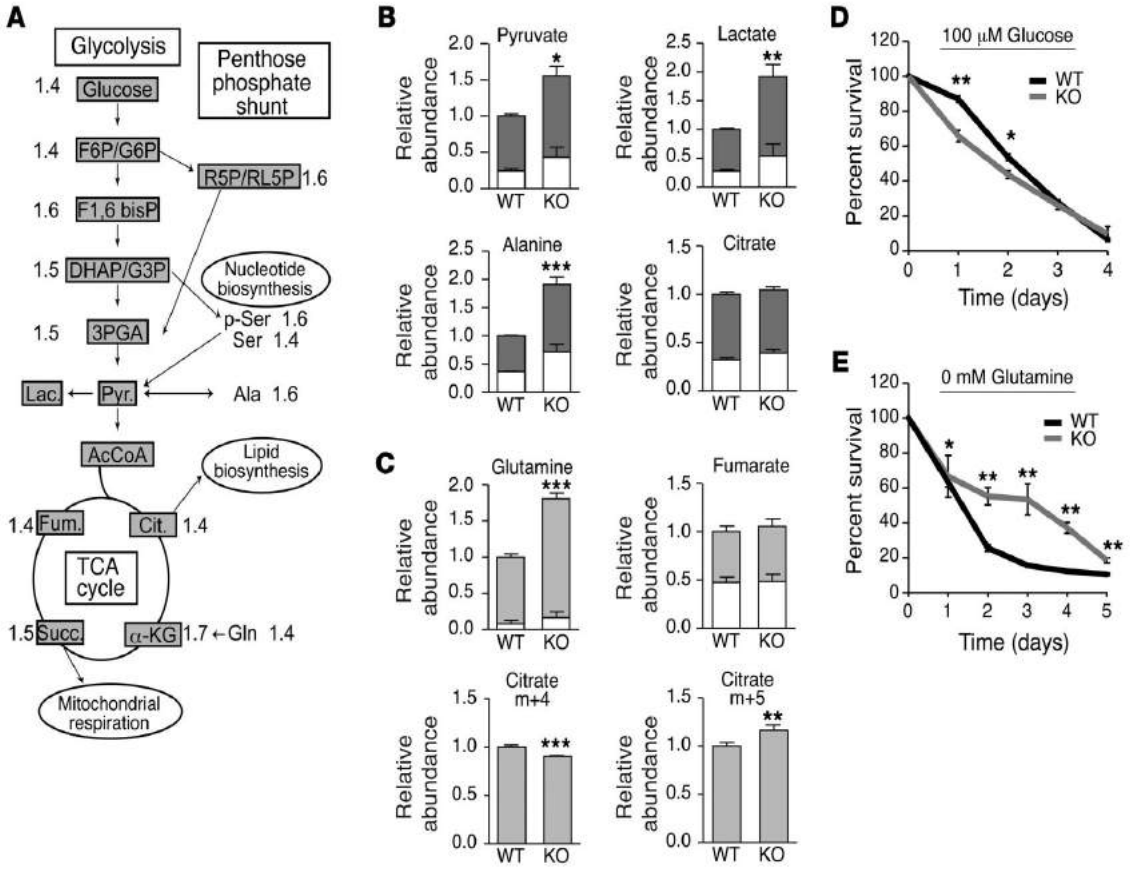

Figure 2.5 FLCN-null cell survival depends on glucose-derived biosynthetic precursor production.

(A) Metabolic signature of *Flcn* KO cells determined by GC/MS and LC/MS. Data are expressed as fold of the WT MEF metabolite quantification and are indicated in the schematic representation of the metabolic pathways. (B and C) Mass isotopomer labeling of MEFs pulsed with (B) 13C glucose or (C) 13C glutamine. Relative incorporation of (B) 13C glucose (dark gray) and (C) 13C glutamine (light gray) to total metabolite pool are indicated, and the metabolite abundance relative to WT condition was measured. (D and E) Percentage cell survival under (D) glucose and (E) glutamine starvation relative to cell number at day 0. Data represent the mean ± SD of (A) 8 or (B–E) 3 independent experiments. *P < 0.05, **P < 0.01, ***P < 0.001.

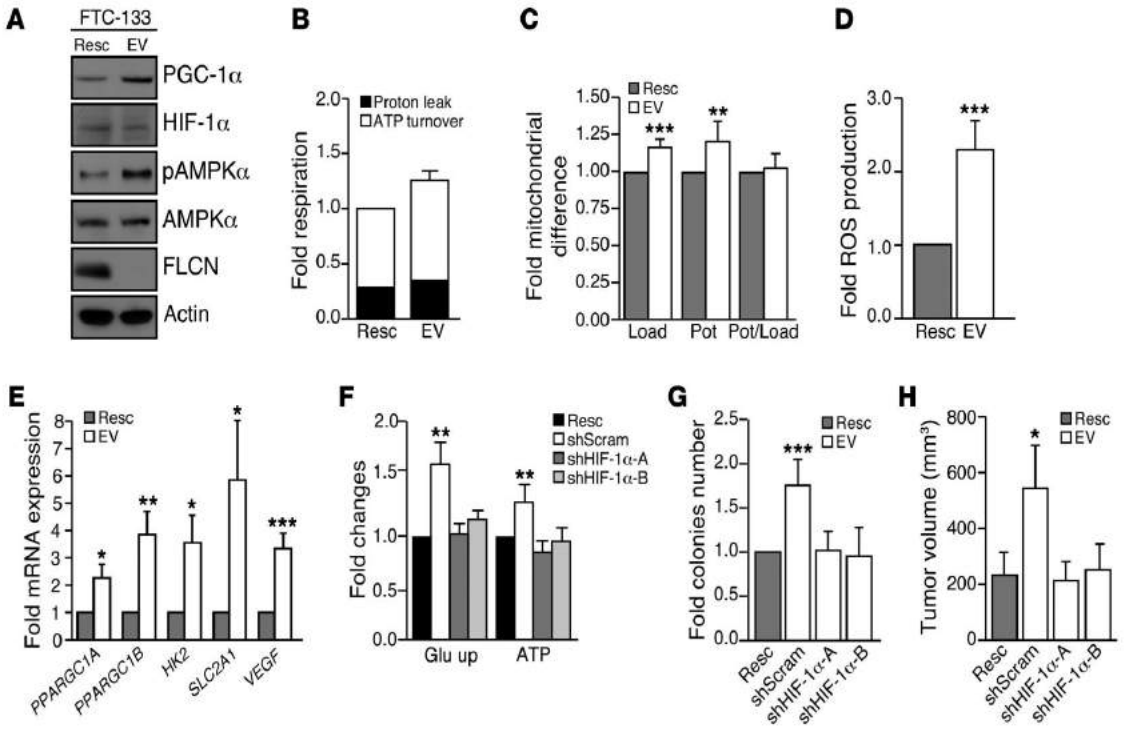

Figure 2.6 HIF-dependent metabolic advantage drives tumorigenesis in FLCN-deficient cancer cells.

(A) Western blot analysis of the AMPK expression (AMPKα) and activation (pT172 AMPKα) and PGC1-α and HIF-1α expression levels in FTC-133 cells deficient (EV) or rescued (Resc) for FLCN expression. (B–D) Fold (B) mitochondrial respiration, (C) load and potential, and (D) ROS production in FTC-133 cells. (E) Fold mRNA levels of the indicated genes relative to FTC-133 cells rescued for FLCN expression. (F) Glycolysis (glucose uptake) and ATP levels quantified in the FLCN-null (EV) cells downregulated (shHIF-1α) or not (shScram) for HIF-1α expression and compared with FTC-133 cells rescued for FLCN expression (Resc). (G) Fold change in soft agar colony number and (H) xenograft tumor volume 42 days after subcutaneous tumor cell injection in nude mice using the indicated FTC-133 cell lines. Data represent the mean ± SD of (A–G) 4 independent experiments or (H) 5 tumors per group. *P < 0.05, **P < 0.01, ***P < 0.001.

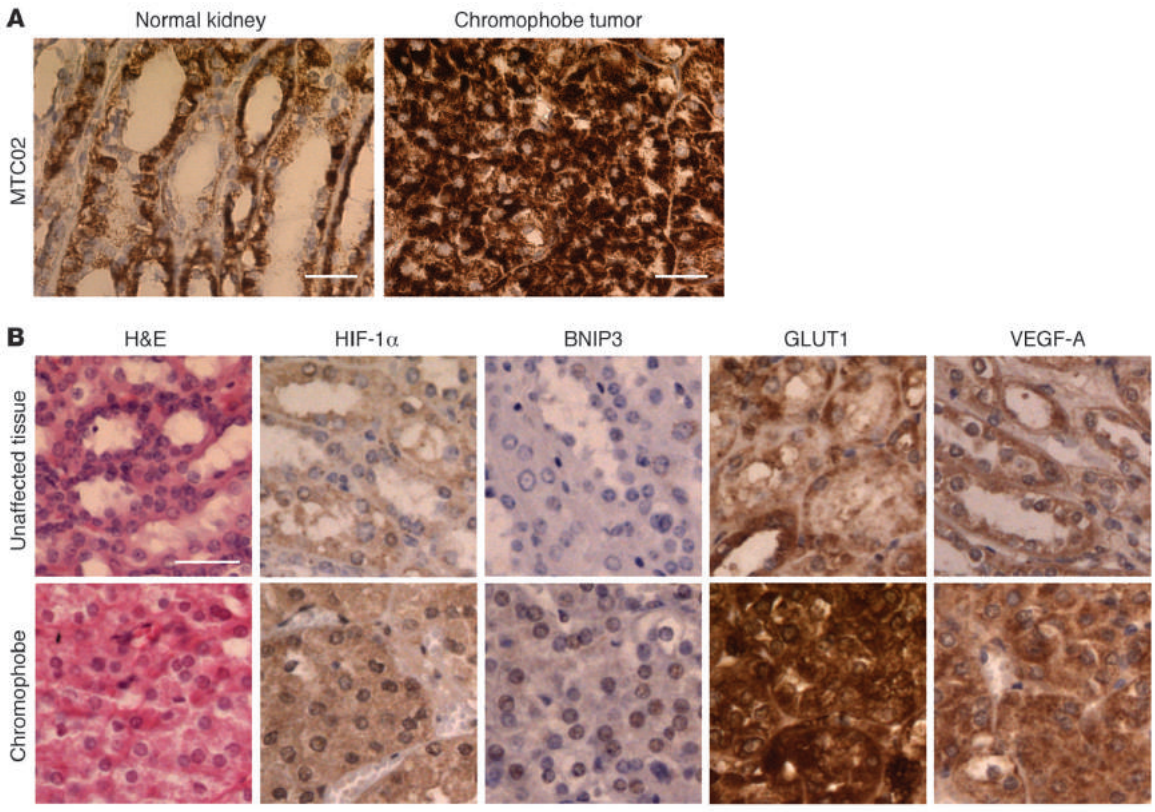

Figure 2.7 Increased mitochondrial content and HIF target gene expression in a BHD tumor

(A and B) Representative images of immunohistochemistry staining performed on a BHD kidney chromophobe tumor and (A) normal kidney or (B) adjacent unaffected tissues. Scale bar: 50 μm (A); 100 μm (B).

2.7 SUPPLEMENTAL INFORMATION

The tumor suppressor folliculin regulates AMPK-dependent metabolic transformation

Ming Yan, Marie-Claude Gingras, Elaine A. Dunlop, Yann Nouët, Fanny Dupuy, Zahra Jalali, Elite Possik, Barry J. Coull, Dmitri Kharitidi, Anders Bondo Dydensborg, Brandon Faubert, Miriam Kamps, Sylvie Sabourin, Rachael S. Preston, David Mark Davies, Taren Roughead, Laëtitia Chotard, Maurice A.M. van Steensel, Russell Jones, Andrew R. Tee, and Arnim Pause.

2.7.1 Supplemental methods

2.7.1.1 Plasmids, Antibodies and biochemical reagents

The SV40LT-pMSCV and Cre-Neo-pMSCV vectors were kind gifts from Dr. N. Sonenberg (McGill University, Montreal, Canada) and the pGL2-TK-HRE plasmid was gifted by Dr. G. Melillo (NCI, Frederick, MD, USA). The mouse-*Flcn*-pMSCV vector was a gift from Dr. M.C. Simon (University of Pennsylvania, Philadelphia, USA) and was subcloned into a 2XFlag-MigR1 retroviral vector. The 2XFlag was first inserted into MigR1 vector by restriction using BglI and EcoR1 sites and then the mouse *Flcn* cDNA was subcloned into EcoR1 site. The mutation of FLCN serine 62 to alanine (S62A) was generated with the Quick Change Site-Directed Mutagenesis kit (Stratagene) according to the manufacturer's instructions, using the *Flcn*-pMSCV construct as template and modified S62A forward and reverse primers (sequence are detailed in Supplemental Table S3). The human-*Flcn* cDNA was obtained from Dr. L.S. Schmidt (NCI, Bethesda, MD, USA) and was subcloned into a 2xFlag-pcDNA3 vector [152]. The anti-mouse FLCN polyclonal antibody was generated by the McGill animal resource center services through injecting purified GST-FLCN recombinant protein in rabbits. The β-actin (AC74; Sigma-Aldrich), HIF-1α (Cayman Chemical Company), HIF-2α (Abcam), Flag (M2; Sigma-Aldrich), PGC-1α (4C1.3; Calbiochem), tubulin (T9026; Sigma), FNIP1 (Novus Biologicals), AMPKα (2532; Cell Signaling Technology), phospho (Thr172) AMPKα (2531; Cell Signaling Technology), ACC (3676; Cell Signaling Technology) and phospho (S79) ACC (3661; Cell Signaling Technology) antibodies are commercially available. The antibodies used for immunohistochemistry staining were HIF-1α (NB100-123; Novus Biologicals), MTC02 Mitochondrial Marker (AB3298), BNIP3 (AB38621 Abcam), GLUT1 (AB652; Abcam) and VEGF-A (sc-152 Santa Cruz Biotechnology) and are commercially available. The N-acetyl cysteine (NAC) was purchased from Sigma-Aldrich.

2.7.1.2 Cell culture

Primary MEFs were isolated from E12.5 *Flcn* floxed mice (generously gifted by Dr. L.S. Schmidt, NCI, Bethesda, MD, USA) and cultured by standard methods [153]. *Flcn* wild-type (WT) and knockout (KO) MEFs were generated after immortalization of primary *Flcn*$^{Flox/Flox}$ MEFs with SV40 large T (hygromycin B) and retroviral infection with a CD8 or CD8-Cre recombinase construct, followed by flow cytometry cell sorting of CD8 positive cells. The FLCN rescued knockout cells (Resc) were generated by retroviral infection with 2X-Flag-Flcn-MigR1 (puromycin) wild type (WT), S62A mutant or empty vector (EV) constructs. *Ampk*$^{+/+}$ and *Ampk*$^{-/-}$ MEFs have been described in [143] and UOK257 (FLCN-) / UOK257-2 (FLCN+) cells were kindly gifted by Dr. L.S. Schmidt (NCI, Bethesda, MD, USA) [43]. The human follicular thyroid cancer cell line FTC-133 cells naturally deficient for FLCN were obtained from Dr. E.R. Maher (University of Birmingham, Birmingham, UK) and were previously described in [128, 129]. FTC-133 cell were stably rescued for FLCN expression using 2XFlag-pcDNA3 human FLCN construct or an empty vector as control. MEFs, UOK257 and UOK257-2 were maintained in Dulbecco's modified Eagle's medium (DMEM), and FTC-133 cells were maintained in 50:50 DMEM:F12 media. Cell culture medium was supplemented with 10% (v/v) fetal bovine serum (FBS), 100 U/ml penicillin and 100μg/ml streptomycin (Invitrogen). UOK257-2 cell medium was supplemented with 5ug/ml blasticidin S and rescued MEFs and FTC-133 with G418 (0.5 mg/ml) to maintain FLCN expression. MEFs and FTC-133 cells stably downregulated for FLCN or HIF-1α expression were generated using the Mission lentivirus shRNA empty vector (shEV), a scrambled sequence (shScram2; Sigma-Aldrich), FLCN knockdown (shFlcn) (purchased from Sigma-Aldrich) or two HIF-1α (shHIF) specific sequences targeting mouse or human. HIF-1α shRNA A was obtained from Dr. RG. Jones (McGill University, Montreal, Canada and described in [143] and targeted mouse and human sequence, while two independent shRNA targeting mouse or human HIF-1α were purchased from Sigma-Aldrich (shHIF-1α B). PGC-1α was downregulated in MEFs using siRNA smart pool (On target plus; Dharmacon) according to the manufacturer's instructions using HiPerFect transfection reagent (Qiagen) and the assays were performed 48 h post-transfection.

2.7.1.3 Cell Proliferation and Survival assays

MEFs were seeded (2×10^4 cells) in 12-well plates in triplicate and 100μM glucose or glutamine free medium was added 24 h after plating. Cell numbers were counted daily using Coulter Counter (Beckman) and proliferation and survival rates were determined as the fold or percent cell number compared to day 0, respectively.

2.7.1.4 Quantification of mitochondria content by genomic qPCR

Total cellular DNA was extracted from UOK257 or MEFs using the DNeasy Blood and Tissue Kit (Qiagen). Relative nuclear (human RPL13A or mouse β-globin) and mitochondrial (human cytochrome B or mouse Cox2) DNA levels were quantified by qPCR (sequences are detailed in Supplementary table S3) and results were expressed as the percent mitochondrial DNA normalized to the nuclear DNA content (% mtDNA/nDNA).

2.7.1.5 RNA Extraction, quantitative PCR (qPCR) and real time PCR (qRT-PCR)

Total RNA was extracted using the RNeasy mini kit (Qiagen) and reverse-transcribed using the Superscript III kit (Invitrogen). Quantitative real-time PCR (qRT-PCR) was performed using Express SYBR Green qPCR supermix (Invitrogen) and specific primers (sequences are detailed in Supplemental table S3). Dissociation curves confirmed single product amplification and results were normalized to housekeeping genes 18S or RPLP0 (sequences are detailed in Supplemental table S3).

2.7.1.6 Protein extraction, immunoprecipitation and western blotting

Cells were washed twice with cold phosphate-buffered saline (PBS), lysed in AMPK lysis buffer [154], supplemented with Complete protease inhibitor (Roche) and DTT (1 mM), and cell lysates were cleared by centrifugation at 13000*xg*. For immunoprecipitation, cleared lysates were incubated with the EZview Red anti-Flag M2 beads (Sigma-Aldrich) for 2 h at 4°C. Beads were washed 3 times with lysis buffer and Flag-FLCN complexes were eluted twice with 150 ng/ml of Flag peptides diluted in PBS. For cell lysates, cells were washed twice with cold PBS and lysed directly in Laemmli buffer (62.5 mM Tris-HCL (pH 6.8), 2% (w/v) sodium dodecyl sulphate, 10% (v/v) glycerol, 5% (v/v) β-mercaptoethanol and 0.01% (w/v) bromophenol blue). Proteins were separated on SDS-PAGE gels and revealed by western blot as we previously described [69] using the antibodies listed above.

2.7.1.7 Soft agar and xenograft assays

Two-layered soft agar assays were undertaken in six-well plates. Briefly, subconfluent FTC-133 or UOK257 cells (3×10^5) were plated in complete media

supplemented with TSH (10U/L), containing 0,35% agar over a 0,6% agar layer. Agar was overlaid with complete media and colonies were grown for 14 to 21 days at 37°C in 5% CO_2. Media were changed twice a week. Cell colonies were then stained with crystal violet (0.0005%) and representative pictures were taken using inverted CKX41 microscope (Olympus) equipped with an Infinity camera (Luminera Corporation). For xenograft assays, 5 x 10^6 FTC-133 cells resuspended in 200µL of PBS were injected subcutaneously into the flank of nude mice. Tumor length (l) and width (w) were measured twice a week using a caliper and the tumor volume (V) was calculated ($V = 1/2(l \times w^2)$).

2.7.1.8 Immunohistochemistry

Procedures have been described in details previously [69]. Briefly, sections of formalin-fixed paraffin-embedded (FFPE) kidney tumor sample and normal controls were deparaffinized in xylene and dehydrated through graded ethanol concentrations. Endogenous peroxidase activity was blocked by incubation in 3 % (w/v) hydrogen peroxide (H_2O_2) in methanol for 30 min, followed by microwave treatment using 10mM citrate buffer (pH 6) for 10 min (90W) for MTC02, BNIP3, GLUT1 and VEGF-A and using 20mM TE buffer (pH 9) for HIF-1α to facilitate antigen retrieval. Sections were incubated with primary antibodies in 3% (w/v) bovine serum albumin overnight at 5ºC. Slides were washed 3 times with PBS and secondary antibody (EnVision, DAKO) was applied for 30 min at room temperature. Slides were washed 3 times with H_2O_2, revealed using DAB solution (EnVision, Dako), counterstained haematoxylin and embedded in Entellan (Electron Microscopy Sciences).

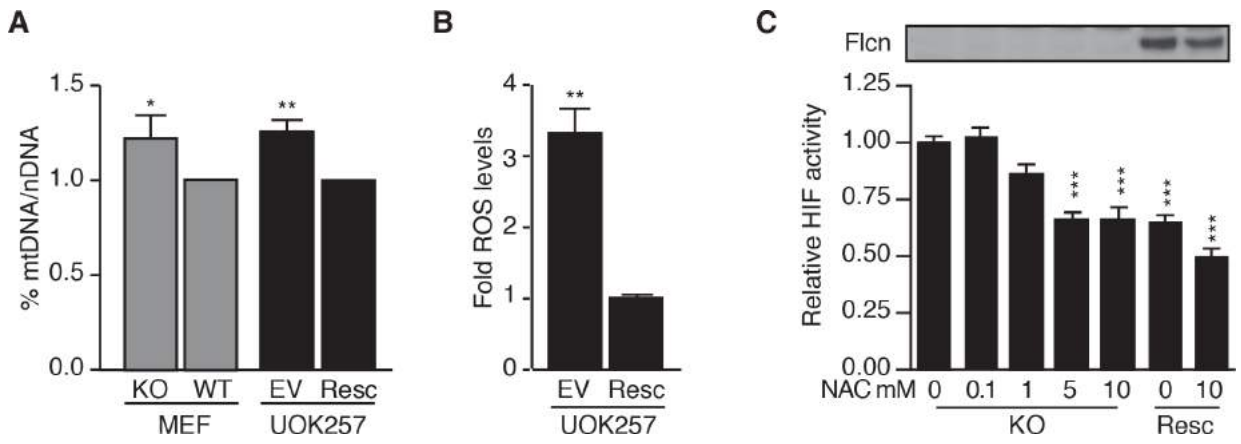

Supplementary Figure S1: **Increase mitochondrial biogenesis in FLCN deficient human kidney cancer cells and ROS-dependent activation of HIF upon loss of FLCN in MEFs under hypoxia.** A) Percent mitochondrial DNA content (mtDNA) normalized to nuclear DNA content (nDNA) measured in the indicated MEFs and the FLCN-deficient UOK257 (EV) and FLCN rescued (Resc) human kidney cancer cells. B) Fold ROS levels measured in the indicated UOK257 cells. C) Relative HIF activity measured under hypoxia using HIF-luciferase reporter assay in *Flcn* knockout MEFs, rescued (Resc) or not (KO) for FLCN expression and treated with the indicated concentrations of the anti-oxidant, N-acetyl cysteine (NAC) for 16 h. Data represent the means ± SD of 3 independent experiments performed in triplicate. **p* < 0.05, ***p* <0.01, ****p* < 0.001.

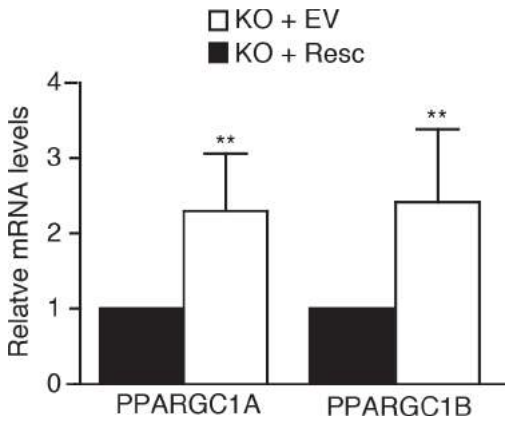

Supplementary Figure S2: PGC-1 upregulation upon loss of FLCN in human kidney cancer cells.

Relative PPARGC1A and PPARGC1B mRNA expression levels measured in FLCN-deficient (EV) and FLCN rescued (WT) human kidney UOK257 cancer cells. Data represent the means ± SD of five independent experiments performed in triplicate. $^{**}p < 0.01$.

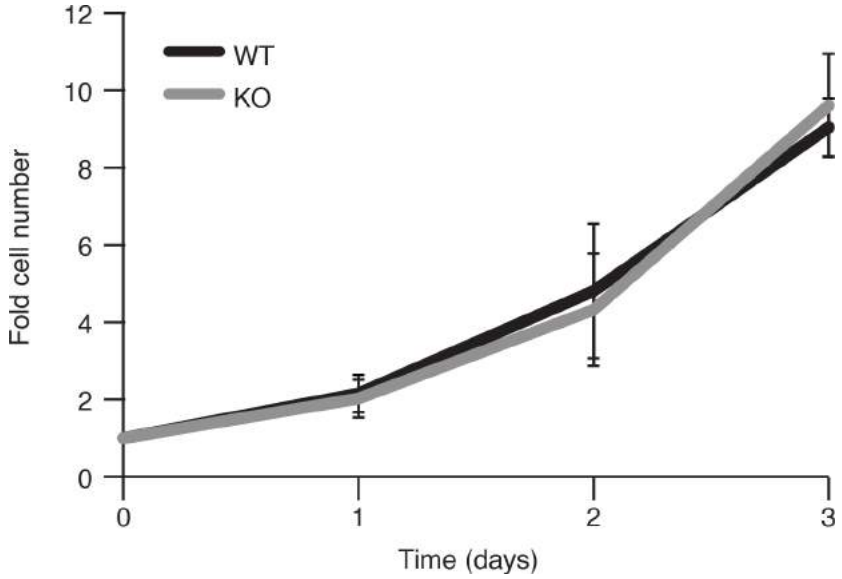

Supplementary Figure S3: **Loss of FLCN in MEF does not affect cell proliferation.** *Flcn* WT and KO MEFs proliferation rate were determined by cell counting in time course experiments. Data represent the mean ± SD of six independent experiments performed in triplicate.

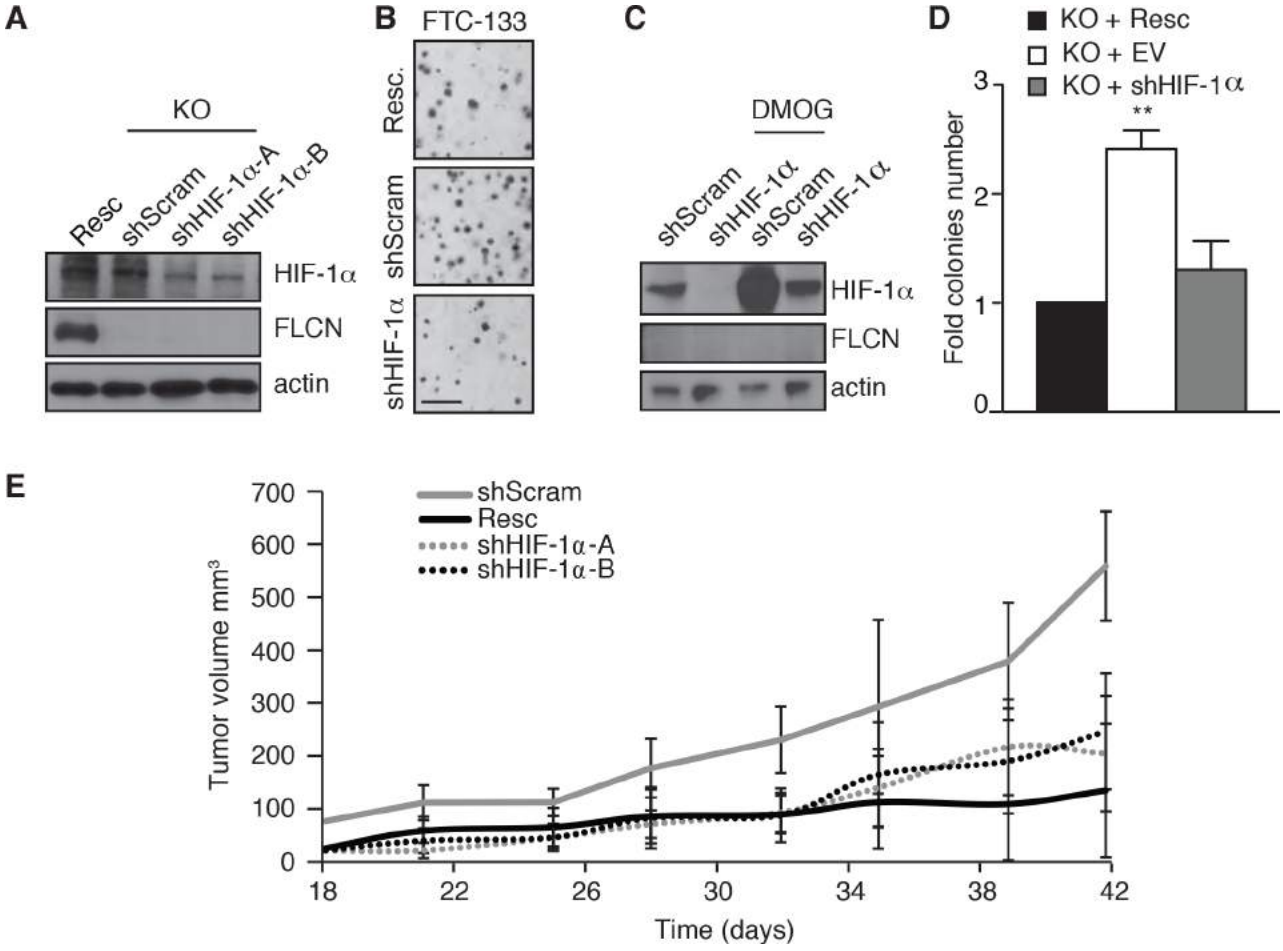
A
KO
Resc
shScram
shHIF-1α-A
shHIF-1α-B
HIF-1α
FLCN
actin
B
FTC-133
Resc.
shScram
shHIF-1α
C
DMOG
shScram
shHIF-1α
shScram
shHIF-1α
HIF-1α
FLCN
actin
D
KO + Resc
KO + EV
KO + shHIF-1α
**
Fold colonies number
0
1
2
3
E
shScram
Resc
shHIF-1α-A
shHIF-1α-B
Tumor volume mm3
0
100
200
300
400
500
600
700
18
22
26
30
34
38
42
Time (days)

Supplementary Figure S4: HIF-dependent metabolic advantage drives tumorigenesis in FLCN null cancer cells. A, C) Western blot analysis of FLCN and HIF-1α expression levels in the indicated FTC-133 (A) and UOK257 (C) cancer cell lines. Actin was shown as loading control. When indicated, cells were pretreated with Dimethyloxaloylglycine (DMOG), an inhibitor of HIF-1α prolyl hydroxylases that prevent HIF-1α degradation. Results are representative of 3 independent experiments. B) Representative pictures of soft agar colonies in the indicated FTC-133 cell lines. Scale bar: 500μM. D) Quantification of soft agar colonies number relative to FLCN-deficient UOK257 cells rescued for FLCN expression (KO + Resc). Data represent the means ± SD of 4 independent experiments performed in triplicate. E) Time course measurement of xenograft tumor volume in the indicated FTC-133 cell lines. n= 5 mice per group.

2.7.2 Supplemental tables:

Table S 1: Fold metabolites levels measured in MEFs

Pathway	Metabolites	WT		KO		p-value	N
		MEAN	SD	MEAN	SD		
glycolysis	Glucose	1,0	0,2	1,4	0,2	0,00002	8
	F6/G6P	1,0	0,1	1,4	0,5	0,01398	8
	F1,6bisP	1,0	0,2	1,6	0,9	0,01621	8
	DHAP/G3P	1,0	0,4	1,5	0,4	0,00979	8
	3PGA	1,0	0,3	1,5	0,4	0,00454	8
	R5P/RL5P	1,0	0,4	1,6	0,3	0,01189	8
	pSer	1,0	0,4	1,6	0,8	0,01614	8
	Ser	1,0	0,2	1,4	0,2	0,00253	8
	Ala	1,0	0,2	1,6	0,4	0,00001	8
TCA cycle	Glutamine	1,0	0,2	1,4	0,4	0,01101	8
	Fumarate	1,0	0,1	1,4	0,2	0,00165	8
	Succinate	1,0	0,1	1,5	0,4	0,00445	8
	Citrate	1,0	0,1	1,4	0,2	0,00055	8
	⟨-ketoglutarate	1,0	0,2	1,7	0,6	0,01260	8

Table S2: Fold metabolites levels derived from Glucose or Glutamine labelled source

Flux	Metabolites		WT		KO		p-value	N
			MEAN	SD	MEAN	SD		
Glucose	Pyruvate	unlabelled	0,24	0,03	0,43	0,14	0,0197	3
		Labelled	0,76	0,03	1.12	0,14		
	Lactate	unlabelled	0,28	0,03	0,54	0,21	0,0017	3
		Labelled	0,72	0,03	1,36	0,21		
	Alanine	unlabelled	0,37	0,01	0,72	0,13	0,0007	3
		Labelled	0,63	0,01	1,20	0,13		
	Citrate	unlabelled	0,32	0,02	0,39	0,03	0,0846	3
		Labelled	0,68	0,02	0,65	0,03		
Glutamine	Glutamine	unlabelled	0,08	0,04	0,17	0,08	0,0040	3
		Labelled	0,92	0,04	1,64	0,08		
	Fumarate	unlabelled	0,47	0,05	0,48	0,08	0,4670	3
		Labelled	0,53	0,05	0,57	0,08		
	Citrate	m+4	1,00	0,02	0,90	0,01	0,0002	3
		m+5	1,00	0,04	1,16	0,06	0,0070	3

Table S3: List of primers used for vector construction and gene targeting

Genes	Forward primers sequence (5'-3')!	Reverse primers sequence (5'-3')!
m HK2	CCGTGGTGGACAAGATAAGAGAGAAC	GGACACGTCACATTTCGGAGCCAG
h HK2	TCCTCAGTAGAACATGGCAG	TGACATTAGCACTGGTGGAG
m LDHA	AGACAAACTCAAGGGCGAGA	GCGGTGATAATGACCAGCTT
m SLC2A1	AGGTCACCATCTTGGAGCTG	ACAGCGACACCACAGTGAAG
h SLC2A1	TTCACTGTCGTGTCGCTGTTT	AGCGCGATGGTCATGAGTAT
m VEGF	GGAGAGCAGAAGTCCCATGA	ACTCCAGGGCTTCATCGTTA
h VEGF	TACCTCCACCATGCAAAGTG	ATGATTCTGCCCTCCTCCTTC
m PPARGC1A	CAGTCCTTCCTCCATGCCTG	GGGTTTGTTCTGATCCTGTGG
h PPARGC1A	CCTGTGATGCTTTTGCTGCTCTTG	AAACTATCAAAATCCAGAGAGTCA
m PPARGC1B	CAGCCAGTACAGCCCCGATG	GGTGTGTCGCCTTCATCCAG
h PPARGC1B	GTACATTCAAAATCTCTCCAGCGACAT	GAGGGCTCGTTGCGCTTCCTCAGGGC
m ATP5J	GCGCGGAAGTAGAACGGT	GAGACTGCTGACCGAAGGAC
m COX7A	CAGTACACTTGAAAGGCGGG	CCAGCCCAAGCAGTATAAGC
m NDUFB5	TGGCAAGAGACTGTTTGTCG	AGCTGCGCTTCACCAATAAA
m TFAM	CGGCAGAGACGGTTAAAAA	GAATCATCCTTTGCCTCCTG m
NRF1	CTTACAAGGTGGGGGACAGA	ATGCTCACAGGGATCTGGAC
m NRF2	TGAGAAACTTAGCCGTGCATT	TGAGAAACTTAGCCGTGCATT
m RPLP0	GCAGCAGATCCGCATGTCGCTCCG	ACCAGACGGTTCAGTTCTGC
h RPLP0	GCAATGTTGCCAGTGTCTG	GCCTTGACCTTTTCAGCAA
h 18S rRNA	AACCCGTTGAACCCCATT	CCATCCAATCGGTAGTAGCG
h *cyt-b mtDNA	GCGTCCTTGCCCTATTACTATC	CTTACTGGTTGTCCTCCGATTC
h RPL13A nDNA	CTCAAGGTCGTGCGTCTG	TGGCTTTCTCTTTCCTCTTCTC
m COX2 mtDNA	GCCGACTAAATCAAGCAACA	CAATGGGCATAAAGCTATGG
m β globin nDNA	GAAGCGATTCTAGGGAGCAG	GGAGCAGCGATTCTGAGYAGA
m Flcn S62A	CGGGTCCGTGCCCACGCTCCAGCCGAG GGTGCCAGC	GCTGGCACCCTCGGCTGGAGCGTGGG C ACGGACCCG

* cyt-b: cytochrome b

Chapter 3:

Chronic AMPK activation via loss of FLCN induces functional beige adipose tissue through PGC-1α/ERRα

Ming Yan[1,2], Étienne Audet-Walsh[1,2], Benjamin Walker[1,2], Sanaz Manteghi[1,2], Chatherine Rosa Dufour[1,2], Julie St-Pierre[1,2], Vincent Giguère[1,2,3], Arnim Pause[1,2]

[1]Goodman Cancer Research Centre, McGill University, Montréal, Québec, Canada
[2]Department of Biochemistry, McGill University, Montréal, Québec, Canada
[3]Medicine and Oncology, McGill University, Montréal, Québec, Canada

Running title: FLCN/AMPK-dependent reprogramming of adipose tissue

This article is in revision at *Genes and Dev.,* 2015 Oct.

3.1 Abstract

The tumor suppressor Folliculin forms a complex with AMP-activated protein kinase (AMPK). Given that AMPK is a master regulator of cellular energy homeostasis we generated an adipose-specific *Flcn* knockout (Adipoq-*Flcn* KO) mouse model to investigate the role of FLCN, a repressor of AMPK, in energy metabolism. Here we show that the absence of FLCN in mouse adipose tissues leads to a complete metabolic reprogramming of white adipocytes. Adipoq-*Flcn* KO mice exhibit increased energy expenditure that protects them from high fat diet (HFD)-induced obesity. Importantly, FLCN ablation leads to chronic hyper-activation of AMPK, which in turns induces and activates two key transcriptional regulators of cell metabolism, PGC-1α and ERRα. Together, the AMPK/PGC-1α/ERRα axis positively modulates the expression of nuclear-encoded mitochondrial genes to promote mitochondrial activity and lipid metabolism. Accordingly, levels of mitochondrial uncoupling proteins are upregulated in *Flcn* KO white adipose tissue. As a consequence, the Adipoq-*Flcn* KO mice are more resistant to cold exposure associated with increased browning of inguinal fat depots. These results show an unexpected role for FLCN in metabolic control and identify a novel molecular pathway involved in browning of white adipocytes.

Key words: FLCN; AMPK; PGC-1α; nuclear receptors; brown fat; metabolic reprogramming

3.2 Introduction

Obesity is one of the most serious public health problems worldwide and is characterized by the excessive accumulation of lipids in adipose tissue. Obesity is initiated from a chronic imbalance between energy intake and expenditure and is a major risk factor for metabolic disorders such as type-2 diabetes, cardiovascular diseases, and certain cancers. There are two major types of adipose tissue with distinct functions: white and brown adipose tissue (WAT and BAT, respectively). WAT is mainly involved in lipid storage, mostly triglycerides, whereas BAT is specialized in lipids oxidation by mitochondria in order to produce heat through a process of non-shivering thermogenesis [155]. Recently, a third type of adipose tissue, named brite ("brown and white") or beige, was identified. It resides in certain depots of WAT and exhibits inducible BAT phenotype in response to appropriate stimuli such as cold exposure or β-adrenergic stimulation [156, 157]. Notably, beige adipocytes are characterized by an induction of thermogenic genes expression such as proliferator activated receptor γ (PPARγ)-coactivator-1α (PGC-1α), uncoupling proteins (UCP1, UCP3), and with at least partial conversion of unilocular adipocytes into multilocular mitochondria-rich adipocytes [158, 159]. The distribution of brite/beige cells differs between WAT depots in mice. A large accumulation of brown-like cells can be found in the subcutaneous inguinal WAT, but is also occasionally observed in gonadal/perigonadal WAT during cold exposure [160]. Remarkably, many studies have reported that mice displaying an increase in the abundance of brite/beige in WAT are associated with resistance to high fat diet (HFD)-induced obesity [161-163]. Therefore, understanding the underlying mechanisms of white adipocytes browning has attracted much interest to prevent, control, or treat obesity.

Birt-Hogg-Dubé (BHD) syndrome is an autosomal dominant hereditary disorder characterized by a predisposition to develop hair follicle tumors, lung and kidney cysts, and renal cell carcinoma. This syndrome is caused by loss-of-function mutations of a tumor suppressor gene that encodes a 64-kDa protein named folliculin (FLCN) [43]. FLCN has no significant sequence homology to any known protein and is highly conserved across species, suggesting an important

biological role, as illustrated by the embryonic lethality of *Flcn* homozygous disruption in mice [164-166]. FLCN interacts with the master energy sensor AMP-activated protein kinase (AMPK) via FLCN interacting protein (FNIP) [43, 69, 105, 165, 167, 168].

AMPK is an evolutionarily conserved serine/threonine protein kinase playing a key role in cellular and whole-body energy homeostasis. When cellular energy levels drop, AMP or ADP bind to the γ subunit of AMPK and induce its allosteric conformational change. This change leads to the activation of AMPK by phosphorylation in an attempt to restore energy balance by switching cells from an anabolic (ATP consumption) to catabolic (ATP production) state [169]. Activation of AMPK leads to a concomitant increase in the phosphorylation of acetyl-CoA carboxylase (ACC), which inhibits fatty acid synthesis and promotes fatty acid oxidation (FAO) by upregulation of CPT-1 activity [170]. Pharmacological activation of AMPK in mice leads to an increase in adipose tissue browning and a decrease in fat mass. Similarly, constitutive activation of hepatic AMPK-α1 in mice induces resistance to HFD-induced obesity [171]. Therefore, FLCN modulation of AMPK activity might affect lipid metabolism and WAT/BAT functions.

We have previously reported that ablation of FLCN expression or loss of FLCN binding to AMPK induces chronic AMPK pathway hyperactivation in nematodes and various cellular contexts leading to increased energy reserves, enhanced metabolic stress resistance, and metabolic transformation [69, 167, 168]. This hyperactivation of AMPK induces the expression of PGC-1α in muscle cells, MEFs, and cancer cells, which triggers mitochondrial biogenesis and promotes transcriptional regulation of nuclear-encoded mitochondrial genes [167, 172]. Upregulation of PGC-1α expression in adipose tissues also leads to increased mitochondrial biogenesis, and protects from HFD-induced obesity in mice [162]. To control mitochondrial gene expression, PGC-1α acts in concert with ERRα, a transcription factor member of the nuclear receptor family [173]. The PGC-1α/ERRα transcriptional axis is now well appreciated as a master transcriptional

regulator of cell metabolism, binding and regulating the vast majority of nuclear-encoded mitochondrial genes [174], illustrative of their positive control of mitochondrial activity and heat production in BAT [175, 176]. Moreover, upon FLCN inactivation and AMPK activation, PGC-1α and ERRα might act as downstream effectors of FLCN to mediate metabolic cellular reprogramming.

To investigate the potential role of FLCN in fat metabolism, we generated an adipose-specific *Flcn* knockout (Adipoq-*Flcn* KO) mouse model. We observed that Adipoq-*Flcn* KO mice exhibit elevated energy expenditure that protects them from HFD-induced obesity. Importantly, loss of FLCN leads to an increase in AMPK-dependent PGC-1α/ERRα transcriptional regulation, thereby inducing mitochondrial biogenesis and activity. In parallel, the *Flcn* KO mice exhibit an increase in the abundance of brite/beige adipocytes in WAT and are more resistant to cold exposure associated with higher UCP1 levels, which promotes uncoupling and FAO generating heat.

3.3 Results

3.3.1 Adipose-specific *Flcn* KO mice are resistant to HFD-induced obesity

Global homozygous deletion of *Flcn* in the mouse results in early embryonic lethality around day 8.5 [164-166]. To elucidate the role of FLCN in adipose tissue we generated an adipose-specific *Flcn* KO mouse model by crossing $Flcn^{lox/lox}$ mice (loxP sites flanking exon 7; Fig. S1; [165]) with adiponectin-Cre mice [177] to generate mice with conditional *Flcn* disruption in both WAT and BAT (Adipoq-*Flcn* KO; Fig. 3.1A). Adipoq-*Flcn* KO mice are born at the expected Mendelian frequency, display no developmental defects, survive without difficulty, are fertile and have similar weight compared to wild type (WT) mice at weaning (4 weeks of age). On normal chow diet, no difference in weight gained between WT and KO mice over a 14-week time course was observed (Fig. 3.1B). On HFD challenge, WT mice gained about ~50% more weight than normal chow. However, KO mice only gained ~15% more weight on HFD compared to normal chow, a 3-fold decrease in weight gain compared to WT mice (Fig. 3.1B, C).

We next investigated the effect of adipose-specific *Flcn* deletion on whole animal metabolism using metabolic cages, simultaneously measuring food/water intake, physical activity, and energy expenditure (VO_2 consumption and VCO_2 production) in individual mice. Four-month-old mice fed with chow or HFD were examined for 3 days. No difference was observed in food/water intake or in total activity between WT and KO mice (Fig. 3.1D, E and S2). However, Adipoq-*Flcn* KO mice exhibited significantly higher VO_2 consumption in a 12-hour dark and 12-hour light cycle (Fig. 3.1F, G, and H), both under chow or HFD. In addition, the respiration exchange ratio ($RER=VCO_2/VO_2$) of Adipoq-*Flcn* KO mice was significantly reduced compare to WT mice on HFD (Fig. 3.1I), suggesting an increase in FAO in response to enriched nutrition stress. These results indicate that

the significantly lower weight gain following HFD in Adipoq-*Flcn* KO mice could be due to an increase in mitochondrial energy expenditure.

3.3.2 FLCN is necessary for proper lipid storage in white adipocytes

To determine the mechanism underlying the Adipoq-*Flcn* KO specific protection against obesity, we dissected individual fat depots and organs to measure their weights relative to the whole body weight from 5-month-old mice. We observed a slight reduction of iWAT and gonadal WAT (gWAT) in Adipoq-*Flcn* KO mice fed with chow compared to WT mice (Fig. 2A). In contrast, iWAT and gWAT of KO mice fed with HFD were significantly decreased compared to WT mice (Fig. 3.2A). There is however no weight difference in BAT and other selected organs (liver, heart, kidney and spleen) between WT and KO mice (Fig. 3.2A and 2B).

Importantly, and consistent with the observed resistance to HFD, white adipocytes isolated from Adipoq-*Flcn* KO tissue were significantly smaller compared to WT mice under HFD, but not under regular diet (Fig. 3.2C, D and E). No difference in cell size of BAT was observed, suggesting that the lower weight gain in Adipoq-Flcn KO mice on HFD was primarily due to white adipocyte metabolism.

3.3.3 FLCN ablation activates AMPK and induces downstream markers associated with browning in WAT

FLCN binds AMPK and has been described as a negative regulator of AMPK signalling pathways [43]; [167]; [75]. Indeed, we recently demonstrated that loss of FLCN constitutively activates AMPKα, which in turn leads to elevation in PGC-1α that stimulates mitochondrial biogenesis [167]. ERRα is now well recognized as one of the major partners of PGC-1α in regulating mitochondrial metabolism and is an important component of the transcriptional network that promotes mitochondrial biogenesis and oxidative capacity in BAT

[175]. Thus, ERRα may play a role as an effector of the induction of energy metabolism in WAT of Adipoq-*Flcn* KO mice. As expected, we observed increased phosphorylation of AMPK (pT172 AMPKα) in the absence of FLCN, under both chow and HFD conditions, as well as induced phosphorylation of acetyl-CoA carboxylase (pS78 ACC), a major downstream target of AMPK that inhibits fatty acid synthesis (Fig. 3.3A, B). Concomitantly, expression of PGC-1α and ERRα were significantly increased at both the protein and the mRNA levels in WAT and BAT (Fig. 3.3 A- E).

One key biomarker of BAT or of browning of WAT is the expression of UCP that allows mitochondria to generate heat instead of ATP through the dissipation of mitochondrial proton gradient. Accordingly, we observed 2-3 fold increase in mRNA expression UCP1 and 5-10 fold increase in UCP3 in Adipoq-*Flcn* WATs (Fig. 3C-E). We also observed increased PR domain-containing 16 (PRDM16) mRNA, another important factor that has been associated with brown-like adipocytes (Fig. 3C- E) [160, 178].

3.3.4 FLCN knockdown in 3T3-L1 adipocytes stimulates PGC-1α/ERRα activity and decreases lipid production

Because WATs of Adipoq-Flcn KO mice displayed increased PGC-1α/ERRα expression, we next examined the effect of FLCN repression on their activity using two independent shRNAs in 3T3-L1 adipocytes (Fig. 3.4A and S3). In agreement with our in vivo results, FLCN repression increased significantly PGC-1α and ERRα expression in 3T3-L1 (Fig. 3.4B), as well as of several metabolic genes (Fig. S3A). In addition, the activity of the PGC-1α/ERRα transcriptional axis was assessed using a luciferase-based system containing 3xERRE (estrogen-related receptor response element). As expected, a significant increase in luciferase activity was observed following FLCN repression. Indeed, we observed a 6-10 fold increase in their activity following FLCN inhibition in 3T3-L1 adipocytes (Fig. 3.4C), indicating a consistent and strong induction of the PGC-1α/ERRα activity following FLCN repression. Moreover, ChIP-qPCR

experiments indicated a significant increase in global ERRα binding at several metabolic target genes in 3T3-L1 adipocytes upon introduction of shFlcn (Fig. S3B).

Concurrently, we observed an inhibition of lipid droplet production following FLCN repression in 3T3-L1 adipocytes compared to shEV (Fig. 3.4D), which is in agreement with what was observed in vivo in WATs of Adipoq-*Flcn* KO mice (Fig. 2C-D-E). As a consequence, FLCN repression in 3T3-L1 adipocytes decreased cell size and increased cell number (saturated monolayer on a tissue culture plate) compared to control adipocytes (shEV; Fig. 3.4E, Fig. S3C-D). Taken together, our data indicate that inhibition of FLCN expression induced both AMPK activity as well as PGC-1α/ERRα expression and activity, resulting in impaired lipid droplet accumulation.

3.3.5 AMPK activates PGC-1α/ERRα transcriptional activity to promote mitochondrial metabolism

In order to study genetic and mechanistic details of these observations, we took advantage of previously described mouse embryonic fibroblasts (MEFs) that were deleted for *Flcn* or *Prkaa1* and *Prkaa2* (encoding the 2 catalytic AMPKα subunits) (Possik et al., 2014; Yan et al. 2014). First, we confirmed that *Flcn* ablation led to an activated AMPK pathway and increased PGC-1α/ERRα expression (Fig. 3.5A). Moreover, many mitochondrial proteins were upregulated in *Flcn* KO MEFs (Fig. 3.5A). At the mRNA level, the expression of several metabolic genes such as *Ucp1, Ucp3*, and *Acad1*, but also *Ppargc1a* and *Esrra* (PGC-1α and ERRα) was increased (Fig. 3.5B). *Flcn* KO increased ERRα binding at several metabolic target genes involved in mitochondrial activity, such as Aco2 and Idh3a, required for the citric acid cycle activity, and several members of the Nduf and Atp5 families, required for the electron transport chain activity (Fig. 3.5C). Similar results were obtained using shRNA against *Flcn* in MEFs (Fig. 3.5D; left). Importantly, genetic inactivation of AMPKα blocked the induction of ERRα-DNA binding independent of FLCN repression (Fig. 3.5D; right). These

results indicate that AMPK is required for ERRα activation following FLCN repression. Accordingly, *Ucp1, Ucp3*, *Acad1, Ppargc1a* and *Esrra* were induced in MEFs upon *Flcn* knockdown (Fig. 3.5E). However, AMPK ablation completely blocked the induction of these genes upon FLCN repression (Fig. 3.5E, F). Altogether, these results clearly demonstrate a functional link between AMPK and ERRα to mediate the metabolic reprogramming induced upon FLCN loss of function.

One major effect of AMPK activation is the induction of mitochondrial biogenesis and activity, which is also a major component of the PGC-1α/ERRα transcriptional program. Hence, *Flcn* KO MEFs exhibited significantly higher oxygen consumption rate (OCR; Fig. 3.5G), which is consistent with an increased AMPK/PGC-1α/ERRα activity. Importantly, siRNA knock down of ERRα strongly blocked this induction of respiration in *Flcn* KO MEFs (Fig. 3.5G, H and S4). Therefore, loss of FLCN dictates an AMPK-dependent PGC-1α/ERRα activation, which leads to an induction of mitochondrial respiration.

3.3.6 FLCN ablation induces thermogenic gene expression, browning of iWAT and resistance to cold

Adaptive non-shivering thermogenesis is a key defense response to maintain body temperature in the cold, particularly in small mammals and newborns, which is mediated by BAT [179]. Both PGC-1α and ERRα are required for proper adaptive thermogenesis under cold exposure as well as for heat production by positively regulating mitochondrial activity and uncoupling [79, 175, 180, 181]. Based on the observation that Adipoq-*Flcn* KO mice were metabolically more active (Fig. 1), and had impaired lipid accumulation (Fig. 3.2), that FLCN inactivation promoted the expression and activity of the PGC-1α/ERRα transcriptional axis (Fig. 3.3-5), we hypothesized that FLCN deletion could be involved in promoting browning of WAT. To test this possibility, we examined the body temperature adaptation to cold exposure of two cohorts of three-month-old mice (Adipoq-*Flcn* KO or WT, n=6 mice/genotype) on normal chow food. The

mice were maintained at thermoneutrality (30°C) for 24 hours then transferred to 4°C in individual pre-cooled cages. Body temperature was equal for the two cohorts at time = 0. Temperature dropped significantly between 3-5 hours in WT mice while Adipoq-*Flcn* KO mice maintained their temperature in this time frame, indicating a higher adaptive thermogenesis (Fig. 3.6A). qRT-PCR analysis revealed a significant increase of adaptive thermogenesis markers in Adipoq-*Flcn* KO mice, notably *Ucp1* and *Ucp3*, *Ppargc1a* and *Prdm16* in BAT, but also in gWAT and iWAT under cold exposure (Fig. 3.6B). Indeed, we observed a 20-fold increase in *Ucp1* mRNA expression in gWAT, and a 30-fold increase in iWAT of Adipoq-*Flcn* KO mice compare to WT mice. UCP1 protein expression was confirmed by western blot and IHC in iWAT, clearly showing increased expression in Adipoq-*Flcn* KO mice under cold exposure (Fig. 3.6C-D). Taken together, our data demonstrate that *Flcn* ablation induces browning of WAT and cold resistance.

3.4 Discussion

In the present study, we have shown that deletion of *Flcn* in mouse adipose tissues leads to a complete metabolic reprogramming of white adipocytes. As a result, adipose-specific *Flcn* KO mice exhibit significantly higher energy expenditure associated with an increase in mitochondrial respiration. Importantly, this remodelling of white adipose tissues metabolism induces several advantages in vivo, including resistance to obesity and increased adaptive thermogenesis. Mechanistically, we demonstrated that the absence of FLCN in WAT activates AMPK, thereby inducing the activity of the PGC-1α/ERRα transcriptional axis. Together, they positively modulated the expression of nuclear-encoded mitochondrial genes to promote mitochondrial activity and lipid metabolism. Overall, our results demonstrate a critical role of *Flcn* as a negative regulator of lipid metabolism in WAT functionally linking the FLCN/AMPK and the PGC-1α/ERRα transcriptional axis.

As observed in vivo and in vitro, FLCN repression activates AMPK, which drives PGC-1α expression and results in increased mitochondrial mass and activity [167]; [75]). It is known that AMPK activation can induce [172]; [167]. Once activated, PGC-1α can increase its own expression as well as that of ERRα, and increases the binding of ERRα to its own promoter [182, 183]. This autoregulation induces a positive feedback loop that enhances PGC-1α and ERRα expression and activity, which suggests a mechanism to explain why both transcriptional regulators are upregulated following FLCN repression or genetic ablation. PGC-1α, together with ERRα, acts as a key regulator of energy homeostasis in both normal and cancer cells [173, 184]. Here, we demonstrate that upon AMPK activation, PGC-1α/ERRα act as downstream effectors of AMPK to stimulate mitochondrial biogenesis and activity. Indeed, the induction of ERRα DNA binding at several of its metabolic target genes following FLCN repression was completely lost in Ampk-/- MEFs (Fig. 3.5D) These target genes, such as *Aco2* and *Idh3a*, are involved in mitochondrial activity, and *Nduf* and *Atp5* are required for the electron transport chain activity. As a consequence, Adipoq-*Flcn* null mice

are resistant to HFD-induced obesity due to the metabolic reprogramming of white adipocytes, which oxidize lipids rather than storing them. Similarly, loss of *Fnip1*, which belongs to the FLCN/FNIP/AMPK complex, results in chronic AMPK activation and in increased oxidative metabolism in B-cells and skeletal muscle in an AMPK/PGC1α-dependent manner [185]. Recently, miR-455 was reported as an activator of AMPKα1 displaying browning of iWAT in transgenic mice upon cold exposure [186].

A lot of focus has been given in the past few years on transcription factors involved in the browning process of white adipocytes. Notably, PRDM16, PPARγ, and the coactivator PGC-1α have been shown to be critical determinants in the transcriptional control of mitochondrial and thermogenic genes during that transition [160, 187]. We can now add FLCN as a negative regulator of the browning process, but also ERRα as participating in maintaining that phenotype, downstream of the hyper-activated AMPK pathway in Adipoq-*Flcn* KO mice. It is interesting to note that Adipoq-*Flcn* KO mice have significantly higher levels of PGC-1α, ERRα and PRDM16 in WAT either under HFD or cold exposure. Additionally, the uncoupling proteins UCP1 and UCP3, which are markers of white adipocyte browning, were also strongly induced in WATs in the Adipoq-*Flcn* null mice, either under HFD or following cold exposure. Even though ERRα does not modulate UCP expression directly, it indirectly modulates their activity by promoting mitochondrial biogenesis, allowing an increase in the cellular capacity to produce heat [175, 181]. As both PRDM16 and PGC-1α were upregulated following FLCN KO or repression, and because they were recently shown to interact together at the *Ucp1* promoter [188] their increased activity most probably explain the increased UCP1 expression observed in vitro and in vivo. Additionally, activation of AMPK promotes FAO through inactivation of ACC, via direct phosphorylation, and by promoting CPT-1 activity, the shuttle allowing entry of fatty acids in mitochondria. Overall, *Flcn* deletion in white adipocytes results in higher FAO, oxygen consumption and heat production. Therefore, by stimulating mitochondrial activity, UCP expression, and FAO, the activation of the AMPK/PGC-1α/ERRα axis upon FLCN repression can strongly modulate white

fat metabolism, shifting them form a "lipid storage compartment" to an active site of lipid metabolism.

The global ERRα deletion has been previously described to confer resistance to HFD-induced obesity, because of the impairment of lipid synthesis in ERRα KO adipose tissues [189], but also because of a decrease in lipid absorption in the intestinal system in mice lacking ERRα [190]. On the other hand, up-regulation of ERRα activity by up-regulation of PGC-1β in mice also conferred resistance to HFD-obesity by a global increase of energy expenditure [191]. Therefore, ERRα appears as a key regulator of lipid handling and processing and these results are consistent with our previous study showing that ERRα activation, following *Flcn* repression, promotes mitochondrial activity. Importantly, this hyper-activation of ERRα is AMPK-dependent, as deletion of AMPK in MEFs blocked ERRα activity, again highlighting its role as a downstream effector of AMPK to mediate transcriptional regulation of cell metabolism.

In conclusion, we revealed that loss of FLCN is involved in an AMPK-dependent browning of white adipose tissues, but also an induction of the PGC-1α/ERRα transcriptional axis that leads to an increase in mitochondrial respiration. These results show an unexpected role for FLCN in metabolic control and identify a novel molecular pathway involved in browning of white adipocytes. The findings described here also highlight new possibilities for obesity treatment strategies through the role of FLCN in adipocyte metabolism.

3.5 Materials and methods

3.5.1 Reagent

Commercial antibodies were purchased as follow: β-actin (AC74; Sigma-Aldrich), PGC-1α (4C1.3; Calbiochem), ERRα (2131; Epitomics), tubulin (T9026; Sigma), AMPKα (2532; Cell Signaling Technology), phospho (Thr172) AMPKα (2531; Cell Signaling Technology), ACC (3676; Cell Signaling

Technology) and phospho (S79) ACC (3661; Cell Signaling Technology), Mito OXPHOS (ab110413; Abcam), UCP1 (10983; Abcam) anti-mouse FLCN polyclonal antibody was generated by the McGill animal resource center services through injecting purified GST-FLCN recombinant protein in rabbits as reported [167].

3.5.2 Animals

All procedures for generating the *Flcn* KO mouse model were performed at McGill University. Maintenance and experimental manipulation of mice were performed according to the guidelines and regulations of the McGill University Research and Ethic Animal Committee and the Canadian Council on Animal Care. All studies were carried out using C57BL/6 female mice obtained from The Jackson Laboratory and housed on a 12:12-hour light–dark cycle at 22°C. *Flcn* f/f (BHDf/f) mice were generated as previously described [165]. To generate adipose-specific *Flcn* knockout (KO), *Flcn* f/f mice were crossed with Adipoq-Cre transgenic mice (Kind gift from Dr. André Marette, Laval University, Quebec, Canada). *Flcn* KO mice were generated by crossing female *Flcn* f/f mice homozygous for the floxed allele with *Flcn* f/+; Adipoq-Cre+/-males. Mice were fed on a chow diet containing 10 kcal % fat (D12450B, Research Diet Inc.) or subjected to a high fat diet (HFD) containing 60 kcal % fat (D12492, Research Diet Inc.) beginning at approximately 6-7 weeks of age as indicated and fed ad libidum. Body weight and food intake were measured weekly.

3.5.3 Metabolic measurements in vivo

Mice were housed individually in metabolic cages for 72 hours at a 12-hour light/dark cycle with a free access to water and food using a comprehensive laboratory animal monitoring system, (CLAMS; Columbus Instruments). Food/water intake, energy expenditure, physical activity, and respiratory exchange ratio (RER), calculated as VCO_2/VO_2, were assessed simultaneously.

3.5.4 RNA isolation and real-time PCR analysis

Total RNA from cultured cells or mouse tissues was isolated by TRIzol (Ambion) extraction and purified using RNeasy mini-columns according to the manufacturer's instructions (Qiagen). For quantitative real-time PCR analysis, 1μg of total RNA was reverse-transcribed using the Superscript III kit (Invitrogen). SYBR Green reactions using the SYBR Green qPCR supermix (Invitrogen) and specific primers (Supp. Table 1) were performed using an MX300 (Stratagene). Relative expression of mRNAs was determined after normalization to housekeeping genes 18S or RPLP0. Student's t-test was used to evaluate statistical significance as previously described [183].

3.5.5 Western Blot Analysis

For whole cell lysates, cells (MEFs or 3T3L1 adipocytes) were washed twice with cold phosphate-buffered saline (PBS) and lysed in AMPK lysis buffer as we previously described (Yan et al 2014). Mouse tissues were isolated, snap-frozen in liquid nitrogen and stored at -80°C. For protein extraction from WAT and BAT, approximately 60mg frozen tissue was homogenized using Tissuelyser (Qiagen) in 1X RIPA buffer containing 0.1% SDS, in 100μl lysis buffer (Tris pH7.5, 2mM EDTA, 2mM EGTA, 0.5M mannitol, 1% triton, phosphatase and protease inhibitors). Extracts were spun down and the fat layer and cell debris were removed before analysis by western blotting.

3.5.6 ERRE luciferase reporter assays

3T3L1 adipocytes or MEFs were transfected with the firefly luciferase PGC-1α/ERRα activity reporter pGL2-TK-ERRE plasmid for 24 hours [183]. Luciferase activity was measured using the Dual Luciferase Assay system (Promega) and normalized to TK-renilla reporter control activity, according to the manufacturer's instructions.

3.5.7 Oxygen consumption in vitro

Oxygen respiration rate (OCR) was accessed using the XF24 Extracellular Flux Analyzer (Seahorse Bioscience). Briefly, 20,000 cells per well were seeded and, after 24 hours, media was changed for the non-buffered Seahorse assay media supplemented with 25mM glucose, 1mM glutamine and 1mM Na-pyruvate and equilibrated in a CO_2-free incubator at 37°C for 1 hour. OCR measurements were obtained at baseline and following injection of Etomoxir (100 μM), oligomycin (10 μM), carbonylcyanide-p-trifluoromethoxyphenylhydrazone (FCCP, 3 μM, Sigma) and rotenone (10 μM, Sigma). The value of basal respiration, mitochondrial proton leak, maximal respiration, and non-mitochondrial respiration was determined as described in the Seahorse Operator's Manual.

3.5.8 Cold exposure studies

Three-month-old mice were housed individually in cages at 30°C for 24 hours with free access to chow food and water, and then were transferred to cold room at 4°C. Body temperature was measured hourly for 6 hours using a digital rectal probe (physitemp Instruments Inc, NJ, USA). At the end of experiment, mice were sacrificed and adipose tissues were harvested (iWAT, gWAT, and BAT), snap-frozen in liquid nitrogen, and stored at -80°C.

3.5.9 Histology

For histological analysis, adipose tissue were fixed in 4% formaldehyde overnight at room temperature immediately after sacrifice, embedded in paraffin, and cut to 6-μm sections on slides. The slides were stained with haematoxylin and eosin (Sigma) according to the standard protocol. Adipocytes area was determined using Metaxpress software for integrated morphology analysis. At least 30 fields from random sections of each mouse sample were quantified. Immunohistochemistry was performed using the Vectastain Elite ABC kit

according to the manufacturer's instructions using rabbit UCP1 antibodies (1:1000) as described previously [178].

3.5.10 Cell Culture

MEFs cell lines with AMPKα1/AMPKα2 (*Prkaa1* and *Prkaa2*) double knockout and *Flcn* knockdown were previously described (Yan et al 2014). 3T3-L1 preadipocytes were obtained from ATCC (Manassas, VA) and *Flcn* knockdown was generated using shRNA pLKO-puro Lentiviral transduction according to the standard protocol (Mission, Sigma). The cells were grown at 37ºC in 5% CO_2 in 10% FBS-DMEM. After two days of post confluence (counted as day 0), adipocytes differentiation was induced with MDI (0.5 mM IBMX, 1 μg/ml insulin, and 10 μM dexamethasone) for two days. Cells were then maintained in growth medium supplemented with 1μg/ml insulin (maintenance medium) and grown for 7-10 days. The medium was changed every two days. By day 8-10, fully differentiated cells were assessed by Oil Red O staining or extracted for RNA for analysis qRT-PCR.

3.5.11 Oil Red O Staining

The differentiated 3T3-L1 adipocytes were assessed using a typical Oil Red O (ORO) staining. Cells were washed with 1 x PBS and fixed with 4% paraformaldehyde for 60 minutes. Cells were rinsed twice with deionized water followed by adding ORO in 60% isopropanol for 20 minutes, and rinsed again. The cells were coverslip mounted and visualized and photographed using a Zeiss microscope under 20X magnification and captured by Axio Cam MRC digital camera.

3.5.12 ChIP-qPCR Analysis

MEFs or undifferentiated 3T3-L1 preadipocytes were cross-linked with 1% formaldehyde and nuclei were enriched by sequential centrifugations. After

sonication, immunoprecipitation was performed overnight at 4ºC with an anti-ERRα rabbit antibody (Epitomics 2131) or a control anti-rabbit IgG antibody (Sigma-Aldrich), using Dynabeads® (Life TechnologiesTM). Enriched DNA was then purified using the QIAGEN PCR purification kit and analyzed by qPCR using a Roche LightCycler 480®. Non-targeted rabbit IgG ChIP was used as a control of antibody non-specific binding and 2 negative regions were used for normalization. ChIP primers can be found in Table S1

3.6 Acknowledgments

We thank Dr. Claire Brown and Erika Tse-Luen Wee for assistance with image analyses (McGill Imaging facility), Ken McDonald for cell sorting analysis (McGill Flow Cytometry Facility), and Jean-Martin Lapointe and Jo-Ann Bader for tissue processing (Goodman Cancer Research Center Histology Facility at McGill University). We thank André Marette (Laval University) for the Adipoq-Cre transgenic mouse strain, Wissal El-Assaad for technical support. We kindly thank Marie-Claude Gingras for critical reading of the manuscript, and our laboratory colleagues for critical comments on this study. M.Y. was a holder of the Canadian Institutes of Health Research (CIHR) Doctoral Research Award. E.A.W. is recipient of a postdoctoral fellowship from CIHR and the Fonds de recherche du Québec–Santé (FRQS). Both M.Y. and E.A.W. are supported by the McGill Integrated Cancer Research Training Program (MICRTP) scholarship. This work is funded by the Kidney Foundation of Canada KFOC100021 (A.P.), the Myrovlytis Trust (A.P.), a Terry Fox Foundation team grant on Oncometabolism (116128), the New Innovation Fund CFI 21875 (V.G.), and McGill University.

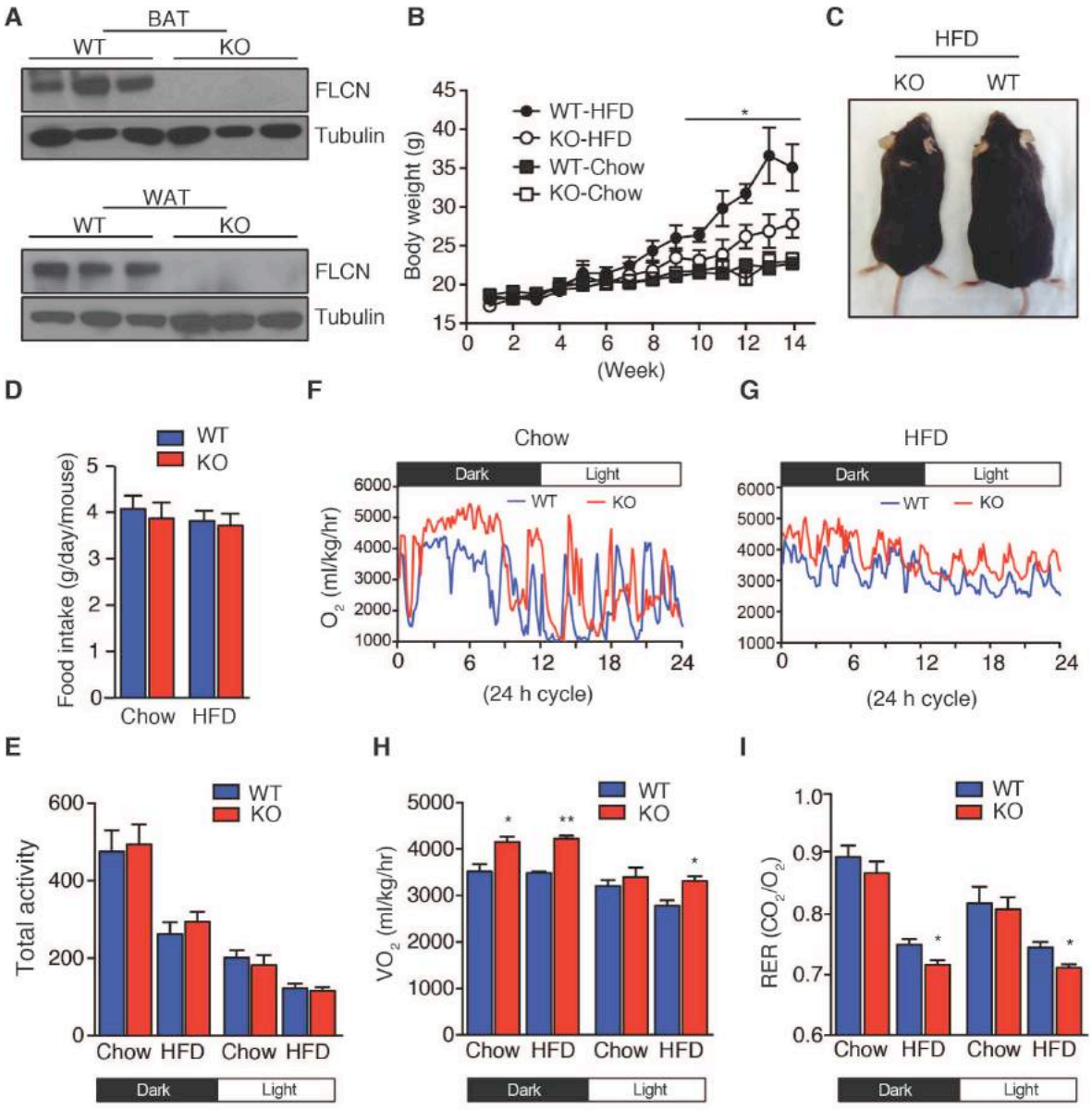

Figure 3.1. Adipose-specific *Flcn* deletion protects from HFD-induced obesity. (A) Western blot analysis of FLCN expression level in BAT (upper) and WAT (lower) of 5-month-old mice. Tubulin was used as loading control. (B-I) 6-week-old Adipoq-*Flcn* WT or KO mice were fed with either chow or HFD for 14 weeks. (B) Body weight was measured weekly (n=6 mice/group). (C) Representative picture taken from Adipoq-*Flcn* WT or KO 5-month-old mice fed with HFD for 13 weeks. (D-I) Metabolic cage analysis of 4-month-old mice fed with chow or

HFD were housed individually for 4 days. The food intake (D), total activity (E), representative VO2 consumption for a 12 hour dark and 12 hour light cycle (F, G), VO2 average (H), and the respiratory exchange ration (RER: VCO2/VO2) (I) were measured simultaneously. Data in B, D, E, H and I are presented as mean ±SEM (n=8-10 mice/genotype/diet). * $p<0.05$, ** $p<0.01$.

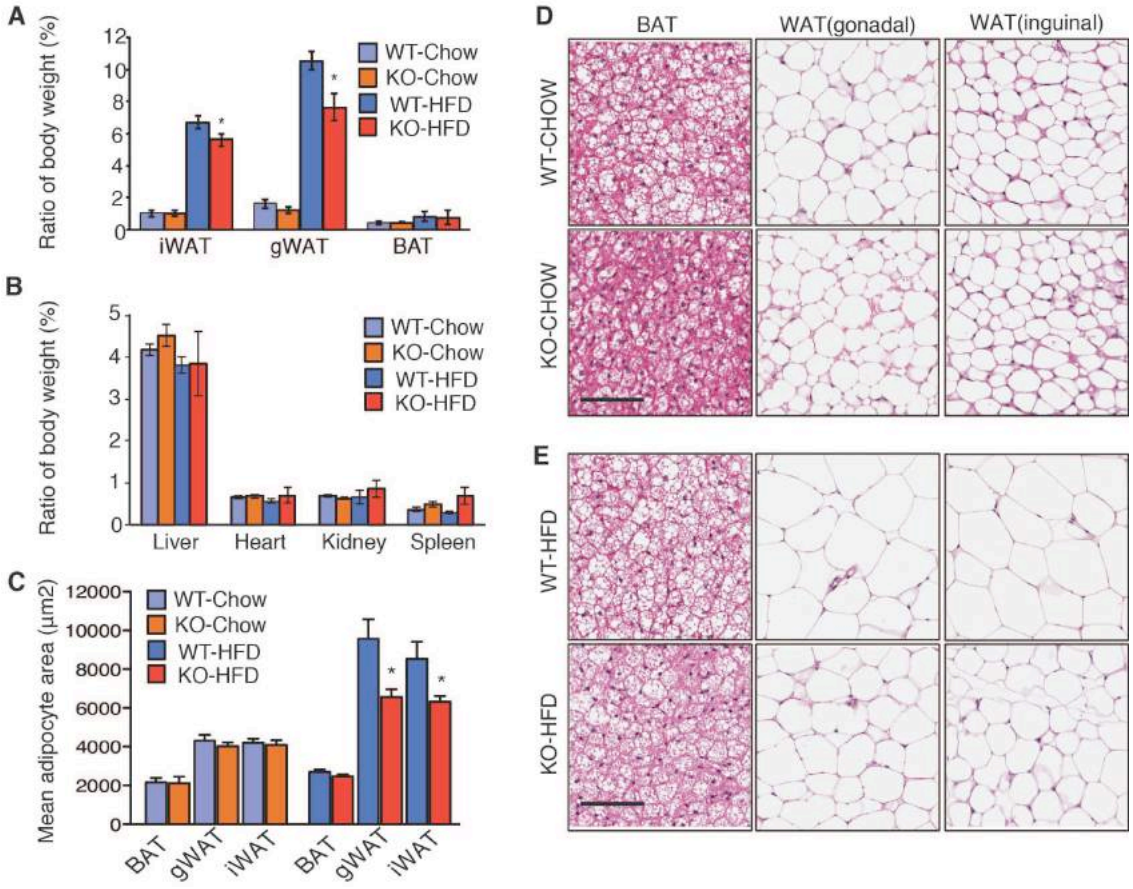

Figure 3.2. Adipose-specific *Flcn* KO mice on HFD display reduced WAT mass and smaller white adipocytes. (A) Fat index (percentage of fat pad weight relative to the whole body weight) of inguinal WAT, gonadal WAT, and BAT. (B) Percentage of liver, heart, kidney and spleen weight relative to body weight. (C) Mean adipocyte area of BAT, gonadal WAT, and inguinal WAT, quantified from H & E stained sections, 5 fields per mouse, using Metaxpress software. (D and E) Representative of H & E stained sections of BAT, gonadal WAT, and inguinal WAT from 5-month-old mice (magnification 20X; scale bar: 100 µm). Data in A, B and C are presented as mean±SEM. (n=6 animals/group). * $p<0.05$.

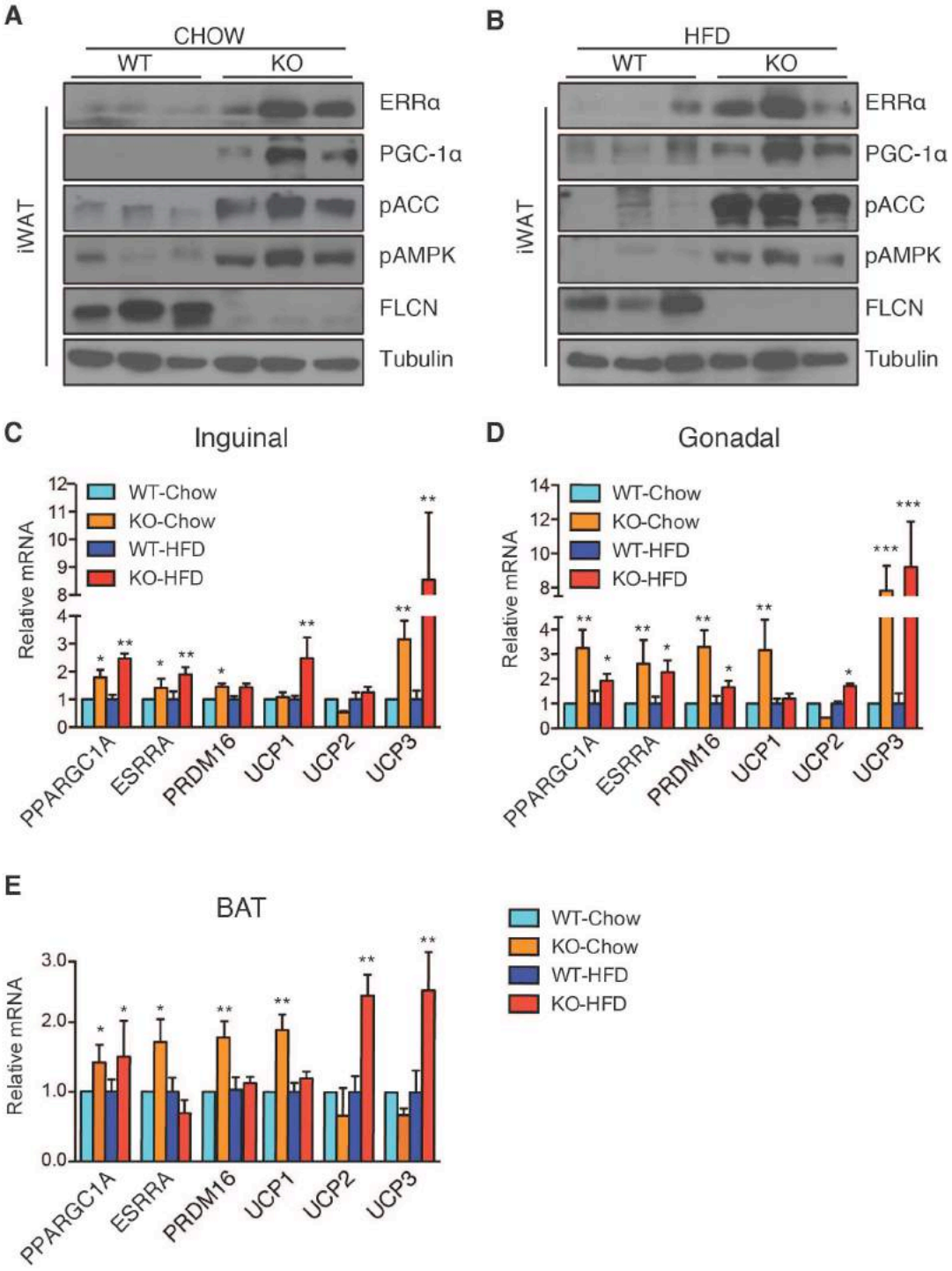
A
CHOW
WT
KO
iWAT
ERRα
PGC-1α
pACC
pAMPK
FLCN
Tubulin
B
HFD
WT
KO
iWAT
ERRα
PGC-1α
pACC
pAMPK
FLCN
Tubulin
C
Inguinal
Relative mRNA
WT-Chow
KO-Chow
WT-HFD
KO-HFD
PPARGC1A
ESRRA
PRDM16
UCP1
UCP2
UCP3
D
Gonadal
Relative mRNA
WT-Chow
KO-Chow
WT-HFD
KO-HFD
PPARGC1A
ESRRA
PRDM16
UCP1
UCP2
UCP3
E
BAT
Relative mRNA
WT-Chow
KO-Chow
WT-HFD
KO-HFD
PPARGC1A
ESRRA
PRDM16
UCP1
UCP2
UCP3

Figure 3.3. Loss of FLCN in WAT results in activation of AMPK and upregulation of downstream mitochondrial marker genes in lipid metabolism. (A-B) Western blot analysis performed with the indicated antibodies on WAT of 4-month-old mice few with CHOW (A) or HFD (B). Relative mRNA expression of indicated thermogenic genes determined by qRT-PCR in inguinal WAT(C), gonadal WAT (D), and BAT (E) of 4-month-old mice few with CHOW or HFD. Data in C, D and E are presented as mean±SEM. (n=6 mice/group). * $p<0.05$, ** $p<0.01$, *** $p<0.001$.

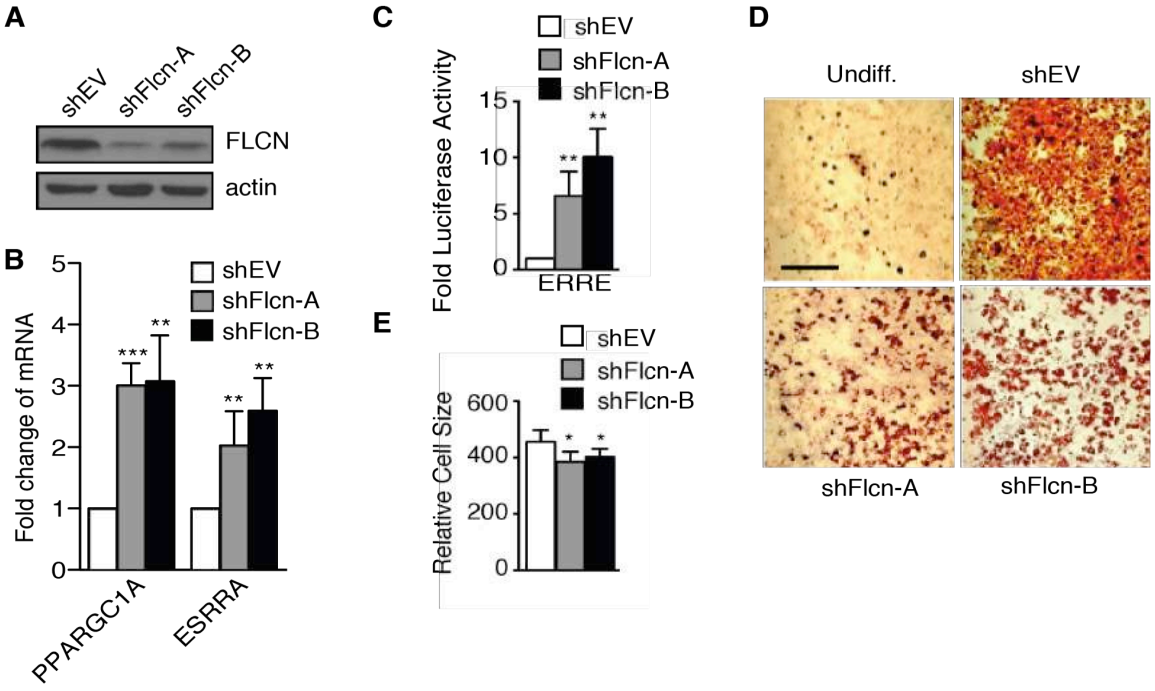

Figure 3.4. FLCN knockdown in 3T3L1 adipocytes inhibits lipid production and storage. (A) Western blot analysis of FLCN expression level in 3T3L1 adipocytes. (B) Relative mRNA expression of PGC-1α and ERRα by qRT-PCR following FLCN knockdown in 3T3L1 adipocytes using shRNA (shFlcn-A and shFlcn–B) or control (shEV). (C) ERRα activity assessed using ERRE luciferase reporter assay in 3T3L1 cells with or without FLCN knockdown. Relative units of cell size (D) measured by FACS analysis, and lipid droplet production (E) stained with oil red O in differentiated 3T3L1 adipocytes at day 6 after MDI (0.5 mM IBMX, 1 µg/ml insulin, and 10 µM dexamethasone) induction or without MDI as un-differentiated control. Pictures taken using a Axio Cam MRC Zeiss, scale bar, 20 µm. Data in B, C and E are presented as mean±SD of 4 independent experiments performed in triplicate. * $p<0.05$, ** $p<0.01$, *** $p<0.001$

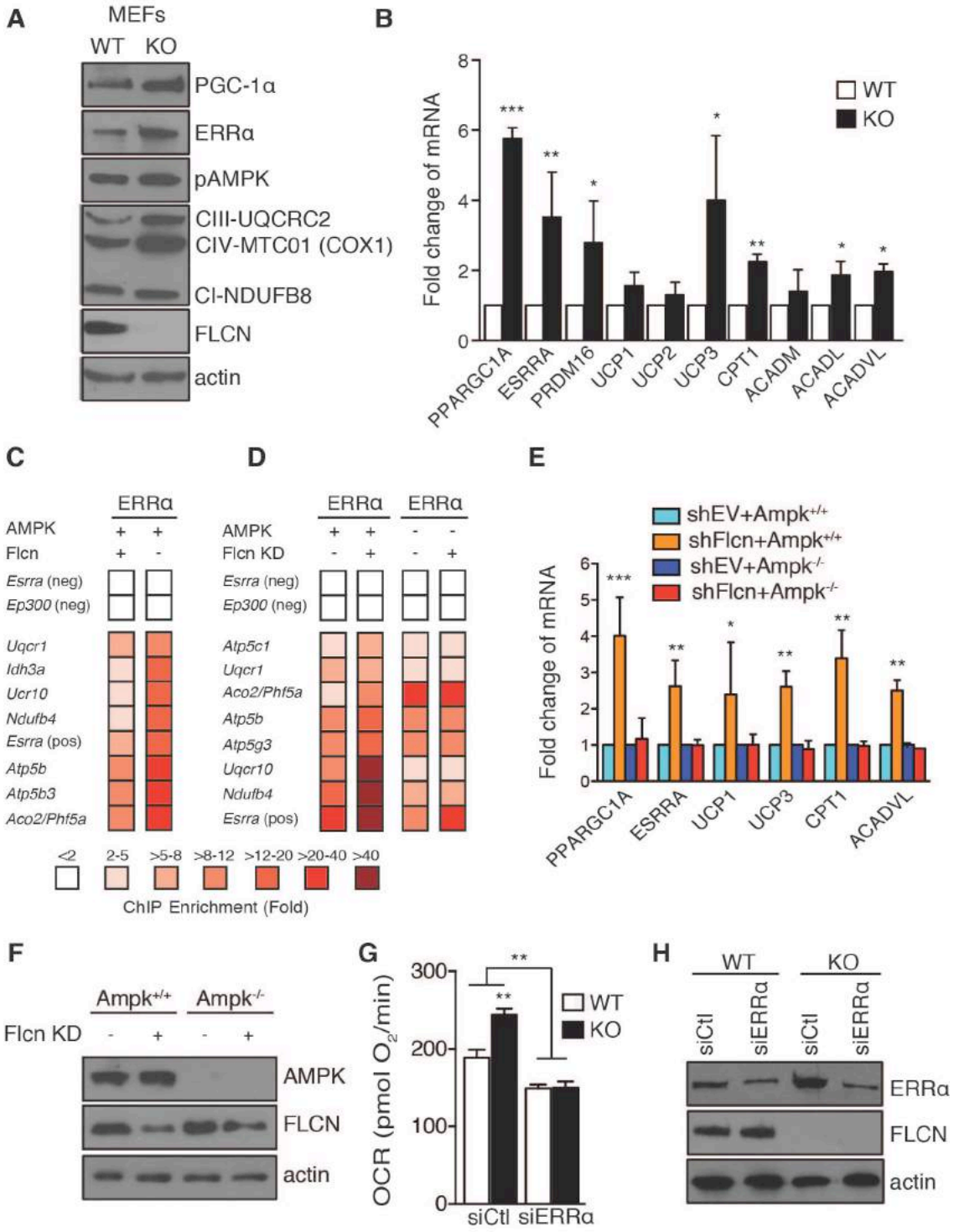
A
MEFs
WT KO
PGC-1α
ERRα
pAMPK
CIII-UQCRC2
CIV-MTC01 (COX1)
CI-NDUFB8
FLCN
actin
B
Fold change of mRNA
WT
KO
PPARGC1A
ESRRA
PRDM16
UCP1
UCP2
UCP3
CPT1
ACADM
ACADL
ACADVL
C
ERRα
AMPK
Flcn
Esrra (neg)
Ep300 (neg)
Uqcr1
Idh3a
Ucr10
Ndufb4
Esrra (pos)
Atp5b
Atp5b3
Aco2/Phf5a
D
ERRα
ERRα
AMPK
Flcn KD
Esrra (neg)
Ep300 (neg)
Atp5c1
Uqcr1
Aco2/Phf5a
Atp5b
Atp5g3
Uqcr10
Ndufb4
Esrra (pos)
<2
2-5
>5-8
>8-12
>12-20
>20-40
>40
ChIP Enrichment (Fold)
E
shEV+Ampk+/+
shFlcn+Ampk+/+
shEV+Ampk-/-
shFlcn+Ampk-/-
Fold change of mRNA
PPARGC1A
ESRRA
UCP1
UCP3
CPT1
ACADVL
F
Ampk+/+
Ampk-/-
Flcn KD
AMPK
FLCN
actin
G
OCR (pmol O2/min)
WT
KO
siCtl
siERRα
H
WT
KO
siCtl
siERRα
siCtl
siERRα
ERRα
FLCN
actin

Figure 3.5. Upregulation of PGC-1α/ERRα upon loss of FLCN is AMPK-dependent. (A) Western blot analysis of pT172 AMPKα, PGC-1α, ERRα and electron transport chain complex (CI-NDUFB8, CIII-UQCRC2, and CIV-MTC01) protein expression levels in MEFs. (B) Fold mRNA levels of the indicated thermogenic and fatty acid oxidation genes analyzed by qRT-PCR in Flcn WT or KO MEFs. Data are presented as mean±SD of 4 independent experiments performed in triplicate. (C) Relative fold enrichments of ERRα binding to metabolic target genes by ChIP-qPCR in Flcn WT or KO MEFs. (D) Relative fold enrichments of ERRα binding to metabolic target genes by ChIP-qPCR in AMPK-/- or AMPK+/+ MEFs with FLCN downregulation (shFlcn) or shEV as control. Data in C and D are presented as the average of 3 independent experiments. (E-F) Fold mRNA level analysis of target genes by qRT-PCR (E), and western blot analysis of FLCN and AMPK (F) in AMPK-/- or AMPK+/+ MEFs downregulated (shFlcn) for FLCN or (shEV) as control. For (E), data are presented as mean±SD of 4 independent experiments performed in triplicate. (G-H) Oxygen consumption rate (OCR) in *Flcn* WT or KO MEFs downregulated for ERRα using siRNA (siERRα) or control (siCtl) (n=5 per group). (H) Western blot analysis of ERRα expression level in Flcn WT or KO MEFs downregulated for ERRα using siRNA (siERRα) or control (siCtl). Actin was used as loading control. * $p<0.05$, ** $p<0.01$, *** $p<0.001$.

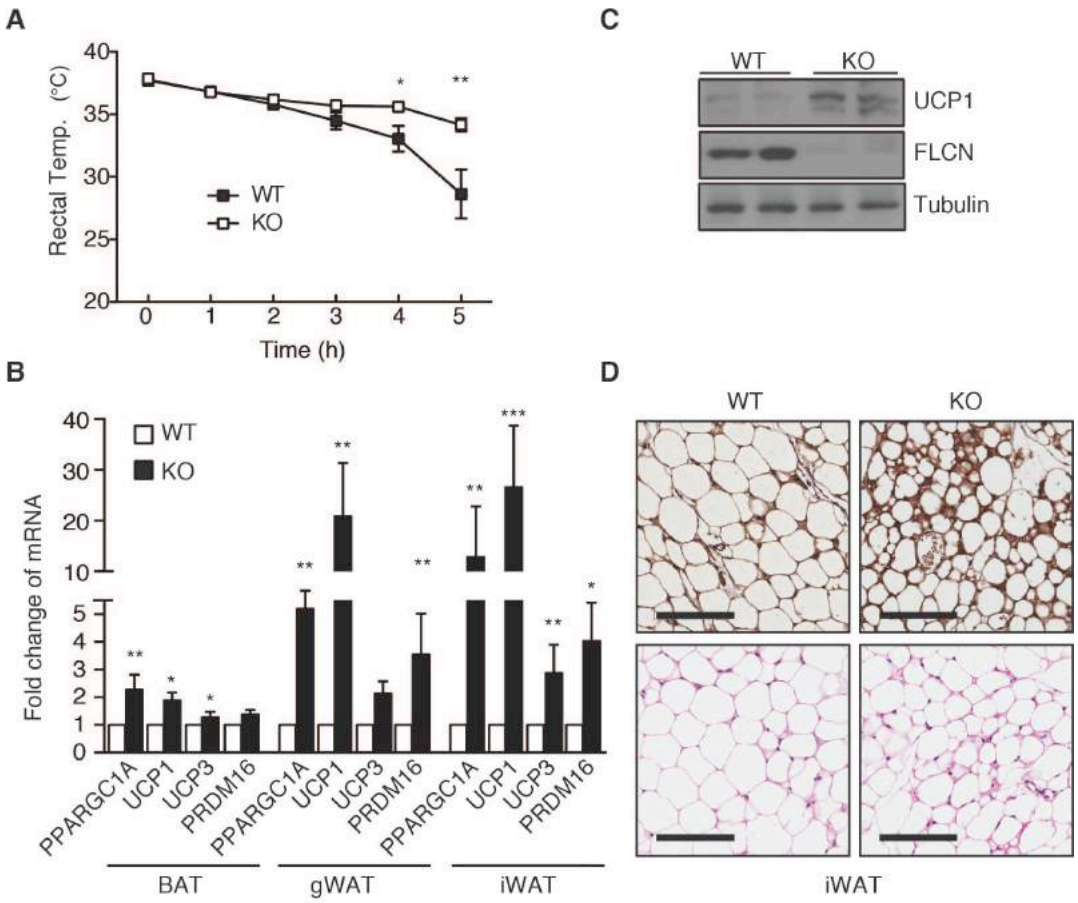

Figure 3.6. *Flcn* ablation in adipose tissue promotes cold resistance and browning of inguinal WAT. Three-month-old mice (Adipoq-FLCN KO or WT, n=6 animals/genotype) were housed at 30° C for 24 hours then transfer to 4° C in individual precooled cages. (A) Rectal temperature was assessed hourly for 5 hours using a rectal probe (Physitemp). (B) Relative mRNA expression of thermogenic marker genes determined by qRT-PCR in inguinal WAT, gonadal WAT, and BAT of *Flcn* WT or KO mice. (C) Western blot analysis of UCP1 in inguinal WAT of *Flcn* WT or KO mice. Tubulin was used as loading control. (D) Immunohistochemistry (IHC) staining with a UCP1 antibody (upper) and H&E

staining (lower) in inguinal WAT section of *Flcn* WT or KO mice. Scale bar, 100 μm. Data in A and B are presented as mean±SEM. (n=6 animal/genotype). * $p<0.05$, ** $p<0.01$, *** $p<0.001$.

Supplemental figures and legends

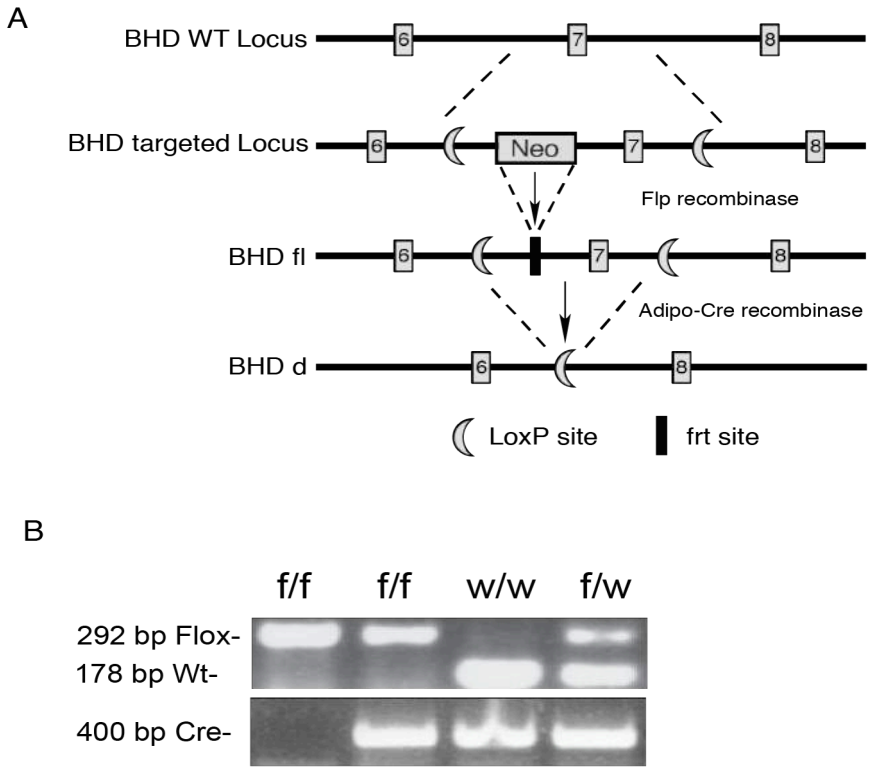

Figure 3.S1. Schematic representation of adipose-specific Flcn deletion. (A) Mice carrying *Flcn* alleles flanked by loxP sites were crossed with Adipoq-Cre transgenic mice to generate adipose-specific *Flcn* knockout mice. (B) Representative PCR based genotyping of *Flcn* WT (Adipoq-*Flcn*+/+), or KO (Adipoq-*Flcn*-/-).

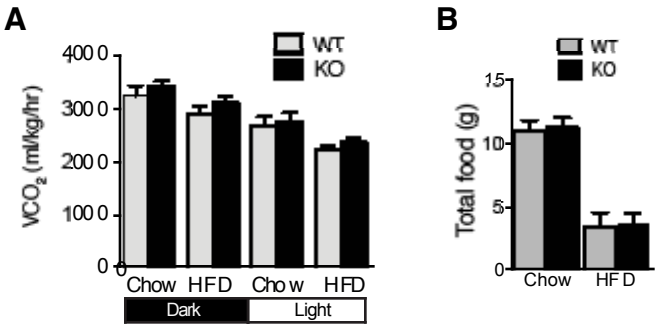

Figure 3.S2. Total CO2 production and food intake in adipose-specific Flcn WT or KO mice (A-B) Metabolic cage analysis of 4-month-old mice fed with chow or HFD were housed individually for 3 days. VCO2 production for a 12 hours dark and 12 hours light cycle (A) and total food intake (B) were measured. Data represent the mean ± SEM (n=8 animals/genotype/diet).

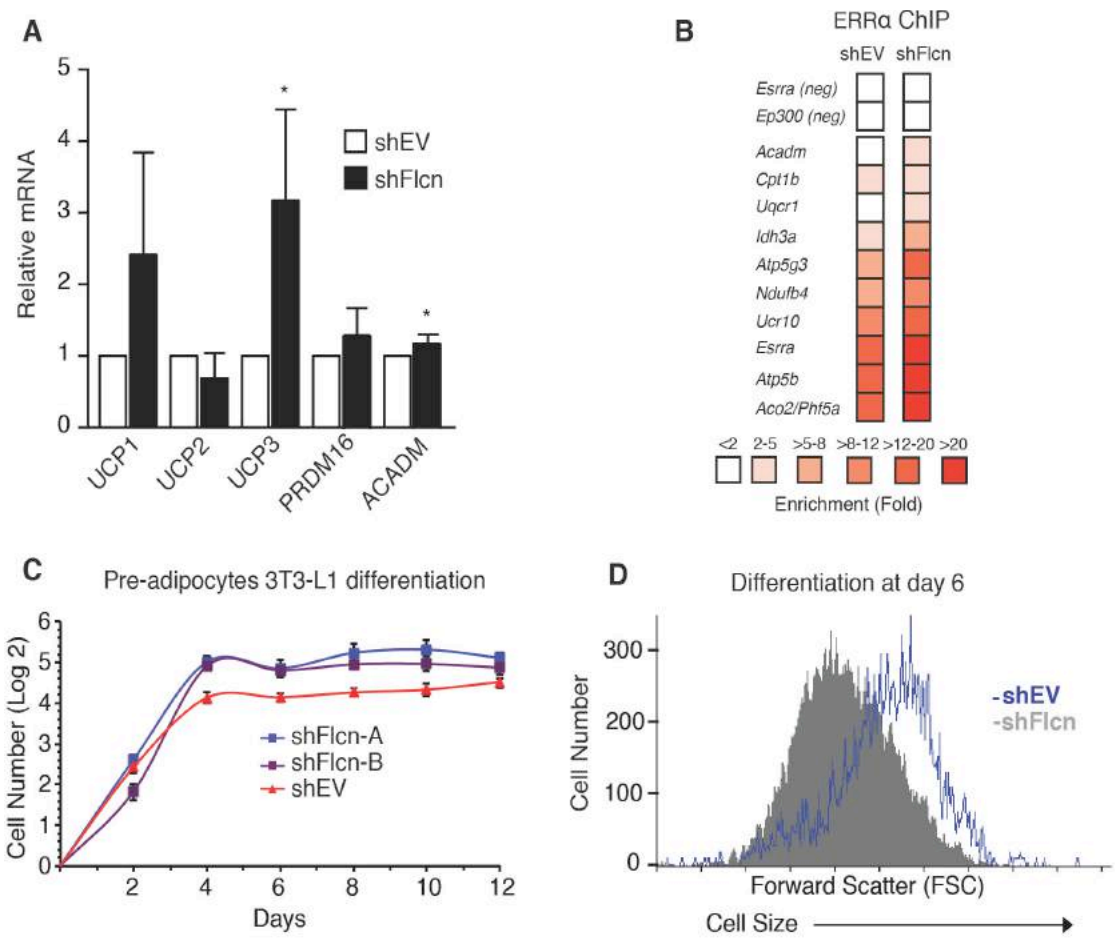

Figure 3.S3. FLCN knockdown in 3T3L1 adipocytes increases ERRα binding to metabolic target genes. (A) Relative fold enrichments of ERRα binding to metabolic target genes by ChIP-qPCR following FLCN repression in 3T3L1 adipocytes using shRNA (shFlcn) or control (shEV). Data are presented as the average of 3 independent experiments. (B) Fold mRNA levels of the indicated thermogenic and fatty acid oxidation genes by qRT-PCR. (C) Proliferation rate of differentiated 3T3L1 adipocytes downregulated (shFlcn-A and shFlcn-B) for FLCN or empty vector (shEV) as control was determined by cell counting in time course. (D) Size of adipocytes assessed by FACS. Data are presented as mean±SD of 4 independent experiments performed in triplicate. * $p<0.05$.

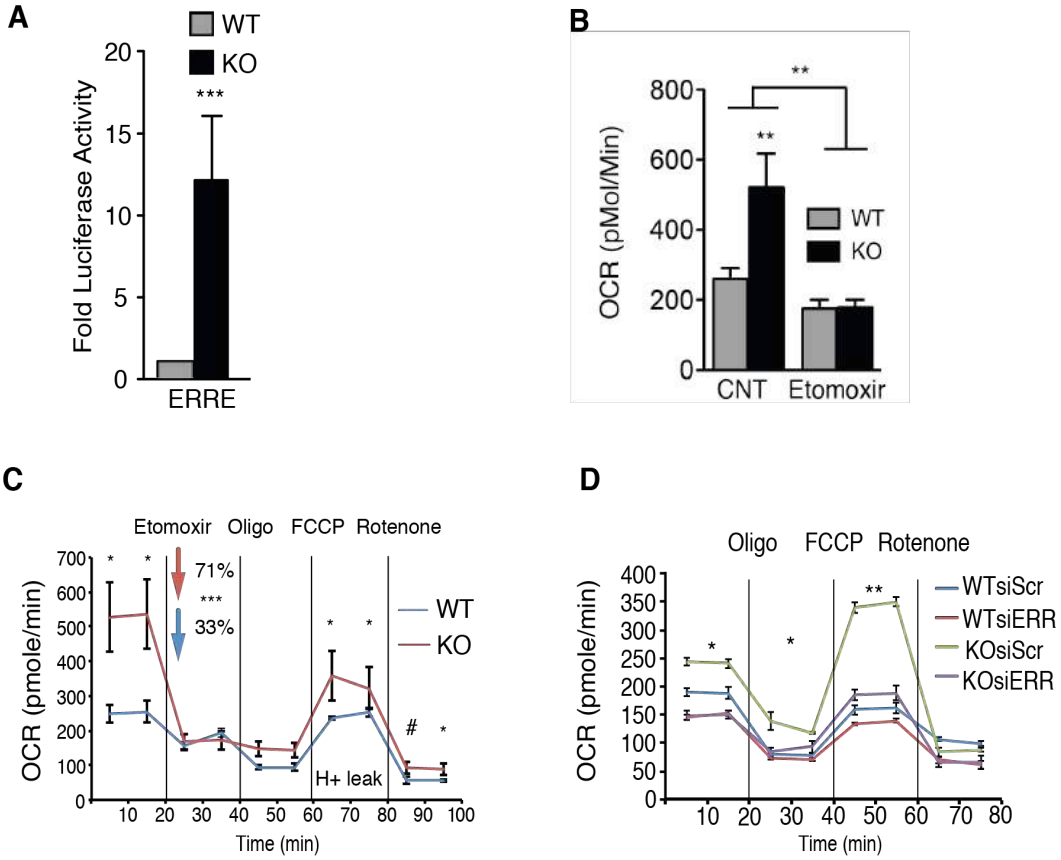

Figure 3.S4. Elevation of oxygen consumption upon loss of FLCN is ERRα dependent. (A) Fold change of ERRα activity assessed using ERRE luciferase reporter assay. (B-C) Oxygen consumption rate (OCR) in *Flcn* WT or KO MEFs assessed using XF24 Extracellular Flux analyzer. Etomoxir was used as CPT-1 inhibitor, to block the entry of fatty acids in the mitochondria. (D) OCR determined in *Flcn* WT or KO MEFs, with or without ERRα downregulation using targeted siRNA (siERRα) or control (siNT). For B-D, representative experiments are shown as mean±SD (n=5). * $p<0.05$, ** $p<0.01$, *** $p<0.001$.

Table 3.S1 Primers used for real-time PCR and ChIP analysis

mRNA	Fwd	Rvs
Ppargc1a	*CAGTCCTTCCTCCATGCCTG*	*GGGTTTGTTCTGATCCTGTGG*
Pparα	*GCGTACGGCAATGGCTTTAT*	*GAACGGCTTCCTCAGGTTCTT*
Pparγ	*AGGCCGAGAAGGAGAAGCTGTTG*	*TGGCCACCTCTTTGCTCTGCTC*
Prdm16	*CAGCACGGTGAAGCCATTC*	*GCGTGCATCCGCTTGTG*
Esrra	*CTCAGCTCTCTACCCAAACGC*	*CCGCTTGGTGATCTCACACTC*
Ucp1	*CTTTGCCTCACTCAGGATTGG*	*ACTGCCACACCTCCAGTCATT*
Ucp2	*CAGGTCACTGTGCCCTTACCAT*	*CACTACGTTCCAGGATCCCAAG*
Ucp3	*GCCTTCTCTCTCGGAGGTTT*	*GCAGATGGAAGACTGAAGGC*
Cpt1	*GACCCTAGACACCACTGGCCG*	*GAGAAGACCTTGACCATAGCC*
Acadm	*ACTTCGTGGCTTCGTCTAGA*	*GAGCAGGTTTCAAGATCGCA*
Acadl	*TTTCCGGGAGAGTGTAAGGA*	*ACTTCTCCAGCTTTCTCCCA*
Acadvl	*GTGAATGACCCTGCCAAGAACGAC*	*CCACAATCTCTGCCAAGCGAGC*
Rplpo	*GCAGCAGATCCGCATGTCGCTCCG*	*ACCAGACGGTTCAGTTCTGC*
ChIP		
Atp5g3	*CAAGGGTGAAGGAGAGCCG*	*CTGTCACCTAGATCCACGCC*
Ndufb4	*CAGTCCAGGGTGGGTTCTTC*	*GGGGCGTAGCTAGGGAAATG*
Atp5b	*TCTTCTCCCCGTGACCTTGA*	*AAATGGGACGCTGCTGGTTA*
Atp5c1	*ACCCAGCAAAGAGTCGGATG*	*GGAGCACAGCTTGCAAAGTC*
Uqcr1	*TCTTGCAATGGTCGCCTTCT*	*CACTTACCGTGCAGGTAGCA*
Uqcr10	*TGGAGTGGTTCAGACCCGTA*	*AGGGAGGTAGGACGGAACTC*
Aco2/Phf5a	*CATGCTTCCGCCAAGTATGTTG*	*CCTTGTCACCTTTGCCCTTG*
Acadm	*GAAGGTCACGTTCTTTCCAGAGG*	*GATCTAGCCCAGAATTTGTTGTTCC*
Cpt1b	*CAGGTTTGCTTCTGTCGGTGTATGG*	*CACCCCTATCTGTTTTCTCCACCCC*
Idh3a	*AAGGCGCTTCAGGTTACATA*	*CCACGACGGCATCAGATGAC*
EP300	*TCCATACCGAACAAAGGCCC*	*CAATCCCCTTGCCATTCCCT*
Ep300 negative region	*TCCATACCGAACAAAGGCCC*	*CAATCCCCTTGCCATTCCCT*
Esrra positive region	*GTGGCCCCGCCTTTCCCCGTGACCTTCATT*	*ACCCCTGAGGACCCTCAAGTGGAGAAGCA*
Esrra negative region	*TTGGCATTGATATTGGGGGTGGGAGCAACT*	*GACTTCTTACTTTGACGCTTTCCTCCATCG*

CHAPTER 4:
DISCUSSION

Although FLCN and its binding partners FNIP1 and 2 were identified as AMPK interactors [43], its tumor suppressor mechanism and metabolic adaptation in cellular energy homeostasis involved in AMPK regulation are not elucidated. Our previous reports using the RCC cell line, UOK-257, demonstrated that loss of FLCN enhances transcriptional activity of HIF and increases the glycolytic rate in hypoxia [192]. Additionally, HIF-1α expression was increased in cystic lung tissue resected from a BHD patient, suggesting that FLCN inhibits HIF signaling in normoxia [71]. Indeed, upon stress, energy levels are maintained by increased mitochondrial biogenesis and glycolysis, controlled by transcriptional coactivator PGC-1α and HIF, respectively. A recent publication by Hasumi and coworkers also indicated that muscle-specific *Flcn* knockout in mice results in increased mitochondrial oxidative phosphorylation through PGC-1α upregulation associated with enhanced ATP synthesis and mitochondrial biogenesis, suggesting that FLCN is highly correlated to cellular energy metabolism [83]. The initial goal of chapter 2 presented in this thesis was to determine how FLCN regulates HIF metabolic adaptation through AMPK energy sensor in normoxia, and if this regulation is linked to tumorigenesis.

4.1 FLCN loss drives AMPK-dependent cellular metabolic transformation, which promotes tumorigenesis

Using untransformed *Flcn*$^{-/-}$ mouse embryonic fibroblasts (MEFs) we observed that loss of FLCN induces transcriptional activity of HIF but not its protein stability, which enhances HIF-dependent aerobic glycolysis and ATP production (Fig 2.1). Importantly, down-regulation of HIF-1α using shRNAs confirmed that the increased aerobic glycolysis and ATP levels observed in *Flcn* KO cells are HIF-1α dependent.

We demonstrate that loss of FLCN binding to AMPK results in AMPK activation and uncover a novel pathway linking for the first time AMPK-PGC-1 and mitochondrial ROS production to HIF transcriptional activity, aerobic

glycolysis metabolic adaptation and ATP production. Our results suggest that in absence of FLCN, AMPK energy sensing function is inhibited leading to constitutive AMPK-dependent metabolic adaptation in the absence of energy demands (Figure 2.4).

Using a non-phosphorylatable form of FLCN (S62A mutation) at a previously identified AMPK phosphorylation and binding site, we established that loss of FLCN binding to AMPK also results in constitutive AMPK activation (Figure 2.4). Chronic AMPK activation leads to upregulation of PGC-1a, a known target of AMPK, which in turn increases mitochondrial content and oxidative phosphorylation rate, leading to enhanced production of ROS.

Since increased ROS and HIF activation have been independently shown to promote tumorigenesis, it would be worthwhile to further determine if this signaling connection from ROS to HIF is relevant to other types of cancers. Interestingly, it was recently shown that FLCN expression negatively correlates with PGC-1α activation in numerous tumors such as breast, cervix, colon, kidney, lung, lymph, ovary, pancreas, prostate, stomach, thyroid, and vulva. Specifically, the PGC-1α gene set and other OXPHOS gene sets correlated negatively with FLCN expression across all tumor types examined [82].

While HIF activation has been associated with tumor development in mammals, it leads to extension of lifespan in nematodes. Indeed, a loss of function mutation of the VHL tumor suppressor gene in *C. elegans* promotes HIF1-α-dependent increase in life span [137]. Interestingly, promotion of *C. elegans* longevity upon transient AMPK-dependent increased of ROS or upon ROS-mediated HIF-1 activation has been independently reported [115, 138, 139]. Together with these studies, our results suggest the existence of an AMPK driven pathway activating HIF-mediated metabolic adaptation through ROS, which appears conserved in lower organisms.

Surprisingly, elevated mitochondrial ROS production is not associated with

increased oxidative protein and DNA damage, but rather acts as a signaling molecule to activate HIF transcriptional activity without affecting HIF-1a protein stability (Figure 2.2). Upon FLCN depletion, the active HIF complex mediates transcription of glycolytic effectors, thus enhancing glucose uptake and the glycolytic rate. Strikingly, knockout of AMPK, knockdown of PGC-1a, or reduction of ROS levels by antioxidants abolish the HIF-dependent glycolytic increase (Figure 2.3).

By concomitantly upregulating mitochondrial oxidative phosphorylation and glycolysis, the chronic AMPK activation induced by FLCN deficiency increases cellular ATP levels and biosynthetic precursors, mimicking the metabolic signature of highly proliferative cells. Interestingly, this metabolic transformation is not associated with a direct effect on cell proliferation or spontaneous transformation of primary cells per se (Figure 2.S3). However, loss of FLCN significantly enhances the HIF-1α -dependent tumor growth of human cancer cell lines (Figure 2.6). Finally, HIF-1α nuclear translocation and upregulation of glycolytic effectors controlled by HIF were observed in a chromophobe tumor from a BHD patient (Figure 2.7), further suggesting that FLCN deficiency induces AMPK- and HIF-dependent metabolic reprogramming that confers a tumorigenic advantage *in vivo*.

Overall in chapter 2 we found that upon loss or S62A mutation of FLCN, AMPK is activated by phosphorylation via an unidentified kinase (Kinase X) which in turn leads to elevation in PGC-1α, which mediates mitochondrial biogenesis and increase reactive oxygen species (ROS) production. Elevated ROS induces hypoxia-inducible factor (HIF) transcriptional activity and drives Warburg metabolic reprogramming. These findings indicate that FLCN exerts tumor suppressor activity by acting as a negative regulator of AMPK-dependent HIF activation and Warburg effect that confers a tumorigenic advantage [75, 193]. However, how AMPK was activated through the 172 phosphorylation site, upon FLCN loss or mutation is not elucidated yet. Further experiments are needed to

screen the upstream of potential kinase, which may phosphorylate and activate AMPK through dynamic of the FLCN/FNIP/AMPK complex (Figure 4.1).

4.2 AMPK/PGC-1/ROS/HIF pathway upon loss of FLCN in cancer cells is conserved

AMPK has been proposed to be a contextual oncogene that may confer a survival advantage under selection pressure, suggesting an involvement in tumor progression rather than in tumor initiation [194]. To determine whether the metabolic transformation induced upon loss of FLCN would promote a tumorigenic advantage in AMPK dependent manner in an established cancer cell line, we choose human follicular thyroid cancer cell line FTC-133, which is naturally FLCN deficiency, to test beneficial for tumor progression and metastasis using soft agar and xenograft. In agreement with our previous observation, FTC-133 cells exhibited an increase in AMPK activation, PGC-1α levels, mitochondrial biogenesis, ROS production, transcriptional upregulation of HIF target genes in absence of HIF-1α stabilization and an increase in aerobic glycolysis (glucose uptake) and ATP levels (Figure 2.6) compared with FLCN-rescued FTC-133 cells.

Strikingly, we observed a significant increase in the number of soft agar colonies in FTC-133 cells (Figure 2.6 and Supplemental Figure 2.S4). In addition, FLCN deficiency in FTC-133 cells was associated with an increased tumour volume and growth rate when compared with that in FLCN-rescued cells (Figure 2.6 and Supplemental Figure 2.S4). Moreover, downregulation of HIF-1α completely abolished the increased colony numbers and an increased tumor volume and growth rate. Taken together, these data suggest that the AMPK/PGC-1α/ROS/HIF pathway identified in FLCN-null MEFs and UOK-257 cells is conserved in the human FTC-133 cancer cell line.

To test the relevancy of our finding for human BHD disease, we performed immunohistochemistry staining on normal kidney tissues and a chromophobe

tumor isolated from a patient with BHD. We observed an increase in the mitochondrial marker (MTC02) (Figure 2.7A). Moreover, we detected an increase in HIF-1α nuclear staining associated with an increase in HIF target gene staining (BNIP3, GLUT1, VEGF-A) (Figure 2.7B), suggesting that loss of FLCN stimulates mitochondrial biogenesis and HIF-1 signaling during renal tumor progression in patients with BHD. Altogether, our data strongly suggest that loss of FLCN induces an AMPK-HIF-dependent metabolic reprogramming, resulting in an energetic advantage, which favors tumor progression *in vivo*.

Our observations in this cell line importantly confirm that our research findings presented in this manuscript have wider implications to other cancers, rather than only being restricted to tumors developed in BHD patients. Our study suggests that loss of FLCN expression lead to activation of the AMPK/PGC-1α/OXPHOS/HIF signaling axis, which is an important driver of sporadic tumors in multiple organs. As a continuation of this work, it will be important to assess these pathways in BHD mouse models and to compare them in cancer models to determine potential therapeutic benefits in the treatment of BHD disease in specific and other kidney cancers.

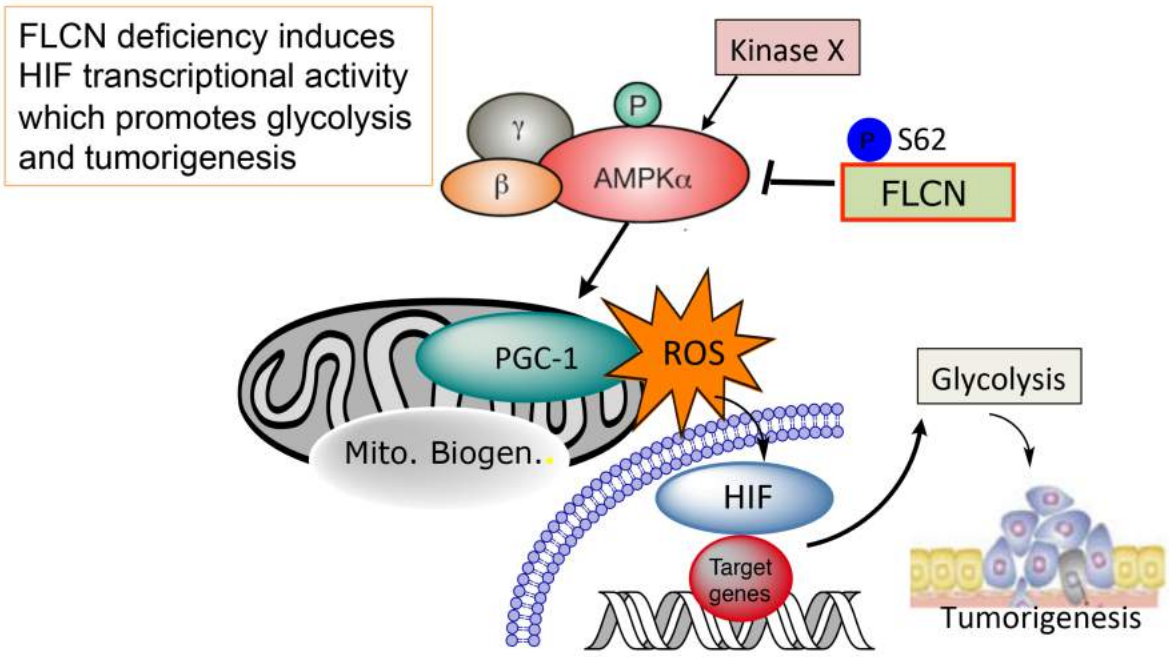

Figure 4.1. FLCN regulates AMPK activation and downstream Warburg metabolic reprogramming and tumorigenesis.

Folliculin (FLCN) binds and inhibits phosphorylation (P) of AMP-activated protein kinase (AMPK) via serine 62 (S62), a previously described AMPK phospho-site. Upon loss of FLCN, AMPK is activated by phosphorylation through an unidentified kinase (Kinase X) and stimulates transcription and expression of peroxisome proliferator-activated receptor g coactivator 1 (PGC-1), leading to enhanced mitochondrial biogenesis and reactive oxygen species (ROS) production. This drives hypoxia- inducible factor (HIF) transcriptional activation and enhances Warburg metabolic reprogramming.

Adapted from [193]

4.3 Does FLCN deficiency reduce or induce mTOR activation?

The functional role of FLCN in mTOR signaling in mammals is unclear since several publications have reported contradictory effects of FLCN deficiency on phosphorylated ribosomal protein S6 (p-S6R), an indicator of mTOR activation. Three studies reported that transient downregulation of FLCN by siRNA in human cell lines results in reduction of phosphorylation of p-S6R [45, 195, 196]. Reduction of p-S6R was also observed in renal cysts developing in mice heterozygous for FLCN [195].

In contrast, kidney-specific homozygous knockout of FLCN resulted in an increase in phosphorylated p-S6R, which contributed to the development of polycystic kidneys [165, 197, 198]. Additionally, an activation of mTOR signaling in the kidney *Flcn*$^{+/-}$ heterozygous mice was observed by Hasumi et al [199]. Interestingly, a third *Flcn*$^{+/-}$ heterozygous mouse model demonstrated both mTOR activation (elevated phosphoS6 in large cysts) and inactivation (reduced phosphoS6 in small cysts) [166]. The conflicting results presented in these *in vitro* and *in vivo* systems raise the question of why FLCN, a tumor suppressor, has variable effects on cellular metabolism.

We proposed that the effect of FLCN deficiency on mTOR activation or inhibition might depend on an AMPK-dependent role in maintaining cellular bioenergetic homeostasis. Normally, FLCN loss leads to AMPK activation. Once activated, AMPK maintains energy balance by switching cells from an anabolic (ATP consumption), to a catabolic (ATP production) state, therefore turning off mTOR pathway, until restoration of enough energy to grow and survive. However, the chronic AMPK activation caused by FLCN knockout in our model was observed in the absence of energy demand. BHD cancer cells need to generate all building blocks necessary to grow and survive in high metabolic rate which was obtained by increased mitochondrial and biogenesis, glycolysis, and as well as an intrinsic mTOR-dependent metabolic adaptation by unknown mechanism. Additional studies are necessary to clarify this hypothesis involved in the multi-function of FLCN "turning on" both of AMPK and mTOR in BHD patients. Interestingly, we recently observed that liver-specific *Flcn* KO mice demonstrate mTOR activation under fasting condition and inactivation under non-fasting as both keep the AMPK hyperactivation (Yan

et.al unpublished data). It is likely that liver-specific *Flcn* KO mice show much plasticity responsible for energy homeostasis.

4.4 **Chronic AMPK activation via loss of FLCN induces functional beige adipose tissue through PGC-1α/ERRα**

Obesity, one of the most serious public health problems worldwide, is initiated from a chronic imbalance between energy intake and expenditure and is a major risk factor for metabolic syndrome such as type-2 diabetes, hypertension, cardiovascular diseases, obesity and certain cancers.

In the past few years, much interest has been put in the study of white adipose tissue browning, notably for its potential as anti-diabetic and anti-obesity function in humans. The underlying mechanism of this inducible conversion of white adipocytes into metabolically active adipocytes has attracted much attention. In chapter 2 we reported that folliculin (*Flcn*), a tumor suppressor responsible for the Birt-Hogg-Dubé cancer syndrome, is a negative regulator of AMPK both in *C. elegans* and mammalian cell systems. Loss of FLCN enhanced mitochondrial biogenesis via AMPK-dependent PGC-1α upregulation. Importantly, both of AMPK and PGC-1α are master regulators of energy homeostasis. These findings led us to hypothesize that FLCN might be involved in whole body energy metabolism. To address this question, and because global knockout of *Flcn* is embryonically lethal, we generated an adipose-specific *Flcn* knockout mouse model to investigate molecular function of FLCN involved in adipocyte metabolism.

4.4.1 Adipose-specific *Flcn* KO mice exhibit elevated energy expenditure and are resistance to high fat diet (HFD)-induced obesity

In Chapter 3, we demonstrate that deletion of *Flcn* in mouse adipose tissues leads to a complete metabolic reprogramming of white adipocytes. This metabolic switch allows these Adipoq-*Flcn* KO mice to exhibit significantly higher energy expenditure associated with an increase in mitochondrial respiration. Importantly, this remodelling of white

adipose tissue metabolism induces several advantages *in vivo*, including resistance to high fat diet-induced obesity by burning more lipids and increased adaptive thermogenesis. (Figure 3.1).

Nevertheless, we only chose the female FLCN adipose KO mice in this study since they showed a stronger phenotype than male. It is not clear how this occurs and which factors or genes are involved in the process of adipose metabolic disorder. Interestingly, it was reported that AMPK-dependent upregulation of PGC-1α in female mice is remarkably higher than male [200]. A further investigation is required to detect where the phenotype is correlated linkage between genders in PGC-1α molecular signalling in fat metabolism.

4.4.2 Loss of FLCN leads to an increase in AMPK-dependent PGC-1α and ERRα signalling

At the molecular level, we demonstrated that the absence of FLCN in WAT leads to a hyperactivation of AMPK, thereby inducing the activity of the PGC-1α/ERRα transcriptional axis (Figure 3.3). Importantly, both AMPK and PGC-1α are master regulators of energy homeostasis. Together, they positively modulated the expression of nuclear-encoded mitochondrial genes to promote mitochondrial activity and lipid metabolism. Overall, our results demonstrate a critical role of FLCN as a negative regulator of lipid metabolism in WAT functionally linking the FLCN/AMPK and the PGC-1α/ERRα transcriptional axis.

Conversely, we first uncover an AMPK-dependent PGC-1α and ERRα signalling pathway in white adipose in this study, but the role of FLCN loss in brown fat adaptive metabolism has not been elucidated yet. Even though there is only a small mass of BAT compared to that of WAT and much less increase of thermogenic genes level induced by the Adipoq-*Flcn* KO mice, its contribution to resistance to obesity and fat burning might be as significant as WAT since the thermogenic genes is rich in BAT.

4.4.3 FLCN ablation enhances resistance to cold

Accordingly, in the thermogenic experiments in chapter 3, we demonstrate that mitochondrial uncoupling proteins (UCP1 and UCP3) are both upregulated in *Flcn* KO white adipose tissue, which produce heat instead of ATP. Moreover, we observed that activation of AMPK promotes β-fatty acid oxidation through pACC and CPT-1 upregulation. Additionally, these mice have increased resistance to cold exposure associated with browning of white adipose tissue (WAT), a phenomenon usually known as adaptive thermogenesis that relies on heat production in brown adipocytes mitochondria through uncoupled respiration (Figure 3.6).

Clearly, the results presented in chapter 3 not only uncover a novel signalling pathway linking AMPK activity to uncoupling via PGC-1/ERRα upregulation, which in turn induce mitochondrial biogenesis and fatty acid oxidation but also shed further light on how FLCN induced AMPK-dependent PGC-1α/ERRα drive a metabolic advantage, which has wider implications for human metabolic disorders such as obesity, fatty liver and diabetes. Further investigations are required to determine if this novel FLCN regulated AMPK/PGC-1/ERRα signalling pathway could benefit human beings.

In summary, we revealed that FLCN ablation leads to AMPK activation through loss of binding of the FLCN-FNIP-AMPK complex. AMPK-dependent upregulation of PGC-1α and ERRα promote nuclear-encoded mitochondrial gene expression, which results in an increase in mitochondrial respiration and uncoupling proteins expression. In parallel, activation of AMPK promotes FAO through inactivation of ACC, and promotes CPT-1 upregulation for increased OXPHOS in mitochondria (Figure 4.2). These results show an unexpected role for FLCN in metabolic control and identify a novel molecular pathway involved in browning of white adipocytes. The findings described here also highlight new possibilities for obesity treatment strategies through the role of FLCN in adipocyte metabolism.

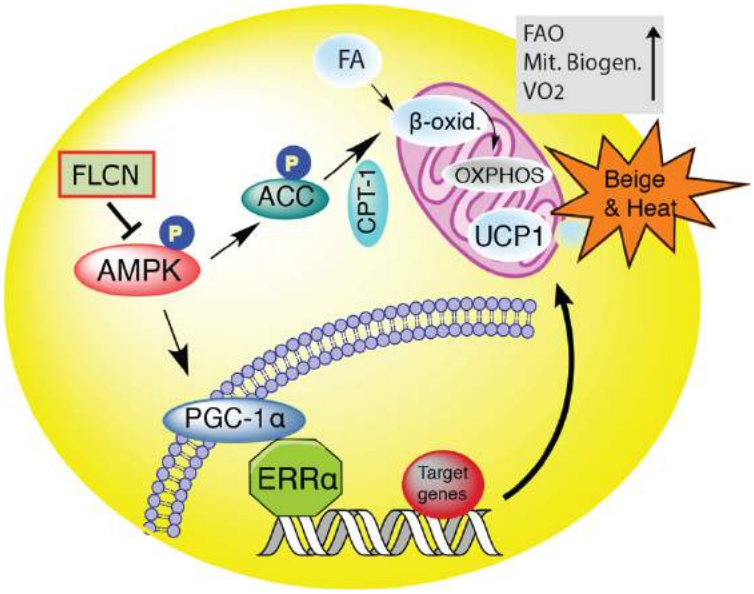

Figure 4.2. A schematic of *Flcn* regulated energy metabolism in white adipocytes through the AMPK/PGC-1α/ERRα pathway.

FLCN ablation leads to AMPK activation through destabilisation of the FLCN-FNIP-AMPK complex. Activated AMPK induces upregulation of PGC-1α and ERRα to promote nuclear-encoded mitochondrial gene expression, which results in an increase in mitochondrial biogenesis, uncoupling protein expression and O2 consumption. In parallel, activation of AMPK promotes FAO through inactivation of ACC, via direct phosphorylation, and promotes CPT-1 upregulation, which functions as a shuttle allowing entry of fatty acids in mitochondria for OXPHOS. Overall, *Flcn* deletion in white adipocytes exhibits a high FAO profile, more oxygen consumption and heat production

4.5 CONCLUSION

The work presented in this thesis contributes important findings to the understanding of the tumor suppressor function of FLCN and the molecular signalling pathways involved in cellular energy metabolism linked to kidney cancers, obesity and diabetes.

Our work represents a major advancement in cell metabolism, being the first characterizing the role of FLCN as a negative regulator of AMPK. We demonstrated that loss of FLCN drives tumorigenic metabolic adaptation by ROS induced by AMPK/PGC-1α/OXPHOS/HIF signalling axis. We also characterized the role of FLCN in white adipocyte browning, identifying the PGC-1α/ERRα axis downstream of AMPK, acting as critical determinant of AMPK-mediated mitochondrial activity and WAT reprogramming.

REFERENCES

1. Birt, A.R., G.R. Hogg, and W.J. Dube, *Hereditary multiple fibrofolliculomas with trichodiscomas and acrochordons.* Archives of dermatology, 1977. **113**(12): p. 1674-1677.

2. Choyke, P.L., et al., *Hereditary Renal Cancers 1.* Radiology, 2003. **226**(1): p. 33-46.

3. Choyke, P.L., *Imaging of hereditary renal cancer.* Radiologic Clinics of North America, 2003. **41**(5): p. 1037-1051.

4. Linehan, W.M., M.M. Walther, and B. Zbar, *The genetic basis of cancer of the kidney.* The Journal of urology, 2003. **170**(6): p. 2163-2172.

5. Liaw, D., et al., *Germline mutations of the PTEN gene in Cowden disease, an inherited breast and thyroid cancer syndrome.* Nature genetics, 1997. **16**(1): p. 64-67.

6. Maehama, T. and J.E. Dixon, *PTEN: a tumour suppressor that functions as a phospholipid phosphatase.* Trends in cell biology, 1999. **9**(4): p. 125-128.

7. Toro, J., et al., *Exclusion of PTEN, CTNNB1, and PTCH as candidate genes for Birt-Hogg-Dube syndrome.* Journal of medical genetics, 2002. **39**(2): p. e10-e10.

8. Ding, Y., et al., *FLCN intragenic deletions in Chinese familial primary spontaneous pneumothorax.* American Journal of Medical Genetics Part A, 2015. **167**(5): p. 1125-1133.

9. Schmeler, K.M., et al., *Prophylactic surgery to reduce the risk of gynecologic cancers in the Lynch syndrome.* New England Journal of Medicine, 2006. **354**(3): p. 261-269.

10. Miura, K., et al., *Birt-Hogg-Dubé syndrome detected incidentally by asymptomatic bilateral pneumothorax in health screening: a case of a young Japanese woman.* thorax, 2015. **1**: p. 3.

11. Toro, J.R., et al., *Birt-Hogg-Dube syndrome: a novel marker of kidney neoplasia.* Archives of dermatology, 1999. **135**(10): p. 1195-1202.

12. Toro, J.R., et al., *Lung cysts, spontaneous pneumothorax, and genetic associations in 89 families with Birt-Hogg-Dubé syndrome.* American journal of respiratory and critical care medicine, 2007. **175**(10): p. 1044-1053.

13. Zbar, B., et al., *Risk of renal and colonic neoplasms and spontaneous pneumothorax in the Birt-Hogg-Dube syndrome.* Cancer Epidemiology Biomarkers & Prevention, 2002. **11**(4): p. 393-400.

14. Furuya, M. and Y. Nakatani, *Birt–Hogg–Dubé syndrome: clinicopathological features of the lung.* Journal of clinical pathology, 2012: p. jclinpath-2012-201200.

15. Canadian Cancer Society, http://www.cancer.ca/en/cancer-information/cancer-type/kidney/statistics/?region=on.

16. Linehan, W.M., et al., *The genetic basis of cancer of kidney cancer: implications for gene-specific clinical management.* BJU international, 2005. **95**(s2): p. 2-7.

17. Cohen, H.T. and F.J. McGovern, *Renal-cell carcinoma.* New England Journal of Medicine, 2005. **353**(23): p. 2477-2490.

18. Pavlovich, C.P., et al., *Renal tumors in the Birt-Hogg-Dube syndrome.* The American journal of surgical pathology, 2002. **26**(12): p. 1542-1552.

19. Pavlovich, C.P., et al., *Evaluation and management of renal tumors in the Birt-Hogg-Dube syndrome.* The Journal of urology, 2005. **173**(5): p. 1482-1486.

20. Schmidt, L.S. and W.M. Linehan, *Clinical features, genetics and potential therapeutic approaches for Birt-Hogg-Dubé syndrome.* Expert Opinion on Orphan Drugs, 2015. **3**(1): p. 15-29.

21. Chung, J.Y., et al., *MULTIPLE LIPOMAS, ANGIOLIPOMAS, AND PARATHYROID ADENOMAS IN A PATIENT WITH BIRT-HOGG-DUBE SYNDROME.* International journal of dermatology, 1996. **35**(5): p. 365-366.

22. Toro, J.R., et al., *BHD mutations, clinical and molecular genetic investigations of Birt–Hogg–Dubé syndrome: a new series of 50 families and a review of published reports.* Journal of medical genetics, 2008. **45**(6): p. 321-331.

23. Kunogi, M., et al., *Clinical and genetic spectrum of Birt–Hogg–Dube syndrome patients in whom pneumothorax and/or multiple lung cysts are the presenting feature.* Journal of medical genetics, 2010. **47**(4): p. 281-287.

24. Hornstein, O.P. and M. Knickenberg, *Perifollicular fibromatosis cutis with polyps of the colon—a cutaneo-intestinal syndrome sui generis.* Archives of Dermatological Research, 1975. **253**(2): p. 161-175.

25. Hornstein, O., *Generalized dermal perifollicular fibromas with polyps of the colon.* Human genetics, 1976. **33**(2): p. 193-197.

26. Khoo, M.L., et al., *Thyroid calcification and its association with thyroid carcinoma.* Head & neck, 2002. **24**(7): p. 651-655.

27. Khoo, S., et al., *Clinical and genetic studies of Birt-Hogg-Dube syndrome.* Journal of medical genetics, 2002. **39**(12): p. 906-912.

28. Jiang, W., et al., *Birt-Hogg-Dubé (BHD) gene mutations in human gastric cancer with high frequency microsatellite instability.* Cancer letters, 2007. **248**(1): p. 103-111.

29. Heinen, C.D. and L. Juel Rasmussen, *Determining the functional significance of mismatch repair gene missense variants using biochemical and cellular assays.* Hered Cancer Clin Pract, 2012. **10**(1): p. 9.

30. Kluger, N., et al., *Birt–Hogg–Dubé syndrome: clinical and genetic studies of 10 French families.* British Journal of Dermatology, 2010. **162**(3): p. 527-537.

31. Jacob, C.I. and J.S. Dover, *Birt-Hogg-Dube Syndrome: Treatment of Cutaneous Manifestations WithLaser Skin Resurfacing.* Archives of dermatology, 2001. **137**(1): p. 98-99.

32. Kahle, B., S. Hellwig, and T. Schulz, *Multiple Mantelome bei Birt-Hogg-Dubé-Syndrom Erfolgreiche Therapie mit dem CO2-Laser.* Der Hautarzt, 2001. **52**(1): p. 43-46.

33. Khoo, S.K., et al., *Birt-Hogg-Dube syndrome: mapping of a novel hereditary neoplasia gene to chromosome 17p12-q11. 2.* Oncogene, 2001. **20**(37): p. 5239-5242.

34. Schmidt, L.S., et al., *Birt-Hogg-Dube syndrome, a genodermatosis associated with spontaneous pneumothorax and kidney neoplasia, maps to chromosome 17p11. 2.* The American Journal of Human Genetics, 2001. **69**(4): p. 876-882.

35. Nickerson, M.L., et al., *Mutations in a novel gene lead to kidney tumors, lung wall defects, and benign tumors of the hair follicle in patients with the Birt-Hogg-Dube syndrome.* Cancer cell, 2002. **2**(2): p. 157-164.

36. Schmidt, L.S., *Birt-Hogg-Dubé syndrome, a genodermatosis that increases risk for renal carcinoma.* Current molecular medicine, 2004. **4**(8): p. 877-885.

37. Murakami, T., et al., *Identification and characterization of Birt–Hogg–Dube associated renal carcinoma.* The Journal of pathology, 2007. **211**(5): p. 524-531.

38. Zhao, J., et al., *Sporadic human renal tumors display frequent allelic imbalances and novel mutations of the HRPT2 gene.* Oncogene, 2007. **26**(23): p. 3440-3449.

39. Gunji, Y., et al., *Mutations of the Birt–Hogg–Dubé gene in patients with multiple lung cysts and recurrent pneumothorax.* Journal of medical genetics, 2007. **44**(9): p. 588-593.

40. Vos, T., et al., *Years lived with disability (YLDs) for 1160 sequelae of 289 diseases and injuries 1990–2010: a systematic analysis for the Global Burden of Disease Study 2010.* The Lancet, 2013. **380**(9859): p. 2163-2196.

41. Dodding, M.P., et al., *A kinesin-1 binding motif in vaccinia virus that is widespread throughout the human genome.* The EMBO journal, 2011. **30**(22): p. 4523-4538.

42. Warren, M.B., et al., *Expression of Birt–Hogg–Dube gene mRNA in normal and neoplastic human tissues.* Modern pathology, 2004. **17**(8): p. 998-1011.

43. Baba, M., et al., *Folliculin encoded by the BHD gene interacts with a binding protein, FNIP1, and AMPK, and is involved in AMPK and mTOR signaling.* Proc Natl Acad Sci U S A, 2006. **103**(42): p. 15552-7.

44. Hasumi, H., et al., *Identification and characterization of a novel folliculin-interacting protein FNIP2.* Gene, 2008. **415**(1): p. 60-67.

45. Takagi, Y., et al., *Interaction of folliculin (Birt-Hogg-Dube gene product) with a novel Fnip1-like (FnipL/Fnip2) protein.* Oncogene, 2008. **27**(40): p. 5339-47.

46. Petit, C.S., A. Roczniak-Ferguson, and S.M. Ferguson, *Recruitment of folliculin to lysosomes supports the amino acid-dependent activation of Rag GTPases.* J Cell Biol, 2013. **202**(7): p. 1107-22.

47. Tsun, Z.-Y., et al., *The folliculin tumor suppressor is a GAP for the RagC/D GTPases that signal amino acid levels to mTORC1.* Molecular cell, 2013. **52**(4): p. 495-505.

48. Racioppi, L. and A.R. Means, *Calcium/calmodulin-dependent protein kinase kinase 2: roles in signaling and pathophysiology.* Journal of Biological Chemistry, 2012. **287**(38): p. 31658-31665.

49. Fryer, L.G., A. Parbu-Patel, and D. Carling, *The anti-diabetic drugs rosiglitazone and metformin stimulate AMP-activated protein kinase through distinct signaling pathways.* Journal of Biological Chemistry, 2002. **277**(28): p. 25226-25232.

50. Zhang, B.B., G. Zhou, and C. Li, *AMPK: an emerging drug target for diabetes and the metabolic syndrome.* Cell metabolism, 2009. **9**(5): p. 407-416.

51. Li, Y., et al., *AMPK phosphorylates and inhibits SREBP activity to attenuate hepatic steatosis and atherosclerosis in diet-induced insulin-resistant mice.* Cell metabolism, 2011. **13**(4): p. 376-388.

52. Matejkova, O., et al., *Possible involvement of AMP-activated protein kinase in obesity resistance induced by respiratory uncoupling in white fat.* FEBS letters, 2004. **569**(1): p. 245-248.

53. Ma, L., et al., *Phosphorylation and functional inactivation of TSC2 by Erk: implications for tuberous sclerosisand cancer pathogenesis.* Cell, 2005. **121**(2): p. 179-193.

54. Kim, I. and Y.-Y. He, *Targeting the AMP-activated protein kinase for cancer prevention and therapy.* Frontiers in oncology, 2013. **3**.

55. Dunlop, E.A., et al., *FLCN, a novel autophagy component, interacts with GABARAP and is regulated by ULK1 phosphorylation.* Autophagy, 2014. **10**(10): p. 1749-1760.

56. Gaur, K., et al., *The Birt-Hogg-Dube tumor suppressor Folliculin negatively regulates ribosomal RNA synthesis.* Hum Mol Genet, 2013. **22**(2): p. 284-99.

57. Nahorski, M.S., et al., *Folliculin interacts with p0071 (plakophilin-4) and deficiency is associated with disordered RhoA signalling, epithelial polarization and cytokinesis.* Hum Mol Genet, 2012. **21**(24): p. 5268-79.

58. Medvetz, D.A., et al., *Folliculin, the product of the Birt-Hogg-Dube tumor suppressor gene, interacts with the adherens junction protein p0071 to regulate cell-cell adhesion.* PLoS One, 2012. **7**(11): p. e47842.

59. Harris, T.E. and J.C. Lawrence Jr, *TOR signaling.* Sci Stke, 2003. **212**(re15): p. 1-17.

60. Hay, N. and N. Sonenberg, *Upstream and downstream of mTOR.* Genes & development, 2004. **18**(16): p. 1926-1945.

61. Budanov, A.V. and M. Karin, *p53 target genes sestrin1 and sestrin2 connect genotoxic stress and mTOR signaling.* Cell, 2008. **134**(3): p. 451-460.

62. Wee, J., et al., *Familial multiple discoid fibromas: unique histological features and therapeutic response to topical rapamycin.* British Journal of Dermatology, 2013. **169**(1): p. 177-180.

63. Petit, C.S., A. Roczniak-Ferguson, and S.M. Ferguson, *Recruitment of folliculin to lysosomes supports the amino acid–dependent activation of Rag GTPases.* The Journal of cell biology, 2013. **202**(7): p. 1107-1122.

64. Semenza, G.L., *HIF-1 and mechanisms of hypoxia sensing.* Current opinion in cell biology, 2001. **13**(2): p. 167-171.

65. Mahon, P.C., K. Hirota, and G.L. Semenza, *FIH-1: a novel protein that interacts with HIF-1α and VHL to mediate repression of HIF-1 transcriptional activity.* Genes & development, 2001. **15**(20): p. 2675-2686.

66. Lewis, C.E. and J.W. Pollard, *Distinct role of macrophages in different tumor microenvironments.* Cancer research, 2006. **66**(2): p. 605-612.

67. Adams, J., et al., *HIF-1: a key mediator in hypoxia (Review).* Acta Physiologica Hungarica, 2009. **96**(1): p. 19-28.

68. Hellwig-Bürgel, T., et al., *Review: hypoxia-inducible factor-1 (HIF-1): a novel transcription factor in immune reactions.* Journal of interferon & cytokine research, 2005. **25**(6): p. 297-310.

69. Preston, R.S., et al., *Absence of the Birt-Hogg-Dube gene product is associated with increased hypoxia-inducible factor transcriptional activity and a loss of metabolic flexibility.* Oncogene, 2011. **30**(10): p. 1159-73.

70. Warburg, O., *On the origin of cancer cells.* Science, 1956. **123**(3191): p. 309-314.

71. Nishii, T., et al., *Unique mutation, accelerated mTOR signaling and angiogenesis in the pulmonary cysts of Birt-Hogg-Dube syndrome.* Pathology international, 2013. **63**(1): p. 45-55.

72. Semenza, G.L., *Hypoxia-inducible factors in physiology and medicine.* Cell, 2012. **148**(3): p. 399-408.

73. Yun, H., et al., *Glucose deprivation increases mRNA stability of vascular endothelial growth factor through activation of AMP-activated protein kinase in DU145 prostate carcinoma.* Journal of Biological Chemistry, 2005. **280**(11): p. 9963-9972.

74. He, C. and D.J. Klionsky, *Regulation mechanisms and signaling pathways of autophagy.* Annual review of genetics, 2009. **43**: p. 67.

75. Possik, E., et al., *Folliculin regulates ampk-dependent autophagy and metabolic stress survival.* PLoS Genet, 2014. **10**(4): p. e1004273.

76. Hong, S.-B., et al., *Tumor suppressor FLCN inhibits tumorigenesis of a FLCN-null renal cancer cell line and regulates expression of key molecules in TGF-β signaling.* Molecular cancer, 2010. **9**(1): p. 1.

77. Hua, X., et al., *Synergistic cooperation of TFE3 and Smad proteins in TGF-β-induced transcription of the plasminogen activator inhibitor-1 gene.* Genes & Development, 1998. **12**(19): p. 3084-3095.

78. Cash, T., et al., *Loss of the Birt–Hogg–Dubé tumor suppressor results in apoptotic resistance due to aberrant TGFβ-mediated transcription.* Oncogene, 2011. **30**(22): p. 2534-2546.

79. Puigserver, P., et al., *A cold-inducible coactivator of nuclear receptors linked to adaptive thermogenesis.* Cell, 1998. **92**(6): p. 829-839.

80. Wu, Z., et al., *Mechanisms controlling mitochondrial biogenesis and respiration through the thermogenic coactivator PGC-1.* Cell, 1999. **98**(1): p. 115-124.

81. St-Pierre, J., et al., *Bioenergetic analysis of peroxisome proliferator-activated receptor γ coactivators 1α and 1β (PGC-1α and PGC-1β) in muscle cells.* Journal of Biological Chemistry, 2003. **278**(29): p. 26597-26603.

82. Klomp, J.A., et al., *Birt-Hogg-Dube renal tumors are genetically distinct from other renal neoplasias and are associated with up-regulation of mitochondrial gene expression.* BMC Med Genomics, 2010. **3**: p. 59.

83. Hasumi, H., et al., *Regulation of mitochondrial oxidative metabolism by tumor suppressor FLCN.* Journal of the National Cancer Institute, 2012.

84. Boström, P., et al., *A PGC1-[agr]-dependent myokine that drives brown-fat-like development of white fat and thermogenesis.* Nature, 2012. **481**(7382): p. 463-468.

85. Gong, D.-W., et al., *Uncoupling protein-3 is a mediator of thermogenesis regulated by thyroid hormone, β3-adrenergic agonists, and leptin.* Journal of Biological Chemistry, 1997. **272**(39): p. 24129-24132.

86. Chartoumpekis, D.V., et al., *Brown adipose tissue responds to cold and adrenergic stimulation by induction of FGF21.* Molecular medicine, 2011. **17**(7-8): p. 736.

87. Wu, J., P. Cohen, and B.M. Spiegelman, *Adaptive thermogenesis in adipocytes: Is beige the new brown?* Genes & development, 2013. **27**(3): p. 234-250.

88. Ohno, H., et al., *PPARγ agonists induce a white-to-brown fat conversion through stabilization of PRDM16 protein.* Cell metabolism, 2012. **15**(3): p. 395-404.

89. Narkar, V.A., et al., *AMPK and PPARδ agonists are exercise mimetics.* Cell, 2008. **134**(3): p. 405-415.

90. Crowley, V.E., G.S. Yeo, and S. O'Rahilly, *Obesity therapy: altering the energy intake-and-expenditure balance sheet.* Nature reviews Drug discovery, 2002. **1**(4): p. 276-286.

91. Baar, K., *Involvement of PPARγ co-activator-1, nuclear respiratory factors 1 and 2, and PPARα in the adaptive response to endurance exercise.* Proceedings of the Nutrition Society, 2004. **63**(02): p. 269-273.

92. DeBerardinis, R.J., *Metabolism, Diet and Disease 2014: Cancer and metabolism.* 2014.

93. Wang, L., et al., *Serine 62 is a phosphorylation site in folliculin, the Birt-Hogg-Dube gene product.* FEBS Lett, 2010. **584**(1): p. 39-43.

94. Piao, X., et al., *Regulation of folliculin (the BHD gene product) phosphorylation by Tsc2-mTOR pathway.* Biochem Biophys Res Commun, 2009. **389**(1): p. 16-21.

95. Baba, M., et al., *Folliculin encoded by the BHD gene interacts with a binding protein, FNIP1, and AMPK, and is involved in AMPK and mTOR signaling.* Proceedings of the National Academy of Sciences, 2006. **103**(42): p. 15552-15557.

96. Linehan, W.M., R. Srinivasan, and L.S. Schmidt, *The genetic basis of kidney cancer: a metabolic disease.* Nat Rev Urol, 2010. **7**(5): p. 277-85.

97. Keith, B., R.S. Johnson, and M.C. Simon, *HIF1alpha and HIF2alpha: sibling rivalry in hypoxic tumour growth and progression.* Nat Rev Cancer, 2012. **12**(1): p. 9-22.

98. Majmundar, A.J., W.J. Wong, and M.C. Simon, *Hypoxia-inducible factors and the response to hypoxic stress.* Mol Cell, 2010. **40**(2): p. 294-309.

99. Schmidt, L.S., et al., *Germline BHD-mutation spectrum and phenotype analysis of a large cohort of families with Birt-Hogg-Dube syndrome.* Am J Hum Genet, 2005. **76**(6): p. 1023-33.

100. Cairns, R.A., I.S. Harris, and T.W. Mak, *Regulation of cancer cell metabolism.* Nat Rev Cancer, 2011. **11**(2): p. 85-95.

101. Greer, S.N., et al., *The updated biology of hypoxia-inducible factor.* EMBO J, 2012. **31**(11): p. 2448-60.

102. Jung, S.N., et al., *Reactive oxygen species stabilize hypoxia-inducible factor-1 alpha protein and stimulate transcriptional activity via AMP-activated protein kinase in DU145 human prostate cancer cells.* Carcinogenesis, 2008. **29**(4): p. 713-21.

103. Oakhill, J.S., J.W. Scott, and B.E. Kemp, *AMPK functions as an adenylate charge-regulated protein kinase.* Trends Endocrinol Metab, 2012. **23**(3): p. 125-32.

104. Liang, J. and G.B. Mills, *AMPK: a contextual oncogene or tumor suppressor?* Cancer Res, 2013. **73**(10): p. 2929-35.

105. Behrends, C., et al., *Network organization of the human autophagy system.* Nature, 2010. **466**(7302): p. 68-76.

106. Koppenol, W.H., P.L. Bounds, and C.V. Dang, *Otto Warburg's contributions to current concepts of cancer metabolism.* Nat Rev Cancer, 2011. **11**(5): p. 325-37.

107. Vander Heiden, M.G., L.C. Cantley, and C.B. Thompson, *Understanding the Warburg effect: the metabolic requirements of cell proliferation.* Science, 2009. **324**(5930): p. 1029-33.

108. Pollak, M., *Targeting oxidative phosphorylation: why, when, and how.* Cancer Cell, 2013. **23**(3): p. 263-4.

109. Schulze, A. and A.L. Harris, *How cancer metabolism is tuned for proliferation and vulnerable to disruption.* Nature, 2012. **491**(7424): p. 364-73.

110. Hasumi, H., et al., *Regulation of mitochondrial oxidative metabolism by tumor suppressor FLCN.* J Natl Cancer Inst, 2012. **104**(22): p. 1750-64.

111. Pavlovich, C.P., et al., *Renal tumors in the Birt-Hogg-Dube syndrome.* Am J Surg Pathol, 2002. **26**(12): p. 1542-52.

112. Finkel, T., *Signal transduction by reactive oxygen species.* J Cell Biol, 2011. **194**(1): p. 7-15.

113. Brunelle, J.K., et al., *Oxygen sensing requires mitochondrial ROS but not oxidative phosphorylation.* Cell Metab, 2005. **1**(6): p. 409-14.

114. Guzy, R.D., et al., *Mitochondrial complex III is required for hypoxia-induced ROS production and cellular oxygen sensing.* Cell Metab, 2005. **1**(6): p. 401-8.

115. Lee, S.J., A.B. Hwang, and C. Kenyon, *Inhibition of respiration extends C. elegans life span via reactive oxygen species that increase HIF-1 activity.* Curr Biol, 2010. **20**(23): p. 2131-6.

116. Wang, D., D. Malo, and S. Hekimi, *Elevated mitochondrial reactive oxygen species generation affects the immune response via hypoxia-inducible factor-1alpha in long-lived Mclk1+/- mouse mutants.* J Immunol, 2010. **184**(2): p. 582-90.

117. Comito, G., et al., *HIF-1alpha stabilization by mitochondrial ROS promotes Met-dependent invasive growth and vasculogenic mimicry in melanoma cells.* Free Radic Biol Med, 2011. **51**(4): p. 893-904.

118. Kelly, D.P. and R.C. Scarpulla, *Transcriptional regulatory circuits controlling mitochondrial biogenesis and function.* Genes Dev, 2004. **18**(4): p. 357-68.

119. O'Hagan, K.A., et al., *PGC-1alpha is coupled to HIF-1alpha-dependent gene expression by increasing mitochondrial oxygen consumption in skeletal muscle cells.* Proc Natl Acad Sci U S A, 2009. **106**(7): p. 2188-93.

120. Savagner, F., et al., *PGC-1-related coactivator and targets are upregulated in thyroid oncocytoma.* Biochem Biophys Res Commun, 2003. **310**(3): p. 779-84.

121. St-Pierre, J., et al., *Suppression of reactive oxygen species and neurodegeneration by the PGC-1 transcriptional coactivators.* Cell, 2006. **127**(2): p. 397-408.

122. Finkel, T., *Cell biology: a clean energy programme.* Nature, 2006. **444**(7116): p. 151-2.

123. Jager, S., et al., *AMP-activated protein kinase (AMPK) action in skeletal muscle via direct phosphorylation of PGC-1alpha.* Proc Natl Acad Sci U S A, 2007. **104**(29): p. 12017-22.

124. DeBerardinis, R.J., et al., *Beyond aerobic glycolysis: transformed cells can engage in glutamine metabolism that exceeds the requirement for protein and nucleotide synthesis.* Proc Natl Acad Sci U S A, 2007. **104**(49): p. 19345-50.

125. Metallo, C.M., et al., *Reductive glutamine metabolism by IDH1 mediates lipogenesis under hypoxia.* Nature, 2012. **481**(7381): p. 380-4.

126. Mullen, A.R., et al., *Reductive carboxylation supports growth in tumour cells with defective mitochondria.* Nature, 2012. **481**(7381): p. 385-8.

127. Gameiro, P.A., et al., *In vivo HIF-mediated reductive carboxylation is regulated by citrate levels and sensitizes VHL-deficient cells to glutamine deprivation.* Cell Metab, 2013. **17**(3): p. 372-85.

128. Lu, X., et al., *Therapeutic targeting the loss of the birt-hogg-dube suppressor gene.* Mol Cancer Ther, 2011. **10**(1): p. 80-9.

129. Reiman, A., et al., *Gene expression and protein array studies of folliculin-regulated pathways.* Anticancer Res, 2012. **32**(11): p. 4663-70.

130. Hong, S.B., et al., *Tumor suppressor FLCN inhibits tumorigenesis of a FLCN-null renal cancer cell line and regulates expression of key molecules in TGF-beta signaling.* Mol Cancer, 2010. **9**: p. 160.

131. Leprivier, G., et al., *The eEF2 Kinase Confers Resistance to Nutrient Deprivation by Blocking Translation Elongation.* Cell, 2013. **153**(5): p. 1064-79.

132. Jeon, S.M., N.S. Chandel, and N. Hay, *AMPK regulates NADPH homeostasis to promote tumour cell survival during energy stress.* Nature, 2012. **485**(7400): p. 661-5.

133. Liu, L., et al., *Deregulated MYC expression induces dependence upon AMPK-related kinase 5.* Nature, 2012. **483**(7391): p. 608-12.

134. Deblois, G., J. St-Pierre, and V. Giguere, *The PGC-1/ERR signaling axis in cancer.* Oncogene, 2012.

135. Haigis, M.C., et al., *SIRT3 is a mitochondrial tumor suppressor: a scientific tale that connects aberrant cellular ROS, the Warburg effect, and carcinogenesis.* Cancer Res, 2012. **72**(10): p. 2468-72.

136. Semenza, G.L., *HIF-1: upstream and downstream of cancer metabolism.* Curr Opin Genet Dev, 2010. **20**(1): p. 51-6.

137. Zhang, Y., et al., *The HIF-1 hypoxia-inducible factor modulates lifespan in C. elegans.* PLoS One, 2009. **4**(7): p. e6348.

138. Schulz, T.J., et al., *Glucose restriction extends Caenorhabditis elegans life span by inducing mitochondrial respiration and increasing oxidative stress.* Cell Metab, 2007. **6**(4): p. 280-93.

139. Zarse, K., et al., *Impaired insulin/IGF1 signaling extends life span by promoting mitochondrial L-proline catabolism to induce a transient ROS signal.* Cell Metab, 2012. **15**(4): p. 451-65.

140. Lisy, K. and D.J. Peet, *Turn me on: regulating HIF transcriptional activity.* Cell Death Differ, 2008. **15**(4): p. 642-9.

141. Lyberopoulou, A., et al., *MgcRacGAP, a cytoskeleton regulator, inhibits HIF-1 transcriptional activity by blocking its dimerization.* Biochim Biophys Acta, 2013. **1833**(6): p. 1378-87.

142. Luo, Z., M. Zang, and W. Guo, *AMPK as a metabolic tumor suppressor: control of metabolism and cell growth.* Future Oncol, 2010. **6**(3): p. 457-70.

143. Faubert, B., et al., *AMPK is a negative regulator of the Warburg effect and suppresses tumor growth in vivo.* Cell Metab, 2013. **17**(1): p. 113-24.

144. Kottakis, F. and N. Bardeesy, *LKB1-AMPK axis revisited.* Cell Res, 2012.

145. Girnun, G.D., *The diverse role of the PPARgamma coactivator 1 family of transcriptional coactivators in cancer.* Semin Cell Dev Biol, 2012. **23**(4): p. 381-8.

146. Bhalla, K., et al., *PGC1alpha promotes tumor growth by inducing gene expression programs supporting lipogenesis.* Cancer Res, 2011. **71**(21): p. 6888-98.

147. Klimcakova, E., et al., *PGC-1alpha Promotes the Growth of ErbB2/Neu-Induced Mammary Tumors by Regulating Nutrient Supply.* Cancer Res, 2012. **72**(6): p. 1538-46.

148. Tennakoon, J.B., et al., *Androgens regulate prostate cancer cell growth via an AMPK-PGC-1alpha-mediated metabolic switch.* Oncogene, 2013.

149. Dupuy, F., et al., *LKB1 is a central regulator of tumor initiation and pro-growht metabolism in ErbB2-mediated breast cancer.* Cancer & Metabolism, 2013. **1**(18).

150. Rapisarda, A., et al., *Identification of small molecule inhibitors of hypoxia-inducible factor 1 transcriptional activation pathway.* Cancer Res, 2002. **62**(15): p. 4316-24.

151. Fantin, V.R., J. St-Pierre, and P. Leder, *Attenuation of LDH-A expression uncovers a link between glycolysis, mitochondrial physiology, and tumor maintenance.* Cancer Cell, 2006. **9**(6): p. 425-34.

152. Welbourn, S., et al., *Hepatitis C virus NS2/3 processing is required for NS3 stability and viral RNA replication.* J Biol Chem, 2005. **280**(33): p. 29604-11.

153. Xu, J., *Preparation, culture, and immortalization of mouse embryonic fibroblasts.* Curr Protoc Mol Biol, 2005. **Chapter 28**: p. Unit 28 1.

154. MacIver, N.J., et al., *The liver kinase B1 is a central regulator of T cell development, activation, and metabolism.* J Immunol, 2011. **187**(8): p. 4187-98.

155. Rosen, E.D. and B.M. Spiegelman, *Adipocytes as regulators of energy balance and glucose homeostasis.* Nature, 2006. **444**(7121): p. 847-853.

156. Wu, J., et al., *Beige adipocytes are a distinct type of thermogenic fat cell in mouse and human.* Cell, 2012. **150**(2): p. 366-376.

157. Schulz, T.J., et al., *Brown-fat paucity due to impaired BMP signalling induces compensatory browning of white fat.* Nature, 2013. **495**(7441): p. 379-83.

158. Harms, M. and P. Seale, *Brown and beige fat: development, function and therapeutic potential.* Nature medicine, 2013. **19**(10): p. 1252-1263.

159. Wang, S.P., et al., *The Adipose Tissue Phenotype of Hormone-Sensitive Lipase Deficiency in Mice.* Obesity research, 2001. **9**(2): p. 119-128.

160. Seale, P., et al., *Prdm16 determines the thermogenic program of subcutaneous white adipose tissue in mice.* The Journal of clinical investigation, 2011. **121**(1): p. 96.

161. Hansen, J.B., et al., *Retinoblastoma protein functions as a molecular switch determining white versus brown adipocyte differentiation.* Proceedings of the National Academy of Sciences, 2004. **101**(12): p. 4112-4117.

162. Ye, L., et al., *TRPV4 is a regulator of adipose oxidative metabolism, inflammation, and energy homeostasis.* Cell, 2012. **151**(1): p. 96-110.

163. Rajakumari, S., et al., *EBF2 determines and maintains brown adipocyte identity.* Cell Metab, 2013. **17**(4): p. 562-74.

164. Chen, J., et al., *Deficiency of FLCN in mouse kidney led to development of polycystic kidneys and renal neoplasia.* PLoS One, 2008. **3**(10): p. e3581.

165. Baba, M., et al., *Kidney-targeted Birt-Hogg-Dube gene inactivation in a mouse model: Erk1/2 and Akt-mTOR activation, cell hyperproliferation, and polycystic kidneys.* J Natl Cancer Inst, 2008. **100**(2): p. 140-54.

166. Hudon, V., et al., *Renal tumour suppressor function of the Birt-Hogg-Dube syndrome gene product folliculin.* J Med Genet, 2010. **47**(3): p. 182-9.

167. Yan, M., et al., *The tumor suppressor folliculin regulates AMPK-dependent metabolic transformation.* The Journal of clinical investigation, 2014. **124**(6): p. 2640.

168. Possik, E., et al., *Folliculin Regulates Ampk-Dependent Autophagy and Metabolic Stress Survival.* Plos Genetics, 2014. **10**(4).

169. Mihaylova, M.M. and R.J. Shaw, *The AMPK signalling pathway coordinates cell growth, autophagy and metabolism.* Nature cell biology, 2011. **13**(9): p. 1016-1023.

170. Dobrzyn, P., et al., *Stearoyl-CoA desaturase 1 deficiency increases fatty acid oxidation by activating AMP-activated protein kinase in liver.* Proceedings of the National Academy of Sciences of the United States of America, 2004. **101**(17): p. 6409-6414.

171. Zhang, W., et al., *AMP-activated protein kinase α1 protects against diet-induced insulin resistance and obesity.* Diabetes, 2012. **61**: p. 3114-3125

.

172. Jäger, S., et al., *AMP-activated protein kinase (AMPK) action in skeletal muscle via direct phosphorylation of PGC-1α.* Proceedings of the National Academy of Sciences, 2007. **104**(29): p. 12017-12022.

173. Giguere, V., *Transcriptional control of energy homeostasis by the estrogen-related receptors.* Endocrine reviews, 2008. **29**(6): p. 677-696.

174. Eichner, L.J. and V. Giguère, *Estrogen related receptors (ERRs): a new dawn in transcriptional control of mitochondrial gene networks.* Mitochondrion, 2011. **11**(4): p. 544-552.

175. Villena, J.A., et al., *Orphan nuclear receptor estrogen-related receptor α is essential for adaptive thermogenesis.* Proceedings of the National Academy of Sciences, 2007. **104**(4): p. 1418-1423.

176. Handschin, C. and B.M. Spiegelman. *Peroxisome proliferator-activated receptor γ coactivator 1 coactivators, energy homeostasis, and metabolism*. 2013. Endocrine Revews.

177. Lee, K.Y., et al., *Lessons on conditional gene targeting in mouse adipose tissue.* Diabetes, 2013. **62**(3): p. 864-874.

178. Harms, M.J., et al., *Prdm16 is required for the maintenance of brown adipocyte identity and function in adult mice.* Cell metabolism, 2014. **19**(4): p. 593-604.

179. Kusminski, C.M. and P.E. Scherer, *Mitochondrial dysfunction in white adipose tissue.* Trends Endocrinol Metab, 2012. **23**(9): p. 435-43.

180. Uldry, M., et al., *Complementary action of the PGC-1 coactivators in mitochondrial biogenesis and brown fat differentiation.* Cell metabolism, 2006. **3**(5): p. 333-341.

181. Schreiber, S.N., et al., *The estrogen-related receptor α (ERRα) functions in PPARγ coactivator 1α (PGC-1α)-induced mitochondrial biogenesis.* Proceedings of the National Academy of Sciences of the United States of America, 2004. **101**(17): p. 6472-6477.

182. Mootha, V.K., et al., *Errα and Gabpa/b specify PGC-1α-dependent oxidative phosphorylation gene expression that is altered in diabetic muscle.* Proceedings of the National Academy of Sciences of the United States of America, 2004. **101**(17): p. 6570-6575.

183. Laganière, J., et al., *A polymorphic autoregulatory hormone response element in the human estrogen-related receptor α (ERRα) promoter dictates peroxisome proliferator-activated receptor γ coactivator-1α control of ERRα expression.* Journal of Biological Chemistry, 2004. **279**(18): p. 18504-18510.

184. Deblois, G., J. St-Pierre, and V. Giguere, *The PGC-1/ERR signaling axis in cancer.* Oncogene, 2013. **32**(30): p. 3483-3490.

185. Reyes, N.L., et al., *Fnip1 regulates skeletal muscle fiber type specification, fatigue resistance, and susceptibility to muscular dystrophy.* Proceedings of the National Academy of Sciences, 2015. **112**(2): p. 424-429.

186. Zhang, H., et al., *MicroRNA-455 regulates brown adipogenesis via a novel HIF1an-AMPK-PGC1α signaling network.* EMBO reports, 2015: p. e201540837.

187. Kleiner, S., et al., *FGF21 regulates PGC-1α and browning of white adipose tissues in adaptive thermogenesis.* Genes & development, 2012. **26**(3): p. 271-281.

188. Iida, S., et al., *PRDM16 enhances nuclear receptor-dependent transcription of the brown fat-specific Ucp1 gene through interactions with Mediator subunit MED1.* Genes & development, 2015. **29**(3): p. 308-321.

189. Luo, J., et al., *Reduced fat mass in mice lacking orphan nuclear receptor estrogen-related receptor α.* Molecular and cellular biology, 2003. **23**(22): p. 7947-7956.

190. Carrier, J.C., et al., *Estrogen-related receptor α (ERRα) is a transcriptional regulator of apolipoprotein A-IV and controls lipid handling in the intestine.* Journal of Biological Chemistry, 2004. **279**(50): p. 52052-52058.

191. Kamei, Y., et al., *PPARγ coactivator 1β/ERR ligand 1 is an ERR protein ligand, whose expression induces a high-energy expenditure and antagonizes obesity.* Proceedings of the National Academy of Sciences, 2003. **100**(21): p. 12378-12383.

192. Preston, R.S., et al., *Absence of the Birt–Hogg–Dubé gene product is associated with increased hypoxia-inducible factor transcriptional activity and a loss of metabolic flexibility.* Oncogene, 2011. **30**(10): p. 1159-1173.

193. Gingras, M.-C. and A. Pause, *FLCN: A new regulator of AMPK-dependent Warburg metabolic reprogramming.* Molecular & Cellular Oncology, 2014. **1**(2): p. e961819.

194. Liang, J. and G.B. Mills, *AMPK: a contextual oncogene or tumor suppressor?* Cancer research, 2013. **73**(10): p. 2929-2935.

195. Hartman, T.R., et al., *The role of the Birt–Hogg–Dubé protein in mTOR activation and renal tumorigenesis.* Oncogene, 2009. **28**(13): p. 1594-1604.

196. Bastola, P., et al., *Folliculin contributes to VHL tumor suppressing activity in renal cancer through regulation of autophagy.* PloS one, 2013. **8**(7): p. e70030.

197. Chen, J., et al., *Deficiency of FLCN in mouse kidney led to development of polycystic kidneys and renal neoplasia.* PloS one, 2008. **3**(10): p. e3581-e3581.

198. Chen, J., et al., *Disruption of tubular Flcn expression as a mouse model for renal tumor induction.* Kidney international, 2015.

199. Hasumi, Y., et al., *Homozygous loss of BHD causes early embryonic lethality and kidney tumor development with activation of mTORC1 and mTORC2.* Proceedings of the National Academy of Sciences, 2009. **106**(44): p. 18722-18727.

200. Yoon, J.C., et al., *Control of hepatic gluconeogenesis through the transcriptional coactivator PGC-1.* Nature, 2001. **413**(6852): p. 131-138.

ORIGINAL CONTRIBUTIONS TO KNOWLEDGE

1. Characterized a novel tumor suppressor mechanism of FLCN: Loss of *Flcn* favors metabolic transformation that confers a tumorigenic advantage through activation of AMPK.
2. Showed *Flcn* deficiency induced HIF activation through mitochondrial biogenesis and ROS.
3. Showed HIF activation and ROS production depends on AMPK-dependent PGC-1 upregulation.
4. Showed FLCN binding to AMPK is essential to the AMPK-PGC-1-ROS-HIF pathway.
5. Demonstrated Loss of FLCN drives a metabolic transformation characterized by enhanced aerobic glycolysis and mitochondrial oxidative phosphorylation in order to boost levels of ATP and biosynthetic precursors.
6. Showed adipose-specific *Flcn* KO mice exhibit elevated energy expenditure.
7. Showed adipose-specific *Flcn* KO mice are resistance to high fat diet (HFD)-induced obesity.
8. Demonstrated loss of FLCN leads to an increase in AMPK-dependent PGC-1α and ERRα signalling.
9. Demonstrated thermogenic genes including uncoupling protein (UCP1) are upregulated in *Flcn* KO white adipose tissue (WAT) to generate heat under cold exposure.
10. Demonstrated that *Flcn* is involved in not only for cancer-associated metabolic transformation mechanism but also to comprehend the general AMPK function as a master regulator of cellular homeostasis.